UNIVERSITY OF UDINE

Department of Medical and Biological Sciences

PhD Course in Biomedical and Biotechnological Sciences

(in agreement with National Cancer Institute, CRO Aviano)

(XXXI Cycle)

PhD Thesis

ABROGATION OF EMILIN-1/$\alpha_4\beta_1$ INTEGRIN INTERACTION AFFECTS EXPERIMENTAL COLITIS AND COLON CARCINOGENESIS ENHANCING LYMPHATIC DYSREGULATION AND INCREASING INFLAMMATORY CASCADE

PhD Student:
Giulia Bosisio

Supervisor:
Paola Spessotto

ACADEMIC YEAR 2017-2018

This thesis was entirely carried out at the Division of Molecular Oncology and Preclinical Models of Tumour Progression Centro di Riferimento Oncologico (CRO) of Aviano, under the direction of Dr. Gustavo Baldassarre.

CONTENTS

ABBREVIATIONS

AF: Anchoring Filament

AOM: Azoxymethane

CAC: Colitis Associated Cancer

CD: Crohn Disease

CRC: Colorectal Cancer

DAI: Disease Activity Index

DSS: Dextran Sulphate Sodium

ECM: Extracellular Matrix

EMILIN-1: Elastin Microfibril Interface Located Protein 1

H&E: Hematoxylin and Eosin

IBD: Inflammatory Bowel Disease

IHC: Immunohistochemistry

LAEC: LymphAngioma-derived Endothelial Cells

LEC: Lymphatic Endothelial Cell

LP: Lamina Propria

LV: Lymphatic Vessel

MEICS: Murine Endoscopy Index of Colitis Severity

ROS: Reactive Oxygen Species

SDS: Sodium Dodecyl Sulphate

TGF-β: Transforming Growth Factor-β

UC: Ulcerative colitis

VEGF: Vascular Endothelial Growth Factor

NOMENCLATURE

In the following tables there are indications about the nomenclature for **E**lastin **M**icrofibril **I**nterface **L**ocated **P**rotein **1** and abbreviations used in this thesis. When it is written in italics font it refers to the murine form, in regular font to the human one. The presence of the dash (-) indicate the protein, its absence the gene.

Nomenclature	Reference
EMILIN-1	**Protein (Human)**
EMILIN1	**Gene (Human)**
EMILIN-1	**Protein (Murine)**
Emilin1	**Gene (Murine)**
E1-E933A	**Transgenic Mouse carrying mutation in E933 residue of EMILIN1 sequence**

Abbreviation	Reference
$E^{+/+}$	**Wild Type murine protein**
$E^{-/-}$	**Knock Out murine protein**
$E1^{-/-}$**/E1-E933A**	**Human protein expressed in a null *Emilin1* background**

ABSTRACT

Colitis-associated cancer (CAC) is one of the principal cancer types in which there is a functional link between inflammation, tumor microenvironment and cancer progression; moreover, it is related to striking changes in the lymphatic vasculature. Development of aberrations that promote tumour initiation is strongly influenced by the contextual microenvironment. The extracellular matrix (ECM) glycoprotein EMILIN-1 is expressed, among several other tissues, in the normal colonic mucosa and exerts a lot of important function associated to its different domains. Most important, EMILIN-1 is a key structural element in the preservation of the integrity of lymphatic vessels (LVs). It is an adhesive ligand of $\alpha_4\beta_1$ and $\alpha_9\beta_1$ integrins via its gC1q domain; this interaction down-regulates cell proliferation unlike from signals generated by ligand-activated integrins that in general favor proliferative processes. $\alpha_4\beta_1$ integrin plays an important role during inflammation and it is expressed in the normal colon but in colon adenomas and carcinomas is moderately or highly expressed, respectively.

Given the structural and functional properties exerted by EMILIN-1, we hypothesized that it could be located in the context of the development of inflammatory colon cancer. In order to investigate how EMILIN-1 properties are crucial to control proliferation and to guarantee the regeneration of a competent and well-functioning lymphatic vasculature, we took advantage from an *Emilin1*$^{-/-}$ (*E1*$^{-/-}$) mouse model and an E933A EMILIN-1 transgenic mouse model (*E1*$^{-/-}$/E1-E933A), in which a mutant EMILIN-1, unable to be engaged by $\alpha_4\beta_1$, is expressed. After a two-steps colon carcinogenesis induction, *E1*$^{-/-}$ and *E1*$^{-/-}$/E1-E933A mice displayed higher tumour incidence, bigger and less differentiated adenomas and lower survival in comparison with *E1*$^{+/+}$ littermates, suggesting a protective anti-proliferative effect in the colon microenvironment exerted by "functional" *EMILIN-1*. The contribution of inflammation was then analysed after induction of chronic experimental colitis; *E1*$^{-/-}$ and *E1*$^{-/-}$/E1-E933A mice presented higher clinical and endoscopic colitis scores and more severe mucosal injury, fibrosis and inflammation than *E1*$^{+/+}$ counterparts. Furthermore *E1*$^{-/-}$ and *E1*$^{-/-}$/E1-E933A mice showed an extensive epithelial damage and an increased infiltration of inflammatory cells in the lamina propria, an up-regulation of several inflammatory response genes and a down-regulation of cell-cell adhesion molecule. Even without colitis induction, *E1*$^{-/-}$ and *E1*$^{-/-}$

/E1-E933A colonic LVs presented morphologic and functional alterations: they formed a dense network and appeared irregular, dilated and leaky. Under inflammatory conditions *E1*$^{+/+}$ displayed a normal pro-lymphangiogenic capacity, whereas *E1*$^{-/-}$ and *E1*$^{-/-}$/E1-E933A showed a reduced number of podoplanin positive vessels and also functional lymphatics impairment. All these results, mostly obtained using transgenic mouse model, allow us to postulate that the local inflammatory response and the consequences on EMILIN-1 structural and regulatory functions could be important events favouring CAC initiation. In an inflammatory colon cancer contest, an unfunctional gC1q domain, as a consequence of degradation by proteolytic enzymes, very likely leads to the loss of EMILIN-1 oncosoppressor properties. Moreover, an EMILIN-1 deficient or mutated protein, favours lymphatic disfunction and metastatic spread that in turn could impair the inflammatory cells drainage with a consequent unresolved inflammation. Avoiding the EMILIN-1 (specifically its gC1q domain) impairment, could represent a novel pharmacological and therapeutic approach: the attempts to block or prevent EMILIN1 degradation could be the basis for a novel ECM strategy aimed to rescue the anti-proliferative properties of EMILIN-1, promote lymphatic function and avoid dysregulation in inflammatory colon cancer.

INTRODUCTION

1. COLORECTAL CANCER (CRC)

Colorectal Cancer (CRC) is one of the three most frequently diagnosed cancers worldwide (**Somayeh *et al.,* 2018)** and one of the major causes of cancer related death **(Tenesa *et al.,* 2009).** In Europe it is the second most common cancer with an overall incidence of 447 per 100.000 (**Arnold *et al.,* 1988**). Less than 25% of CRC cases are hereditary and genetically attributed to familiar history (**Carethers et al., 2105; Rustgi 2007);** most of cases in fact are sporadic (~65%) with any genetic predisposition (**Burt 2007**). About this category of CRCs, ~85% are characterized by a chromosomal instability and the remaining ~15% of sporadic cases present high frequency microsatellite instability phenotypes (**Grady *et al.,* 2014**). The exact etiology for CRC is still unknown, but many are the risk factors implicated in this disease: genetic and environmental factors, specific intestinal commensals and pathogens, food-borne mutagens (**Terzic *et al*., 2010**), changes in lifestyle, such as a diet rich in processed foods or animal fat, decrease of physical activity, obesity (**Watson *et al.*, 2011**) and chronic intestinal inflammation that predisposes the tissue to cancer by inducing gene mutation, inhibiting apoptosis or stimulating angiogenesis and cell proliferation (**Danese *et al.,* 2011**). Patients with Inflammatory Bowel Disease (IBD) have 2- to 3-fold increased risk of developing CRC. In fact, it is reported that there is an association between IBD and the development of CAC: the most important risk factors for CAC are duration, severity and extent of IBD (**Molodecky *et al.,* 2012**).

1.1. INFLAMMATORY BOWEL DISEASE (IBD)

IBDs are chronic relapsing disorders that affect the gastrointestinal tract and are characterized by severe intestinal damage which comprises microbiota influx and barrier disruption, and inflammation (**Neurath 2014**). The pathogenetic process of these diseases is not clear yet but it is presumed that an interaction between a genetically susceptible host, the environmental factors and the intestinal microbiota (both dysbiosis and commensal flora) could be crucial (**Lakatos *et al.,* 2014; Xavier *et al.,* 2007).**

In normal conditions, the maintenance of intestinal epithelium is mediated by intestinal stem cells that undergo differentiation, proliferation and migration from the crypt base along the crypt-villus axis; this mechanism ends with the apoptosis of intestinal epithelial cells. In IBD patients this process is dysregulated, resulting in hyperplasia of inflamed mucosa (**Asquith *et al.,* 2010**).

Crohn's disease (CD) and *Ulcerative colitis* (UC) are the two major forms of IBDs and, although some similar pathophysiological manifestations, they are different and distinct diseases. In fact, in CD inflammation extends in all layers of the bowel, whereas in UC it occurs in the mucosal areas (**Francescone *et al.,* 2015**).

Thanks to genome-wide association studies, 160 loci associated with IBD susceptibility have been identified (**Jostins *et al.,* 2012**), among which some are involved in intestinal immune responses (**Ihara *et al.,* 2017**). Also cytokines play a crucial role during the pathogenesis of IBDs; the imbalance in the release of pro and anti-inflammatory cytokines, typical of the IBD frame, prevents the correct resolution of inflammation, leading to tissue destruction (**Neurath 2014**). Moreover, studies on human patients revealed that UC is driven by the production of Interleukin-13 (IL-13) whereas CD by the production of Interleukin-12 (IL-12) and Interferon-γ (IFN-γ) (**Bouma *et al.,* 2003**).

Taking into consideration that chronic inflammatory response is characterized by persistently activated immune cells, DNA damage and tissue destruction, there is an evident link between chronic inflammation and gastrointestinal cancer (**Danese *et al.,* 2010**). It's widely proven that IBDs predispose to the development of a CRC form, known as CAC and its incidence increases up to 20% depending on the duration of the inflammatory precursor diseases (**Grivennikov 2013**). It is also well known that CD increases the risk of CAC up to ~8% and UC up to ~33% compared to the risk of developing CRC in general and healthy population (**Kim ER *et al.,* 2014**).

1.2. COLITIS-ASSOCIATED CANCER (CAC)

CAC is characterized by poor prognosis and a relatively high mortality rate (~50%) and represents ~2% of all CRC cases (**Munkholm 2003**). This kind of tumor is characterized by an intrinsic connection with chronic inflammation (**Danese *et al.,* 2011**) that is therefore a key factor in CAC development (**Kanneganti *et al.,* 2011**). It has been demonstrated that the inflammation generated from pre-existing IBDs is able to trigger tumorigenesis and promote cancer progression (**Francescone *et al.,***

2015). Moreover, many animal models of CAC provide evidences that some inflammatory mediators play a key role in the initiation and progression of colitis and CAC (**Danese *et al.,* 2010**).

Usually, the gradual development of CAC is represented by the accumulation of mutations during the consequential phases of "inflammation-dysplasia-carcinoma" (**Zisman *et al.,* 2008**). An important role in tumor pathogenesis is played by the tumor microenvironment that is constituted, as reported in Figure 1, by a lot of different cell types including stem cells, endothelial cells, immune cells, mural cells and fibroblasts. All these cells interact together to promote or inhibit tumorigenesis by releasing cytokines and chemokines (**Grivennikov 2013**).

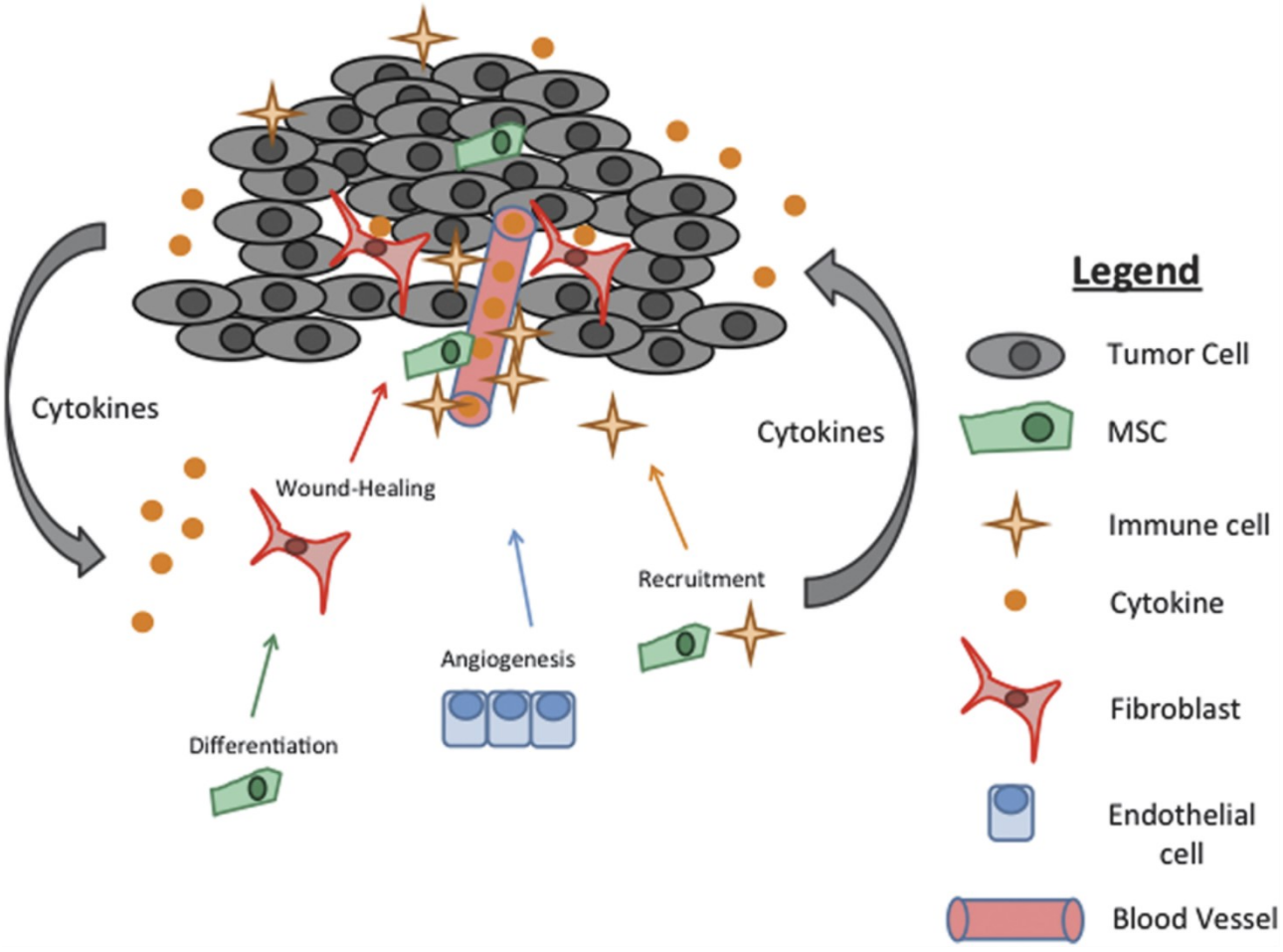

Figure 1: The tumor microenvironment. Tumors are a complex and heterogeneous mixture of various cell types that dynamically interact with each other. Endothelial cells, fibroblasts, stem cells, and immune cells get recruited to and support tumor progression, and cytokines are major drivers of this process. The uneven distribution of the different cell types creates local environments that are dissimilar from one another and can act as niches for certain cell types or program cells differentially. Wound-healing processes seem to promote tumorigenesis, although they are beneficial to damaged epithelia in colitis (from **Francescone *et al.,* 2015**).

Thanks to animal models of CAC, it was possible to study and better understand how and which cytokines are able to drive immune cells in the tumor microenvironment. Tumor Necrosis Factor (TNF-α) is a potent cytokine involved in both inflammation and carcinogenesis and its main source are monocytes/macrophages (**Aggarwal *et al.,* 2012**). Many studies demonstrated that the neutralization of TNF-α protects IBD in mouse models and in patients (**Ford *et al.,* 2011**). Interleukin-6 (IL-6) is a cytokine produced particularly by monocytes/macrophages, B and T lymphocytes and $CD4^+$ cells of IBD patients as well as in experimental colitis models (**Kai et al., 2005**). Moreover, high levels of IL-6 expression are associated to the increased risk to develop colorectal adenomas (**Herbeuval *et al.,* 2004**). Colon carcinogenesis models showed that IL-$6^{-/-}$ mice have a reduced number of tumors compared to the WT counterpart (**Grivennikov *et al.,* 2009**). Dendritic cells and macrophages secreted also the pro-inflammatory cytokine Interleukin-1 (IL-1) into the inflamed mucosal of IBDs after their activation in response to commensal microbiota (**Ng *et al.,* 2011**). Interleukin-10 (IL-10) acts as a regulator factor during IBD pathogenesis; in patients, mutations of this interleukin lead to early and aggressive development of inflammation. IL-$10^{-/-}$ mice developed spontaneous colitis and CAC and, histopathologically, they are characterized by epithelial hyperplasia and inflammatory infiltrates in mucosa and submucosa (**Berg *et al.,* 1996**).

Many evidences support that, besides inflammation itself, another important risk factor that leads to CAC initiation is represented by the inflammation-dependent oxidative stress that occurs as a lack of a balance of the generation and removal of Reactive Oxygen Species (ROS). The oxidative stress induces DNA damage such as single and double strand breaks or nucleotide modification (**Gorrini *et al.,* 2013**). During the duplication of crypts by branching (fission) these DNA changes expand from a crypt to the next one; in this way, some of these changes can induce a clonal expansion of colon epithelial cells with the consequence that a mutation present in one crypt can be found also in other adjacent (**Chen *et al.,* 2005**).

Besides some commensals have a passive role in IBD prevention thanks to their ability to educate immune system and staying in gut niches making them unavailable for pathogen (**Mazmanian *et al.,* 2008**), gut microorganisms also can play an active role in the pathogenesis of both IBDs and CAC for their capacity to induce pro-inflammatory responses (**Round *et al.,* 2009**)**.** In the scenario of IBD and CAC, TLRs play an important role to protect intestinal barrier function and control of microbiota, thus limiting the inflammation damage. Commensal bacteria are recognized by TLRs and this

interaction plays a crucial role in the maintenance of intestinal epithelial homeostasis (**Rakoff-Nahoum *et al.,* 2004).**

1.3. LYMPHANGIOGENESIS and CRC

The lymphatic system plays a crucial role in maintaining tissue homeostasis by returning back, from interstitium to the circulation, of water, plasma proteins and electrolytes (**Olszewski 2003**). Moreover, it transports activated immune cells into draining lymph nodes (LNs), adsorbs fat from the intestine, induces inflammatory immune response and, subsequently, resolves inflammation (**Angeli *et al.,* 2006**). Besides these fundamental functions, lymphatic system is also involved in many pathological processes such as tumor metastasis.

So far, the knowledge on the relationship between LVs and pathological conditions is rather limited, maybe for the fact that only few years ago novel specific antibodies, such as D2-40 (anti podoplanin) and anti LYVE-1 (lymphatic endothelial hyaluronan receptor), were developed and able to significantly increase the accuracy for the identification of LVs (**Sundlisæter *et al.,* 2007**). Little was known about mechanisms through which tumour cells entered into the lymphatic system and the role attributed to LVs was controversial and debated: some authors suggested that LVs had a passive role with tumor cells infiltrating pre-existing peritumoral lymphatics (**Karpanen *et al.,* 2001**); some others have indicated that lymphangiogenesis (formation of new tumor associated lymphatics) played an active role in the metastatic spread (**Hall *et al.,* 2003**).

What we now know is that, in the process of invasion and metastasis, cancer cells migrate nearby LVs and enter lymphatic system to invade distant tissue (**Hanahan *et al.,* 2011**). In this process, LVs provide one of the routes for cancer cells metastasis, especially for tumors of the gastrointestinal tract, breast and lung (**Saharinen *et al.,* 2004).** Moreover, the number and diameter of LVs increase in peritumoral tissues, providing a larger contact area and facilitating tumor cell metastasis. The mechanism through which these LVs born and develop is unclear. Several studies have proposed that it could be regulated by the VEGF-C/VEGF-D/VEGFR-3 pathway and only few indicated that also the ECM is involved (as shown in Figure 2). The VEGF-C/VEGF-D/VEGFR-3 specific signaling pathway is able to trigger lymphangiogenesis, with ligand-receptor binding, stimulating proliferation, survival and migration of lymphatic endothelial cells (LECs) (**Stacker *et al.,* 2001**). In a specific way, VEGF-C disrupts the endothelial lymphatic barrier, promoting CRC invasion and VEGF-D is able to increase

LVs number, lymph flow and vascular leakage (**Saharinen *et al.,* 2004**). There are also evidences in animal tumor models that, blocking the VEGF-C/VEGF-D/VEGFR-3 signaling pathway, the formation of new LVs is inhibited, and the metastasis formation reduced (**Su *et al.,* 2007).** As mentioned before, also the ECM plays an important role in lymphangiogenesis; in fact, interactions that occur between ECM and LVs have crucial consequences for tumor formation, growth and metastasis (**Wiig *et al.,* 2008**). Many are the ligands in the microenvironment (integrins, collagens, fibronectin, tenascin-C and EMILIN-1) that interact with receptors on LVs, affecting normal lymphatic function and lymphangiogenesis (**Tammela et al., 2010**). For example, fibronectin is a ligand for integrin $\alpha_5\beta_1$ and selectively promoted the growth of LEC as compared with vitronectin in the presence of VEGFR-3 (**Zhang *et al.,* 2005**); a study conducted by *Bazigou et al.* (2009) indicated that the deletion of *Itga9* (encoding integrin α9) in mouse embryos leads to the formation of dysplastic lymphatic valve leaflets, with consequent inverted lymphatic flow. Also the lack of EIIIA domain of fibronectin, a ligand for integrin α9, induced similar defects, indicating that LEC interactions with the ECM play a key role in lymphatic valve formation. (**Bazigou *et al.,* 2009**).

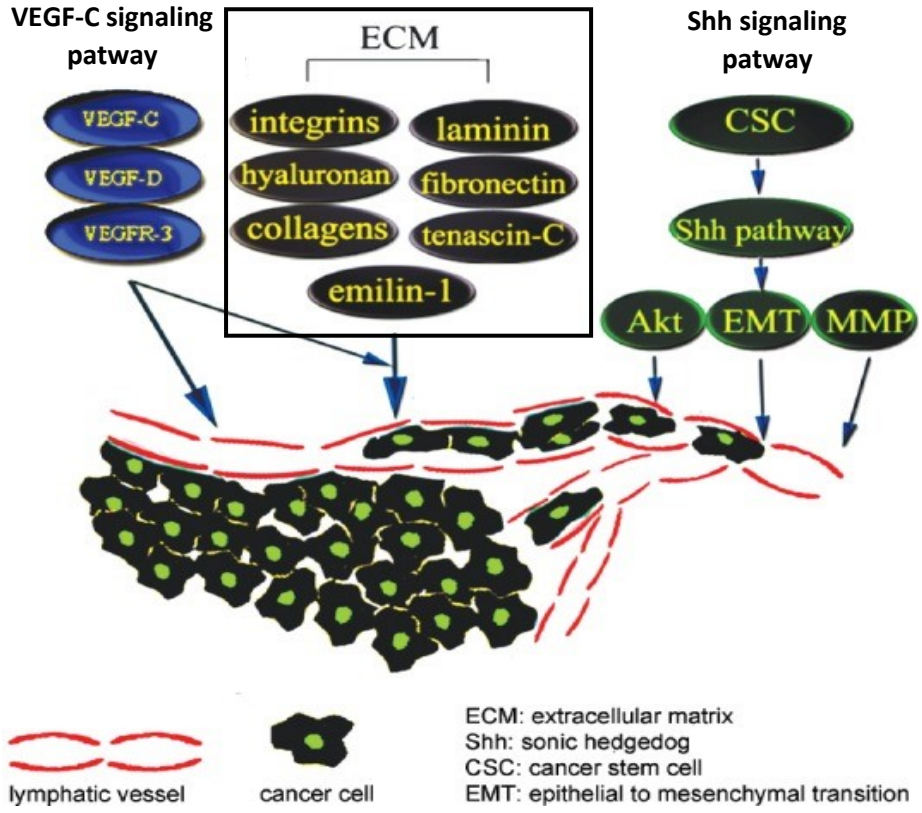

Figure 2: A simplified scheme of the possible mechanism of lymphangiogenesis in cancer cell metastasis. In this multi-factorial and multi-step process, the VEGF-C/VEGF-D/VEGFR-3 pathway, Shh signaling pathway and extracellular matrix have important roles in tumor associated lymphatic sprout formation and cancer cell migration (modified image from **Huang and Chen, 2017**).

2. THE EMILIN/MULTIMERIN PROTEIN FAMILY

EMILINs represent a family of ECM glycoproteins that show high structural similarity **(Colombatti *et al*., 2000; Zanetti *et al*., 2003).** These proteins are characterized by the presence of an N-terminus EMI domain and a C-terminus globular C1q-like domain (gC1q) (**Doliana *et al*., 2000: Mongiat *et al*., 2000).** The EMILIN family includes seven protein members (Figure 3) that can be divided in three groups based on the presence of majors domains **(Braghetta *et al*., 2004);** the first, that comprises proteins with a characteristic domain structure (EMI domain, coiled-coil region and gC1q domain), is the EMILIN group that includes EMILIN-1 (**Colombatti *et al*., 1985**, **Doliana *et al*., 1999**), EMILIN-2 **(Doliana *et al*., 2001)**, MULTIMERIN1 (MNR1) **(Christian *et al*., 2001)** and MULTIMERIN2 (MNR2) **(Hayward *et al*, 1991).** EMILIN3 belongs to the second group and it is similar to members of the first group but differs from the lack of the gC1q C-terminal domain **(Leimester *et al*., 2002).** The last group comprises other two genes, Emu1 and Emu2, that contain the EMI domain but not the gC1q domain and shows a different structure compared to the other members because part of the sequence is collagenous **(Leimeister *et al*, 2002).**

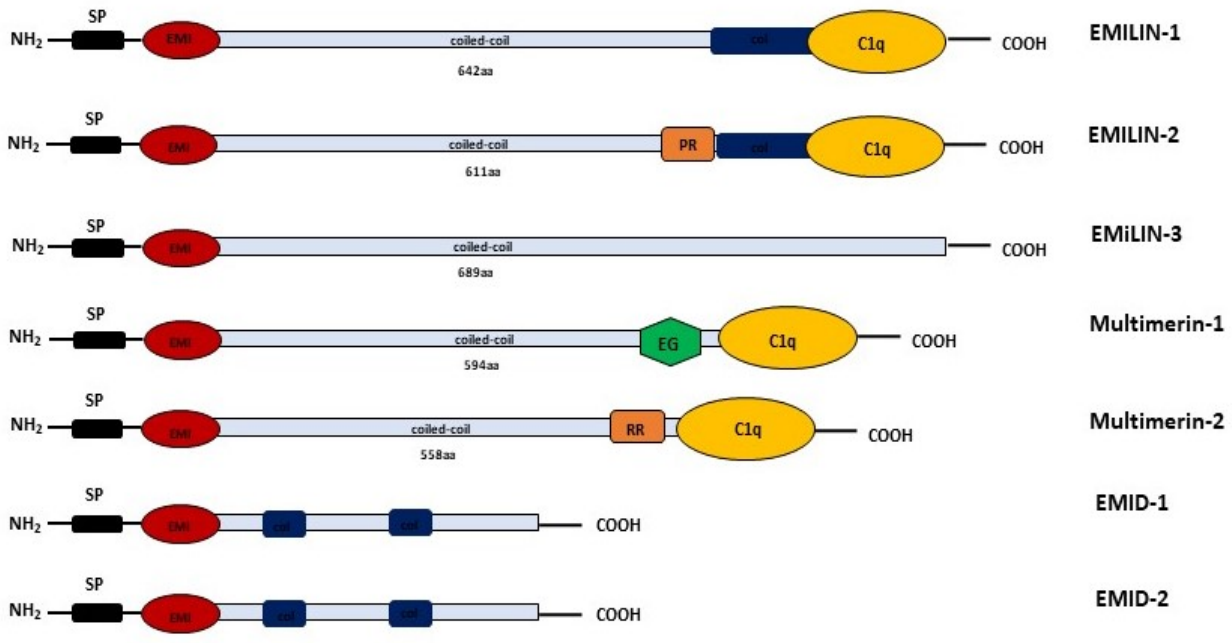

Figure 3: The EMILIN protein family. (C1q) C1q-like C-terminal domain; **(EMI)** EMI N-terminal domain; **(COL)** collagenous domain; **(PR)** prolin-rich domain, **(RR)** arginine-rich domain; **(EG)** region with partial similarity with EGF domain; **(SP)** signal peptide.

2.1. EMILIN-1

2.1.1. Distribution/Expression

EMILIN1 gene maps on human chromosome 2, specifically in positions p23.2 and p23.3 (**Doliana *et al.,* 2000; Colombatti *et al.,* 2000**). The EMILIN-1 protein was the first member of EMILIN family isolated from the heterogeneous fraction of a newborn chick aorta (**Bressan *et al.,* 1983**) and because of its localization between the amorphous elastin surface and microfibrils it was named **E**lastin **M**icrofibril **I**nterface Located Prote**IN 1** (**Bressan *et al.,* 1993**). Highest expression levels of EMILIN-1 protein was found in the wall of large blood vessels, but it was also been detected in the connective tissue of numerous organs (heart, skin, lung, intestine, LNs, skeletal muscle, cornea, kidney) (**Colombatti *et al.*, 1985, Danussi *et al.,* 2008**).

EMILIN1 expression levels were investigated also during mouse development; its mRNA was detected in both morula and blastocyst thanks to RT-PCR analysis. High levels of mRNA were at first expressed in embryonic blood vessels, perineural mesenchyme and somites and then in the mesenchymal component of different organs. At the final stages of gestation, EMILIN1 was found distributed in interstitial connective tissue and in tissues particularly rich of smooth muscle cells. After birth the expression levels decreased with the age (**Braghetta *et al.,* 2002**).

Previous studies demonstrated that EMILIN-1 co-localizes with elastin, suggesting that it might functionally interacts with elastin fibers. After synthesis, the protein is deposited in the ECM as a fine and organized network (Figure 4); it was also found that EMILIN-1 is deposited by fibroblasts grown *in vitro* as a diffuse network (Figure 5).

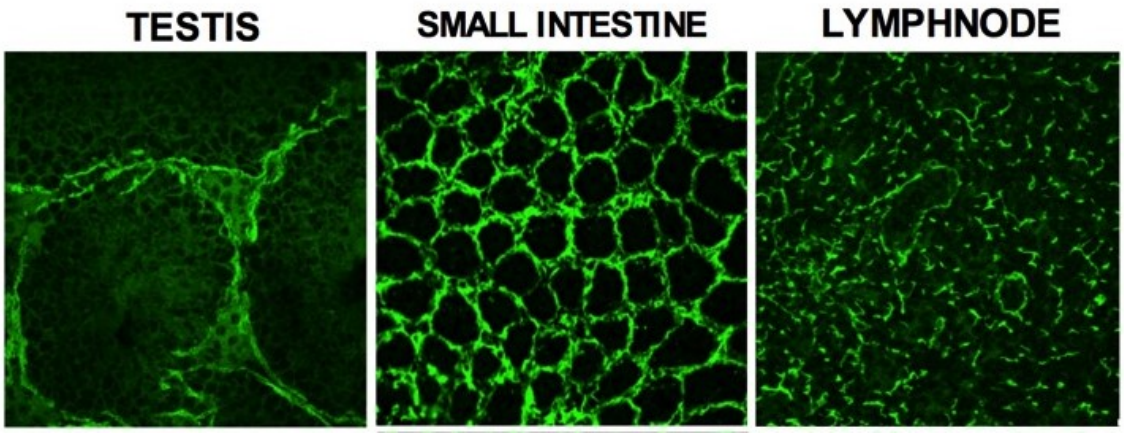

Figure 4: EMILIN-1 expression in mouse tissues. Courtesy by Roberto Doliana.

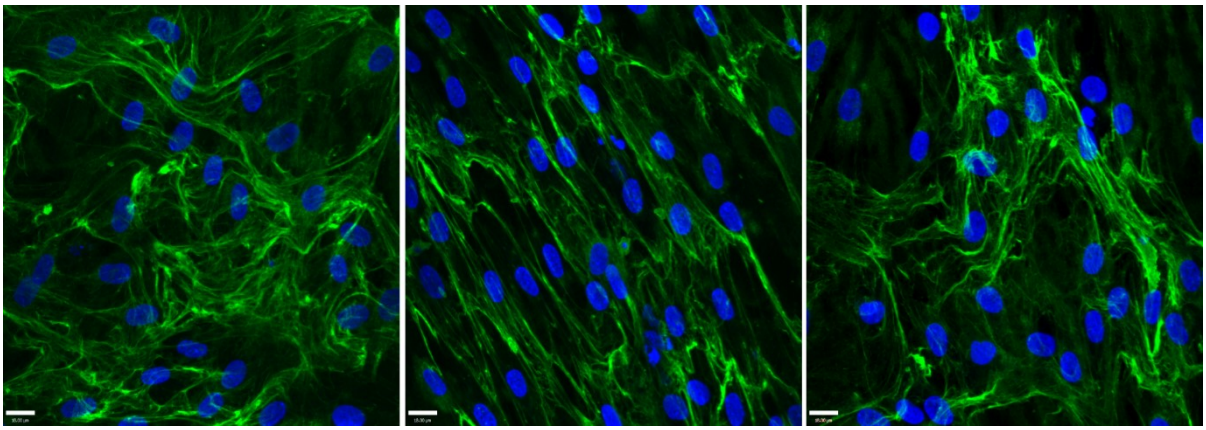

Figure 5: Deposition of EMILIN-1 by human skin fibroblasts (after 10 days of culture). Courtesy by Paola Spessotto.

Gene Expression analysis indicated the presence of EMILIN1 mRNA in human placenta tissue (**Chen *et al.,* 2003**). Subsequent in vitro studies confirmed that stromal cells of decidua represent the main source of EMILIN-1 in this kind of tissue (**Spessotto et al., 2006**).

Thanks to a comparative microarray analysis of gene expression profile of Lymphatic Endothelial Cells (LECs) and Blood Endothelial Cells (BECs) it was also demonstrated that EMILIN-1 is abundantly expressed by LECs (**Podgrabinska *et al.,* 2002**).

2.1.2. Structure

The mature form of EMILIN-1 correspond to a glycoprotein with a modular architecture consisting of 995 amino acids. The N-terminal EMI domain is characterized by a sequence of ~80 amino acids in which seven cysteine residues are included. Moreover, also the spatial organization of this domain is different in comparison to other domains such as the Epidermal Growth Factor (EGF) domain, representing a specific feature of this sequence (**Doliana *et al.,* 2000**).

A region made of 650/700 amino acids with high probability for a coiled-coil structure, is located in the central part of the molecule. Between the coiled-coil region and the C-terminal gC1q domain, EMILIN-1 has a region of 91 residues containing two sequences similar to leucine zippers. Close to these leucine repeats there is a collagenous stalk that is composed of 17 GXY triplets (**Colombatti *et al.,* 2000**).

The C-terminal region of the protein is represented by the gC1q domain, that is constituted by 151 amino acids (mostly hydrophobic); it is highly conserved and is has a great homology with the C1q subunit of the complement. The importance of this peculiar domain is due to its role in the whole protein homotrimerization (**Mongiat *et al.,* 2000, Colombatti *et al.,* 2000, Verdone *et al.,* 2008**) and to its interaction with $\alpha_4\beta_1$ and $\alpha_9\beta_1$ integrins that leads to cell adhesion and migration and to the regulation of cell proliferation (**Spessotto *et al.,* 2003 and 2006; Danussi *et al.,* 2011 and 2013, Capuano *et al.,* 2018**).

2.1.3. Functions

As represented in Figure 6, the multi-domain protein EMILIN-1 is involved in several biological processes. Whereas the role of the coiled-coil region has not been elucidated yet, for the whole structure, because of its association with elastic fibers and microfibrils in blood vessels, it has been demonstrated that it's implicated in elastogenesis and maintenance of vascular cell morphology (**Zanetti *et al.,* 2004**). EMILIN-1 regulates structure and functions of LVs: EMILIN1 deficiency causes hyperplasia, enlargement and irregular pattern of superficial and visceral LVs (**Danussi *et al.,* 2008 and 2013**). Lymphatic vascular morphological alterations in *E1*$^{-/-}$ mice are, accordingly, accompanied by functional defects, such as mild lymphedema, a highly significant drop in lymph drainage, and enhanced lymph leakage (**Danussi *et al.,* 2008; Pivetta *et al.,* 2016**). Very recently, we have demonstrated that the domain responsible for the regulation of lymphatic functions is represented by the C-terminus gC1q (see results section of this thesis and **Capuano *et al.,* in press**).

An important function, related to its EMI domain, is the control of blood pressure: *Emilin1* deficient animals display a hypertensive phenotype characterized by decreased diameter of arteries and elevated systemic blood pressure compared to *E1*$^{+/+}$ mice (**Zacchigna *et al.,* 2006**). The capacity of EMILIN-1 to exert a Transforming Growth Factor-β (TGF-β) antagonist role, binding the pro TGF-β form and thus inhibiting its maturation by furin convertases, is at the basis of this mechanism. In the absence of *Emilin1*, as occurs in *E1*$^{-/-}$ mice, the levels of TGF-β increased reducing, as a consequence, blood pressure levels (**Raman *et al.,* 2006**; **Zacchigna *et al.,* 2006**). This mechanism has represented a novel link between an ECM molecule and TGF-β in the field of blood vessels homeostasis.

Furthermore, through its globular gC1q domain, EMILIN-1 is involved in the regulation of its homotrimerization process (**Mongiat *et al.,* 2000**), skin homeostasis and carcinogenesis (**Danussi et**

***al.,* 2011 and 2012**). The interaction with $\alpha_4\beta_1$ or with the very homologous $\alpha_9\beta_1$ integrin mediates cell adhesion and migration (**Spessotto *et al.,* 2003 and 2006; Danussi *et al.,* 2011; Verdone *et al.,* 2008**). Specifically, the interaction that occurs with $\alpha_4\beta_1$ is particularly efficient because low ligand concentrations provide very strong adhesion (**Spessotto *et al.,* 2003**) and migration (**Spessotto et *al.,* 2006**). Notably, despite a large body of evidence demonstrating that signals generated by ligand-activated integrin are in general pro-proliferative, the binding between gC1q domain and integrin reduces cell proliferation (**Danussi *et al., 2011*).**

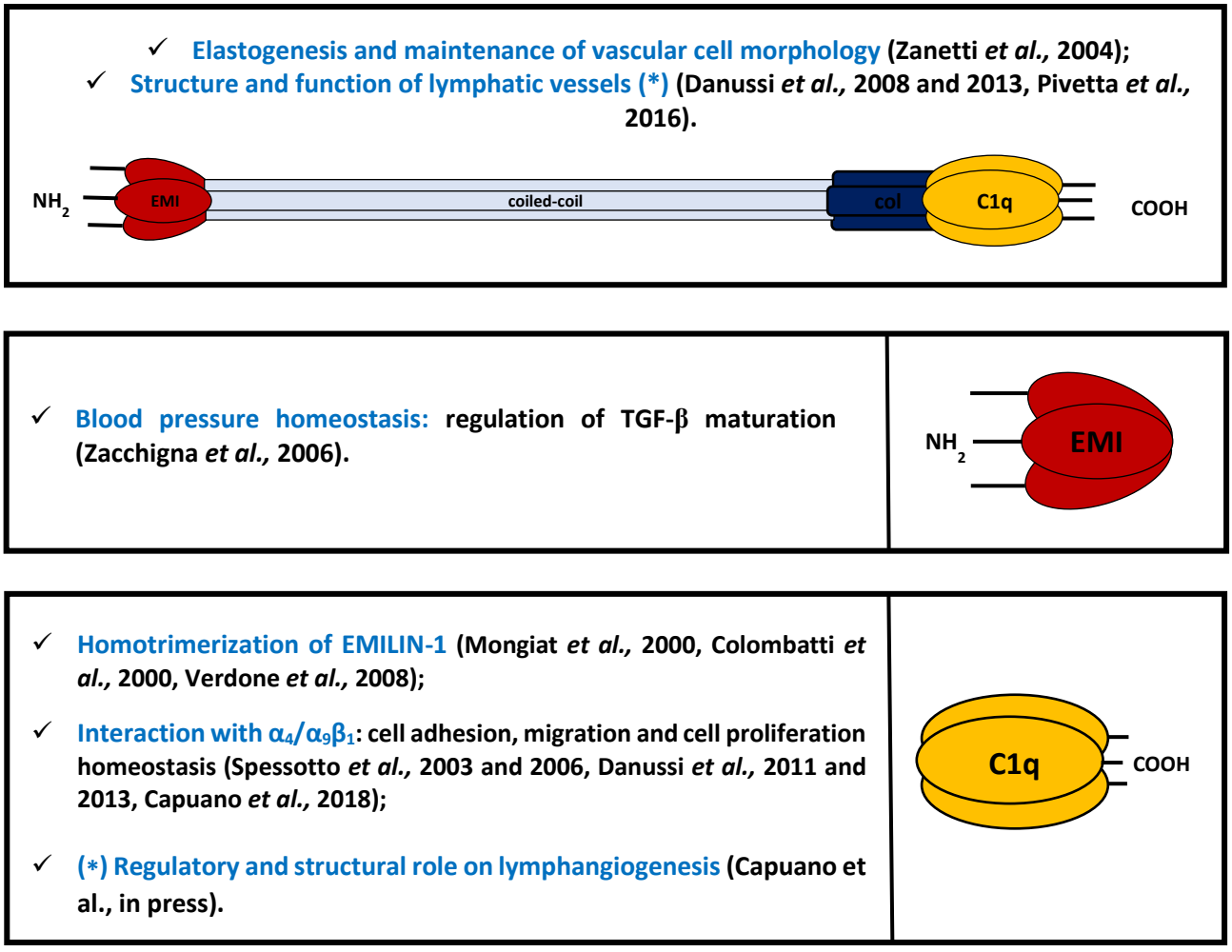

Figure 6: Scheme of EMILIN-1 structure and function profile. EMILIN-1 is represented in the peculiar trimeric organization; biological properties are schematically reported in association with the respective involved domains. **(C1q)** C1q-like domain; **(EMI)** EMI domain; **(COL)** collagenous domain; **(*)** until recently, it seemed that the whole molecule was responsible for the properties played in the lymphatic system; our very recent study (**Capuano *et al;* in press**) demonstrates that this function is carried out by the C-terminal gC1q domain.

2.1.4. EMILIN-1 *and lymphatic system*

The lymphatic system is fundamental for the maintenance of tissue fluid homeostasis, gastrointestinal lipid absorption, and immune trafficking (**Jiang *et al.,* 2018**). As reported in Figure 7, it is composed by branched network of lymphatic capillaries and ducts that are responsible of the lymph uptake from the tissue interstitium and by collecting vessels, which transport the lymph back to the vascular blood system. Lymphatic vasculature, unlike the blood one, is composed by blind-ended vessels, supported by a single layer of LECs that are directly connected to the ECM through elastic anchoring filaments (AFs) that are essential to prevent vessel collapse under conditions of increased interstitial pressure (**Gerli *et al.,* 1991**). Starting from lymphatic capillaries, the lymph is first drained into pre-collecting LVs, which consists of a series of functional units, named lymphangions, separated by intraluminal valves, that are responsible for guaranteeing unidirectional lymph flow (**Schulte-Merker *et al.,* 2011**).

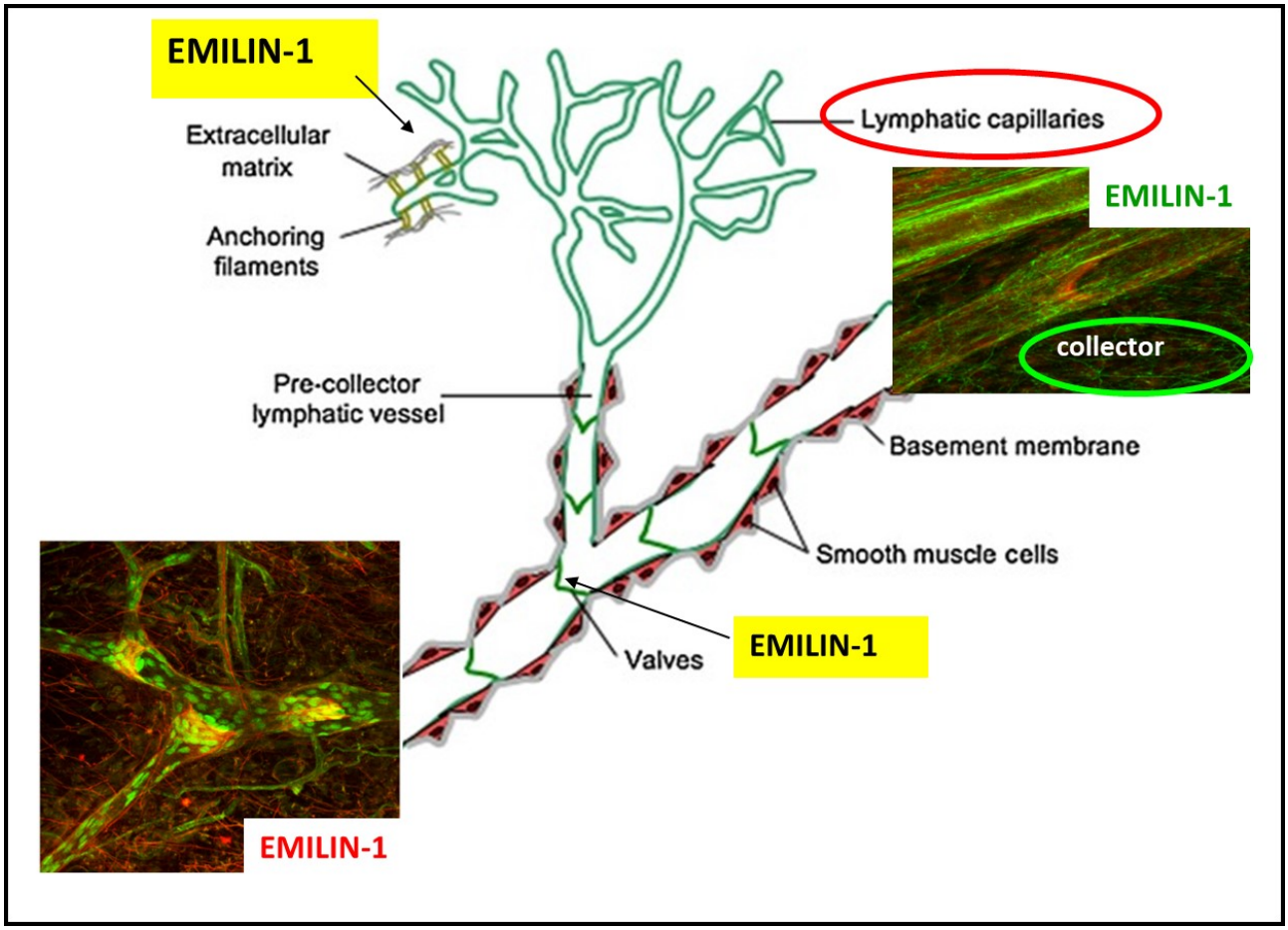

Figure 7: Lymphatic system composition. Schematic representation of the lymphatic system; lymphatic capillaries drained lymph in pre-collector vessels and then in collecting vessels in which the lymph flow is maintained unidirectional by the presence of lymphatic valves. The localization of EMILIN-1 in lymphatic capillaries and collectors is indicated by arrows. The immunofluorescence images are modifications from **Danussi *et al.,* 2013**.

It is well established that LVs have a central role in the regulation of tissue homeostasis and are important regulators of immunity and inflammation (**Kim H *et al.,* 2014**). Recently, different research groups demonstrated that LECs are implicated not only in the transport of leukocyte and antigens from tissues to LNs, but also in the direct control of the traffic of immune cells, thus promoting peripheral tolerance and eliminating inflammatory regulators (**Aebischer *et al.,* 2014; Dieterich *et al.,* 2017**). Accordingly, LVs are essentials for the correct function of several tissues: dysfunctions that affect lymphatics bring to a vast array of consequences as lymphedema, persistent inflammation and fibrosis (**Piller *et al.,* 1990; Alitalo *et al.,* 2005**). These alterations are closely related with the ECM, that can play an active regulatory role. For this reason and for the fact that the real implications in this contest have not been elucidated yet, understanding how ECM molecules influence LEC functions is fundamental to clarify how lymphangiogenesis occurs and takes part to local lymph drainage in disordered tissues. EMILIN-1 is not only involved in the regulation of blood vasculature but, also in the maintenance of LVs integrity. As demonstrated by *Danussi et al.,* in 2008, *Emilin1* deficiency results in hyperplasia and enlargement of the superficial and visceral LVs which display an irregular pattern. Strong evidences show that EMILIN-1 is a component of AFs, indicating a structural role of the protein probably exerted by the whole molecule; in fact, *E1*$^{-/-}$ mice have a significant reduction in the number of AFs and abnormal over-lapping intercellular junction. An absence of EMILIN-1 causes defective ECM anchorage of LECs, dilation of lumen of LVs and variation in interstitial pressure (**Danussi *et al.,* 2008**). Few years ago, through a post-surgical tail lymphedema model, *Pivetta et al.,* demonstrated that the acute phase of acquired lymphedema was correlated to EMILIN-1 degradation by neutrophil elastase (NE) released by neutrophils during the early phases of inflammation after tail surgery. As a consequence, the intercellular junctions of LECs appeared weakened with a compromised lymph drainage; the administration of Sivelestat, a specific inhibitor of NE, prevented the degradation with a consequent reduced lymphedema. These results lead to establish that EMILIN-1 is an important structural element and that its integrity is indispensable to guarantee a proper functionality of the LEC intercellular junctions (**Pivetta *et al.,* 2016**). EMILIN-1 gC1q domain is implicated in the regulation of many functions through the interaction with $\alpha_4\beta_1$ and $\alpha_9\beta_1$ integrins (**Spessotto *et al.,* 2003; Danussi *et al.,* 2011; Maiorani *et al.,* 2017**) and it has been proposed as the domain responsible for the lymphangiogenic role (**Danussi *et al.,* 2008 and 2013, Pivetta *et al.,* 2016**) played by EMILIN-1. Only very recently we demonstrated that the interaction with the integrin is absolutely necessary to obtain a biological response to drive lymphangiogenesis (**Capuano *et al.,* in press**).

3. PECULIARITY OF THE gC1q DOMAIN

3.1. "STRUCTURAL" ASPECTS OF THE gC1q DOMAIN

The gC1q domain has been found in a variety of proteins clustered in the C1q-TNF (Tumor Necrosis Factor) superfamily. It is characterized by a highly conserved conformation of ~150 amino acids that are assembled in trimers (**Kishore *et al,* 2004; Innamorati *et al*, 2006**).

The peculiar C-terminal EMILIN1 gC1q domain presents strong homology to the other domains belonging to the C1q/TNF family; in fact, its aminoacidic sequence shows high level of conservation of some hydrophobic and aromatic residues. A first prediction of EMILIN-1 C1q domain goes back in 1999 when *Doliana et al.* obtained a 3-D structure comparing the molecule with other members of the superfamily. In 2008 and 2009, *Verdone et al.* determined a more accurate 3-D solution structure of the gC1q; the results confirmed the peculiar gC1q spatial conformation that is characterized by two antiparallel β-sheets arranged in a jelly roll topology (Figure 8). This study demonstrated that in solution the recombinant EMILIN1 gC1q domain looks like a stable trimeric protein formed by three identical polypeptide chains of 150 amino acids with a whole molecular mass of 51.624 KDa (**Verdone *et al.,* 2008 and 2009**).

So far, the reduction to nine, rather than ten, of the number of antiparallel strands (A, A', B', B, C, D, E, G, H) and also the presence of an unstructured loop spanning from Y927 to G945 represent the most pertinent changes between EMILIN-1 gC1q domain and other gC1q domain crystal structures (Figure 6 A and B). Specifically, the unstructured loop is located at the apex of each monomer of the trimer and is followed by the "molten strand F" that is an interfacial sequence without any secondary classification (**Verdone *et al.,* 2008**). Furthermore, it is highly dynamic and accessible to solvent, with a number of 10-11 residues protruding from the main globular structure that make this region a good candidate for hosting an interaction site (**Colombatti *et al.,* 2011**). As already mentioned, the gC1q domain is responsible of the self-assembly (trimerization) of the whole protein. This characteristic property was first investigated with the use of two hybrid system and then by other successive biochemical analyses that excluded the involvement of the disulfide bond (**Mongiat *et al.,* 2000**).

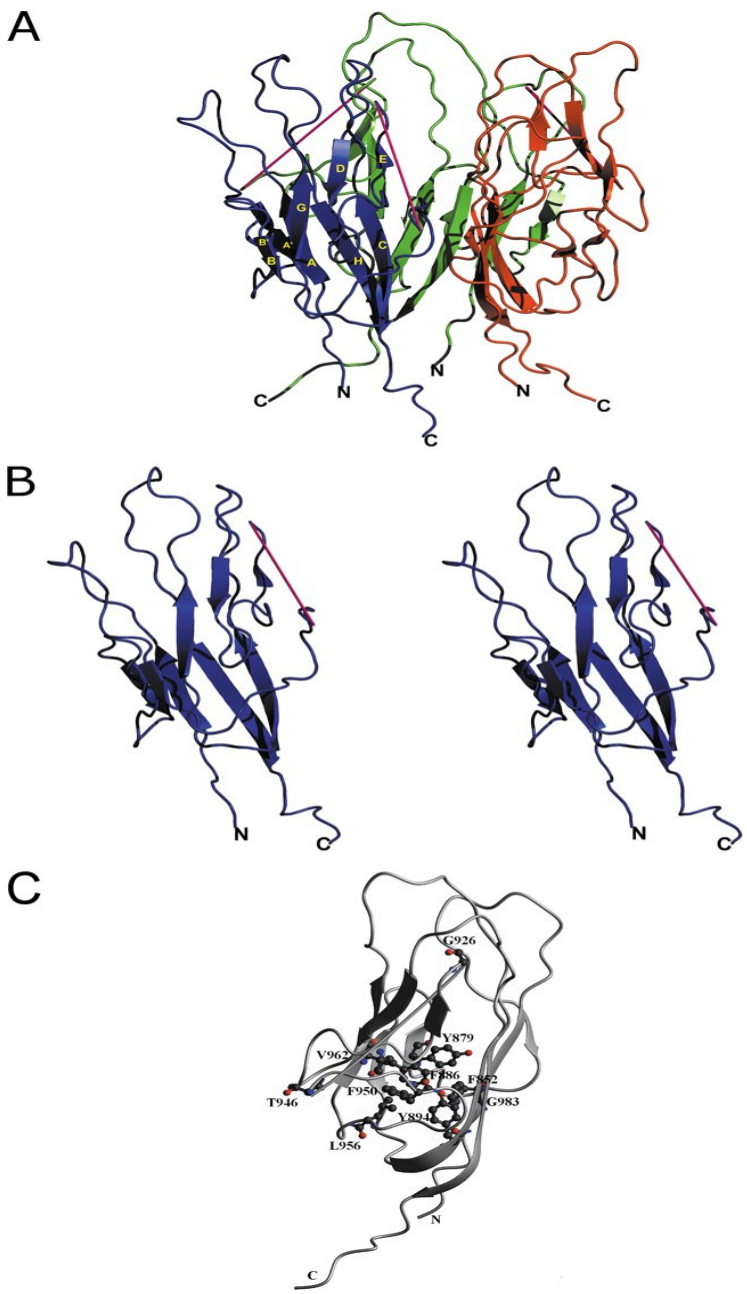

Figure 8: Structure of the homotrimeric EMILIN1 gC1q domain in solution. Structure of the homotrimeric EMILIN1 gC1q domain as obtained by homology model refinement with Residual Dipolar Coupling (RDC). A ribbon representation of the assembly, as side view, is presented in panel **A**. The three protomers in the trimer are shown in different colours (red, blue, and green). Each monomer has a nine-stranded folding topology represented in **B** as stereoview. β-Strands are labelled according to the C1q/tumour necrosis factor superfamily nomenclature. The location of the unstructured segment Tyr927–Gly945 is highlighted in magenta (in **A** and **B**). **C** shows the amino acids forming the monomer hydrophobic core (from **Verdone *et al.*, 2008**).

3.2. $\alpha_4\beta_1$ AND $\alpha_9\beta_1$ INTEGRIN RECEPTORS

Integrins are receptors belonging to a family of 24 transmembrane αβ heterodimers glycoproteins involved in cell-cell and cell-ECM interactions. Mammals express 18 α and 8 β subunits forming distinct αβ integrin dimers (**Shimaoka *et al.,* 2003).** Integrins α_4 and α_9 present a high homology grade: they share 39% amino acid identity. Both engage the β_1 subunit and exert distinct as well similar functions in vivo (**Palmer *et al.,* 1993**).

The **$\alpha_4\beta_1$ integrin** (Very Late Activating Antigen - VLA) is a heterodimer composed by the α_4 (155 kDa) and β_1 (150 kDa) subunits. The α_4 subunits is encoded by the Integrin Subunit Alpha 4 (ITGA4) gene and expressed on circulating leukocytes (**Lobb *et al.,* 1994**), differentiated smooth muscle cells of blood vessel (**Duplaa´ *et al.,* 1997**), epicardial progenitor cells (**Pinco *et al.,* 2002**) and also tumor cells (**Qian *et al.,* 1994**). There are a lot of studies showing that $\alpha_4\beta_1$ integrin binds to the cell adhesion molecule VCAM-1, the CS-1 and CS-5 alternatively spliced domains of the ECM protein fibronectin (**You *et al.,* 2002; Yang *et al*, 2003**), fibrinogen, Von Willebrand factor and EMILIN-1 gC1q domain (**Spessotto *et al.,* 2003**). Differently from many other integrins, that bind Arginin-Glycin-Aspartic acid (RGD) sequence, it recognizes ligand in an RGD independent manner. $\alpha_4\beta_1$ integrin plays important roles during different processes, such as hematopoiesis, myogenesis, lymphopoiesis, cardiac development embryogenesis and, most importantly, in immune response. In fact, it has a prominent role in the pathogenesis of chronic inflammatory response of different disease conditions such as colitis, diabetes, encephalomyelitis, transplant reaction, psoriasis and asthma (**Masumoto *et al*, 1993; Yusuf-Makagiansar *et al*, 2002**).

The **$\alpha_9\beta_1$ integrin** is another member of the VLA integrins subfamily that in humans is encoded by the Integrin Subunit Alpha 9 (ITGA9) gene. It mediates cell adhesion and migration thanks to the recognition of various ligands in the ECM (including Tenascin-C, osteopontin, VCAM-1, Extra Domain A Fibronectin (EDA), EMILIN-1) and VEGF-C and D (**Smith *et al.,* 1996; Stepp *et al.,* 1997; Taooka *et al.,* 1999; Danussi *et al.,* 2011 and 2013**). Also for $\alpha_9\beta_1$, the binding is independent from the RGD sequence. It is particularly expressed in cardiac and skeletal muscles, hepatocytes, visceral smooth muscle, squamous epithelium and airway epithelium (**Palmer *et al.,* 1993).**

3.3. INTERACTION BETWEEN gC1q and INTEGRIN RECEPTOR

In general, all polypeptides that interact with integrins present aspartic or glutamic residues localized in loops that protrudes from the core of the ligand (**Leahy *et al.,* 1996**). Both of them are pivotal residues for integrin recognition. In 2008, by site-direct mutagenesis experiments focused on the unstructured loop located at the apex of the gC1q homotrimer, *Verdone et al.,* demonstrated that the glutamic residue at the position 933 (E933) represents the site of interaction between gC1q and $\alpha_4\beta_1$ integrin. The introduction of a single amino acid mutation to substitute the glutamic acid (E933) with an alanine (E933A) prevented the normal native conformation; all the other tested mutations around the E933 region were unable to impair integrin recognition, confirming that the interaction between EMILIN-1 gC1q domain and $\alpha_4\beta_1$ integrin is exclusively due to glutamic residue present in that region. As a functional point of view, the E933A mutation totally impaired cell adhesion (**Verdone *et al.,* 2008**).

An interesting question is: "How does a homo-trimeric molecule such as EMILIN-1 gC1q domain mechanistically interact with $\alpha_4\beta_1$ integrin?" Considering its homo-trimeric nature, there are three putative binding sites (three E933 residues) for the engagement of integrins. Thus, there are two possible patterns of interaction: the first is that only one single E933 acid residue located in the disorder loop of a monomer is enough to bind $\alpha_4\beta_1$ integrin; the second is that all three E933 residues are indispensable to interact with a single integrin molecule.

A very recent study demonstrated that the E933A substitution in just one of the three monomers that form the gC1q domain is sufficient to completely inhibit the $\alpha_4\beta_1$ mediated cell adhesion (**Capuano *et al.,* 2018**). These results allow to affirm that the engagement of $\alpha_4\beta_1$ integrin is strictly dependent on the simultaneous presence of the E933 residues in all the three monomers (Figure 9). Furthermore, and more importantly, this binding mode is very peculiar because for the very first time an integrin binding site is located on a homotrimeric assembly**.** This novel interaction mode reflects differences also in functional properties exerted by $\alpha_4\beta_1$/gC1q (and even if not directly demonstrated also for $\alpha_9\beta_1$) interaction. It has been proven that gC1q binding leads to stronger and prolonged cell adhesion unlike other specific $\alpha_4\beta_1$ ligand such as CS1 (**Capuano *et al.,* 2018**).

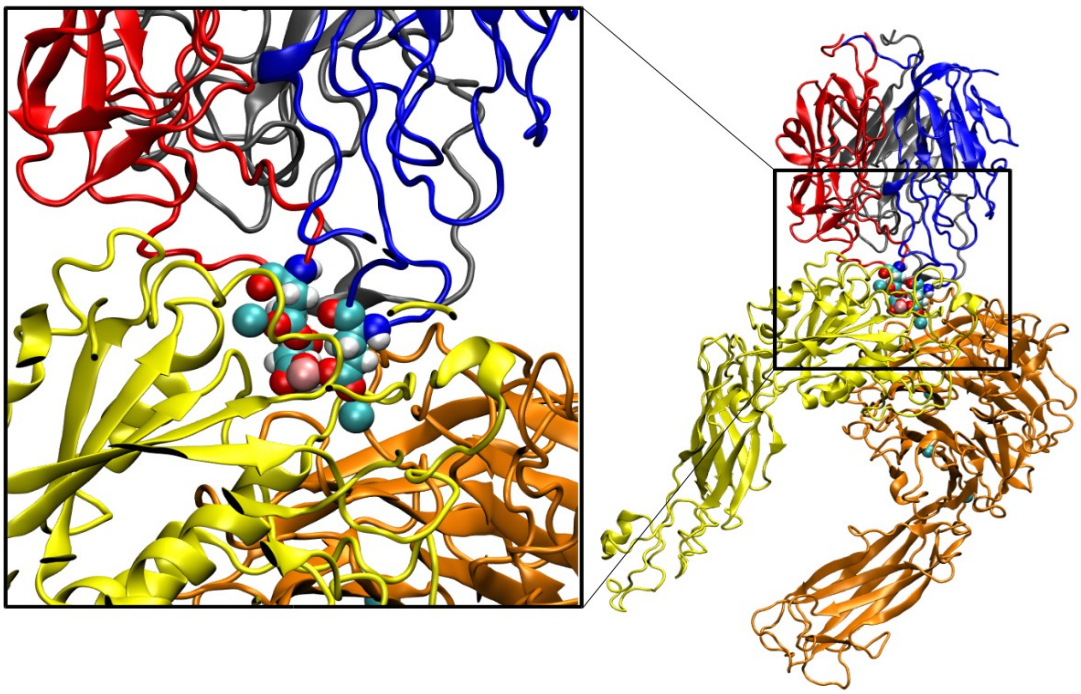

Figure 9: Modeling of the interaction between the $\alpha_4\beta_1$ integrin and the gC1q homotrimer. Complex of the gC1q homotrimer and integrin $\alpha_4\beta_1$. EMILIN1 gC1q chains are displayed in grey, red and blue. Integrin is displayed in yellow (β_1) and orange (α_4). The Mg^{2+} ion is shown in pink and Ca^{2+} ions coordinated by $\alpha_4\beta_1$ integrin chain are shown in light blue. E933 in the EMILIN gC1q domain are shown as van der Waals sphere (from **Capuano *et al.*, 2018**).

3.3.1. Functional consequences of gC1q/$\alpha_4\beta_1$ interaction

Cell adhesion: whereas the binding of integrins $\alpha_5\beta_1$ or $\alpha v\beta_3$ to fibronectin and vitronectin leads to cytoskeletal reorganization (**Campbell 2008**), the interactions with $\alpha_4\beta_1$ integrin drive only the initial and intermediate stages of cell adhesion (such as attachment and spreading), whereas focal adhesion and stress fiber formation, characterizing strong cell adhesion, are rarely observed (**Iida *et al.*, 1995**). EMILIN-1 is the only member of C1q/TNF superfamily able to mediate $\alpha_4\beta_1$ dependent cell adhesion through its gC1q domain (**Spessotto *et al*, 2003 and 2006**). These adhesive properties were demonstrated for the EMILIN-1 gC1q domain using blocking antibodies direct against different epitopes of the protein. Interestingly and differently from the general behavior of other ligands, the interaction between $\alpha_4\beta_1$ and EMILIN-1 gC1q is particularly efficient because even very low concentrations of gC1q provide very strong adhesion. On the other hand, accordingly to an α_4-mediated adhesion model, the distribution pattern of actin and paxillin of cells adhering to EMILIN1

leads to an accumulation of ruffles-inducing signals and a lack of stress fiber formation (**Spessotto *et al.*, 2003**).

Cell migration: there are a lot of cell types able to migrate toward EMILIN-1 using the $\alpha_4\beta_1$ integrin and among these, the trophoblast cells are particularly interesting. In fact, in a study based on both *ex vivo* and *in vitro* cellular model of trophoblast cells, it was demonstrated that EMILIN-1 played an important role in the promotion of extravillous trophoblast migration and invasion in the maternal decidua (**Spessotto *et al.*, 2006**). An *in vitro* study demonstrated that the ability of LECs to adhere and migrate on EMILIN1 was regulated by $\alpha_9\beta_1$ integrin (**Danussi *et al.*, 2013**).

Cell proliferation: *Danussi et al.* demonstrated that the interaction between gC1q and α_4 or $\alpha_9\beta_1$ integrins was able to down-regulate cell proliferation; the deficiency of *Emilin1* gene, and so the absence of the interaction with the integrin, induced both dermal and epidermal hyperproliferation and an increase of skin thickness. These effects were due to a reduction of PTEN phosphatase and a consequently strong up-regulation of pErk1/2. The mechanism by which EMILIN-1 exerts this anti-proliferative property is specific and well defined (Figure 10); the presence of mature TGF-β triggers cytostatic signal pathways through pSmad2 (Ser465/467) activation and modulates PI3K/Akt signaling by regulating PTEN expression. EMILIN-1, binding to $\alpha_4/\alpha_9\beta_1$ integrins expressed on dermal fibroblast and basal keratinocytes, empowers the down-regulation of proliferative cues induced by TGF-β. This effect is mediated by $\alpha_4/\alpha_9\beta_1$-dependent PTEN activation and inhibition of pErk1/2 pro-proliferative activity (**Danussi *et al.*, 2011**).

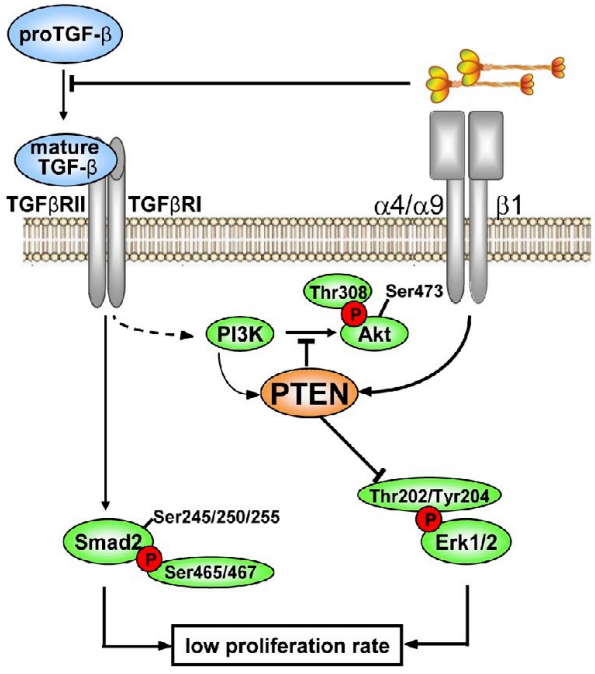

Figure 10: Proposed model for the regulatory role of EMILIN-1 in skin homeostasis. (modified from **Danussi *et al.*, 2011**).

AIM OF THE STUDY

CAC is a CRC subtype characterized by a poor prognosis and a relatively high mortality (**Feagins *et al.,* 2009**). Chronic inflammation plays a role at all stages of tumorigenesis (**Itzkowitz *et al.,* 2004**): it generates genotoxic stress during cancer initiation, induces cellular proliferation, tissue repair and secretion and deposition of ECM molecules in cancer promotion and finally enhances angiogenesis and tissue invasion during cancer progression (**Grivennikov *et al.,* 2010; Francescone *et al.,* 2015**). Striking changes in the lymphatic vasculature are associated with inflammation (**Alitalo *et al.,* 2005**) and alterations of lymphatics lead to a vast array of consequences, such as the persistence of the inflammatory process (**Piller *et al.,* 1990**). It is well-established that intestinal lymphatic network displays dysfunction in both human and experimental IBD (**Vetrano *et al.,* 2010**). In this context the stabilizing and regulatory role of ECM on LVs is poorly taken into consideration; moreover, tissue responses to the interplay between local inflammation, lymphangiogenesis and ECM remodeling in CAC are slightly understood. The ECM glycoprotein EMILIN-1 interacts with $\alpha_4\beta_1$ (**Spessotto *et al.,* 2003**) and $\alpha_9\beta_1$ integrins (**Danussi *et al.,* 2011 and 2013**) via its C-terminus gC1q domain, promotes cell adhesion and migration (**Spessotto *et al.,* 2003**) and provides an ECM cue for a correct homeostatic skin proliferation, playing an important suppressor role in tumour growth (**Danussi *et al.,* 2011 and 2012**). Furthermore, EMILIN-1 plays a direct role in growth and maintenance of LVs and its integrity is necessary to assure stability of LEC junctions (**Pivetta *et al.,* 2016**).

All these evidences allow us to propose EMILIN-1 as a structural regulator for a competent vasculature. Moreover, by its multifaceted functions, it could be centrally located in the context of the development and progression of inflammatory colon cancer. All these considerations lead us to:

- investigate and confirm the antiproliferative role of EMILIN-1/$\alpha_4\beta_1$ integrin interaction in a two steps AOM/DSS colon carcinogenesis mouse model;
- demonstrate that EMILIN-1 is crucial for the establishment of a functional lymphatic vasculature and determine if the aberrant lymphangiogenesis is only driven by DSS-induced inflammation or if lymphatic dysfunction could drive disease.

RESULTS

1. CHARACTERIZATION OF THE *E1*$^{-/-}$/E1-E933A TRANSGENIC MOUSE MODEL

1.1. Generation of the *E1*$^{-/-}$/E1-E933A transgenic mouse model

In order to understand the role exerted exclusively by the EMILIN-1 gC1q domain, separating the effects due to the regulation of TGF-β by the EMI domain, a transgenic mouse model expressing an E933A mutated human EMILIN-1, unable to be engaged by $\alpha_4\beta_1/\alpha_9\beta_1$ integrins, was generated (**Verdone *et al.*, 2008; Capuano *et al.*, 2018 in press**).

The specific construct used for the generation of transgenic lines is sketched in Figure 11 A; among the several different transgenic lines generated, two (G and P lines, Figure 11 B) were selected for their mRNA levels which corresponded to the half (G line) or close (P line) to those of the endogenous *EMILIN-1* (Figure 11 B). Founders expressing the E933A transgenic selected lines were then matched with the *Emilin1*$^{-/-}$ line, in order to obtain littermates expressing only the mutated EMILIN-1 in an *Emilin1* null background (thereafter *E1*$^{-/-}$/E1-E933A), and animals expressing both the endogenous murine wild type (*E1*$^{+/+}$) *EMILIN-1* and mutated human EMILIN-1.

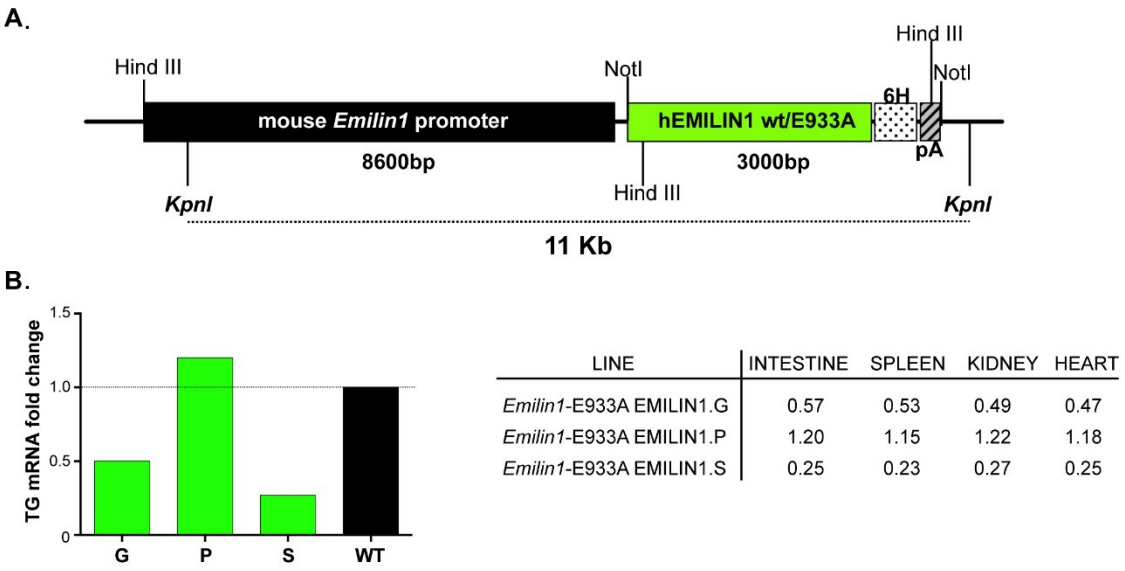

LINE	INTESTINE	SPLEEN	KIDNEY	HEART
Emilin1-E933A EMILIN1.G	0.57	0.53	0.49	0.47
Emilin1-E933A EMILIN1.P	1.20	1.15	1.22	1.18
Emilin1-E933A EMILIN1.S	0.25	0.23	0.27	0.25

Figure 11: Generation of E1-E933A mouse. (A) Construct used for the generation of *Emilin1*-E933A EMILIN1 transgenic mice. The construct is the fusion of mouse *Emilin1* promoter and human EMILIN1 cDNA. 6H, 6-histidines tag. pA, SV40 polyadenylation signal. **(B)** Transgene mRNA expression levels in different mouse lines. On the right, table indicating the relative amounts of transgene mRNAs expressed as fold change to the expression of one chromosomal gene copy.

1.2. Tissue expression and adhesive properties of E933A-EMILIN1 protein

To evaluate the tissue-specific expression and the distribution pattern of the transgene coding for the mutated EMILIN-1, immunofluorescence staining was performed in an *Emilin1*$^{-/-}$ background.

As reported in Figure 12 the transgenic protein deposition reproduced very nicely the pattern of the endogenous *EMILIN-1* in several tissues and organs: a similar network organization was in fact detected in *E1*$^{+/+}$ as well as in *E1*$^{-/-}$/E1-E933A mice.

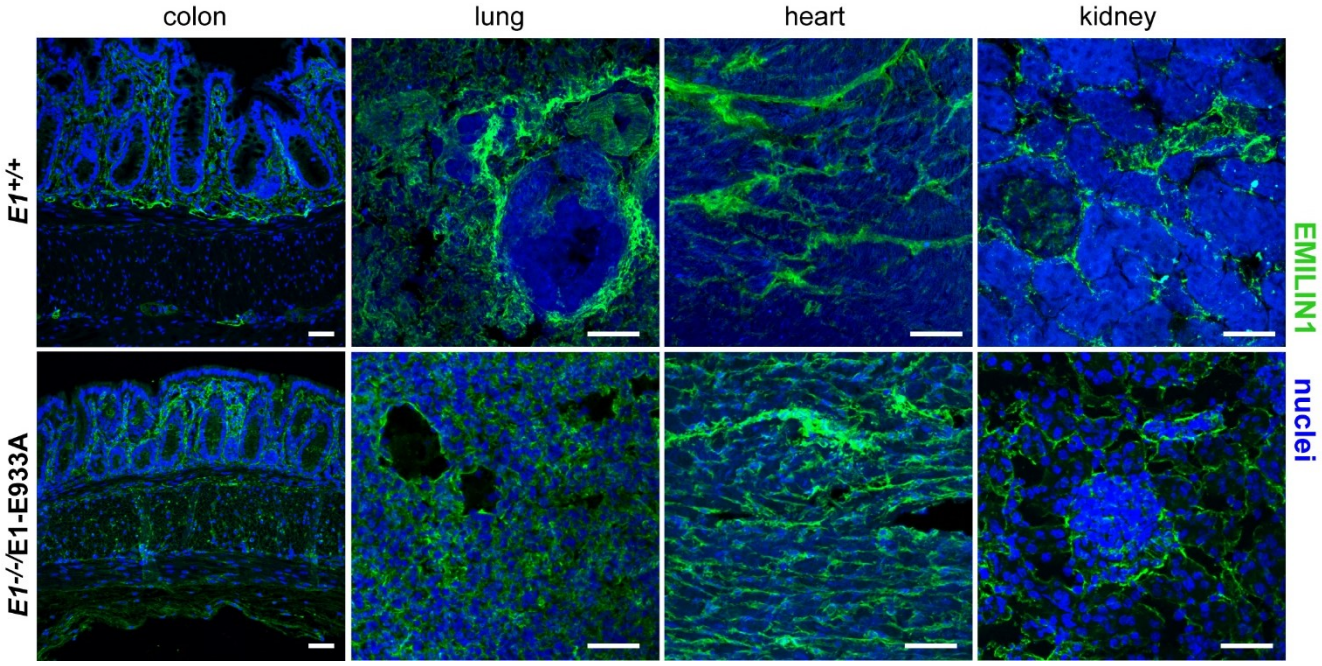

Figure 12: Tissue expression of E933A-EMILIN1 protein. Expression of transgenic E933A EMILIN1 in an *E1*$^{-/-}$ background. Immunofluorescence staining of cryostat sections (colon, lung, heart, kidney) from *E1*$^{+/+}$ and *E1*$^{-/-}$/E1-E933A mice. Labelling was performed with a polyclonal antibody (As556) that recognizes the human protein and a monoclonal antibody (C11A8) that is specific for the murine protein. Scale bar: 50 µm.

Recombinant human gC1q, both wild type (WT gC1q) and mutant (E933A gC1q) were tested in a quantitative cell adhesion assay (CAFCA) using the murine B16F10 cells. As showed in Figure 13, the WT gC1q displayed a very strong adhesive capacity as well as FN that we used as a positive control of adhesion; on the other hand, the mutant E933A gC1q was completely unable to bind cells. After 30 minutes cells appeared well spreaded on both WT gc1q and FN respect to the E933A gC1q and BSA (negative adhesive control). These results indicate that the human sequence of EMILIN1 (and of its gC1q) is able to engage the integrin present in cells of murine, as well as of human origin (see results published in **Spessotto *et al.*, 2003**).

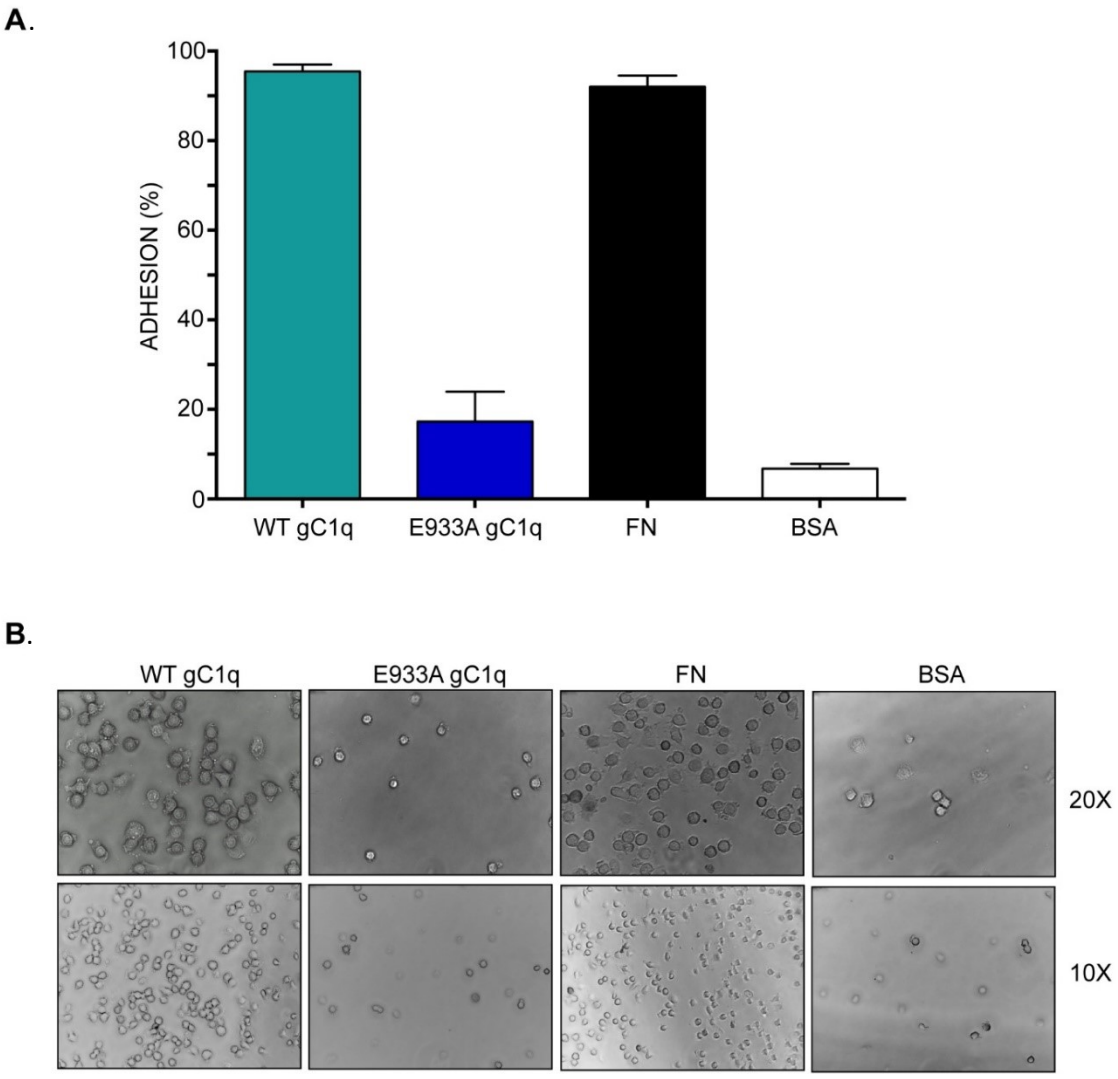

Figure 13: Adhesive properties of human gC1q. Recombinant human EMILIN-1 gC1q (wild type, WT gC1q; mutant E933A gC1q, E933A gC1q) domains were used to perform the quantitative CAFCA adhesion assay with the murine B16F10 cells **(A)**. Fibronectin (FN) and BSA were introduced as positive and negative adhesion controls, respectively. The mutant E933A was totally unable to bind cells whereas WT gC1q displayed a very strong adhesive capacity as well as FN. **(B)** Representative images of cells adhering to the different substrates after 30 minutes. Cells appear well spread on both WT gC1q and FN.

1.3. Evaluation of the mature TGF-β expression levels

To confirm if the properties related to the EMI domain in the transgenic mouse model were unaltered compared to *E1*$^{+/+}$ counterpart, western blotting was performed. The expression levels of mature TGF-β1 in lysates from colon specimens of *E1*$^{-/-}$/E1-E933A mice were similar to those of *E1*$^{+/+}$ counterparts (Figure 14), whereas in *E1*$^{-/-}$ samples a huge amount of TGF-β1 was presented as expected.

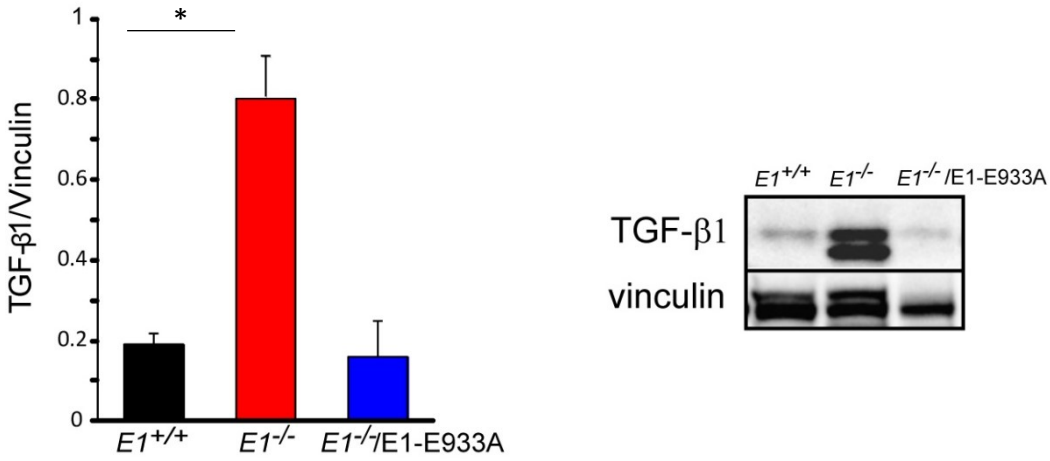

Figure 14: Western blotting analysis of mature TGF-β1 levels in lysates from colon specimens of *E1*$^{+/+}$, *E1*$^{-/-}$ and *E1*$^{-/-}$/E1-E933A mice. The graph represents the mean ± SD of TGF-β1 levels normalized versus vinculin, used as a loading control (n = 3 mice per genotype). **P* < 0.05 (Student's t test).

Thus, we can assert that the human sequence present in the transgene properly works in a murine model and that it is able to rescue the correct regulation of TGF-β (**Zacchigna *et al.*, 2006**). We can conclude that our transgenic mouse is a good model to study the effects dependent only by the gC1q domain.

During my Ph.D. program, I also carried out a series of analyses and experiments aimed to investigate the role of the EMILIN-1 gC1q domain specifically in the regulation of lymphatic system. In fact, experimental evidence for the involvement of a specific domain of EMILIN-1 responsible for its lymphangiogenic functions had not been provided yet. The results obtained (**Capuano *et al.,* in press**) were important not only for the analysis of lymphatic phenotype but also for a better characterization of our transgenic mouse model and for highlight the structural and functional importance of the interaction between gC1q/$\alpha_4\beta_1$. For these reasons, I have included in this thesis the experiments that I performed to evaluate the functional contribution of gc1q.

1.4. *In vitro* and *in vivo* assessment of lymphatic phenotype

Among the different techniques that could be used for the study of the ability of EMILIN-1 gC1q domain to induce a correct lymphangiogenesis, we decided to perform the thoracic duct sprouting assay that allows to analyze different steps of lymphangiogenesis (spreading from a pre-existing vessel, cell proliferation and differentiation). Furthermore, the importance of gC1q domain as a functional point of view, was studied using a model of dissemination of melanoma cancer cells to LNs.

1.4.1. "Sprouting" activity

The evaluation of the interconnected network of capillary-like structures was performed qualitatively by assigning an arbitrary score, from 0 to 4 according to increasing sprouting ability (as detailed in paragraph 5 of Material and Methods section) and quantitatively by measuring the LV sprouting area using the ImageJ software.

After 4 days of culture, only lymphatic rings derived from *E1*$^{+/+}$ were able to sprout; on the contrary, any capillary-like structures were detectable in both *E1*$^{-/-}$ and *E1*$^{-/-}$/E1-E933A rings that, only occasionally, sprouted at day 8 (Figure 15 A and B). Also the calculated area covered by the lymphatic network, reproduced the analysis obtained through the qualitative score evaluation, showing that *E1*$^{-/-}$ and *E1*$^{-/-}$/E1-E933A thoracic ducts were unable to sprout and form an organized capillary network (Figure 15 C).

As reported in Figure 15 A, after 8 days of culture, lymphatic rings of *E1*$^{+/+}$ mice showed an outgrowth of cells that were able to organize into well-established and complex capillary-like structures. On the contrary, the cell outgrowth of both the *E1*$^{-/-}$ and *E1*$^{-/-}$/E1-E933A rings was very limited or absent.

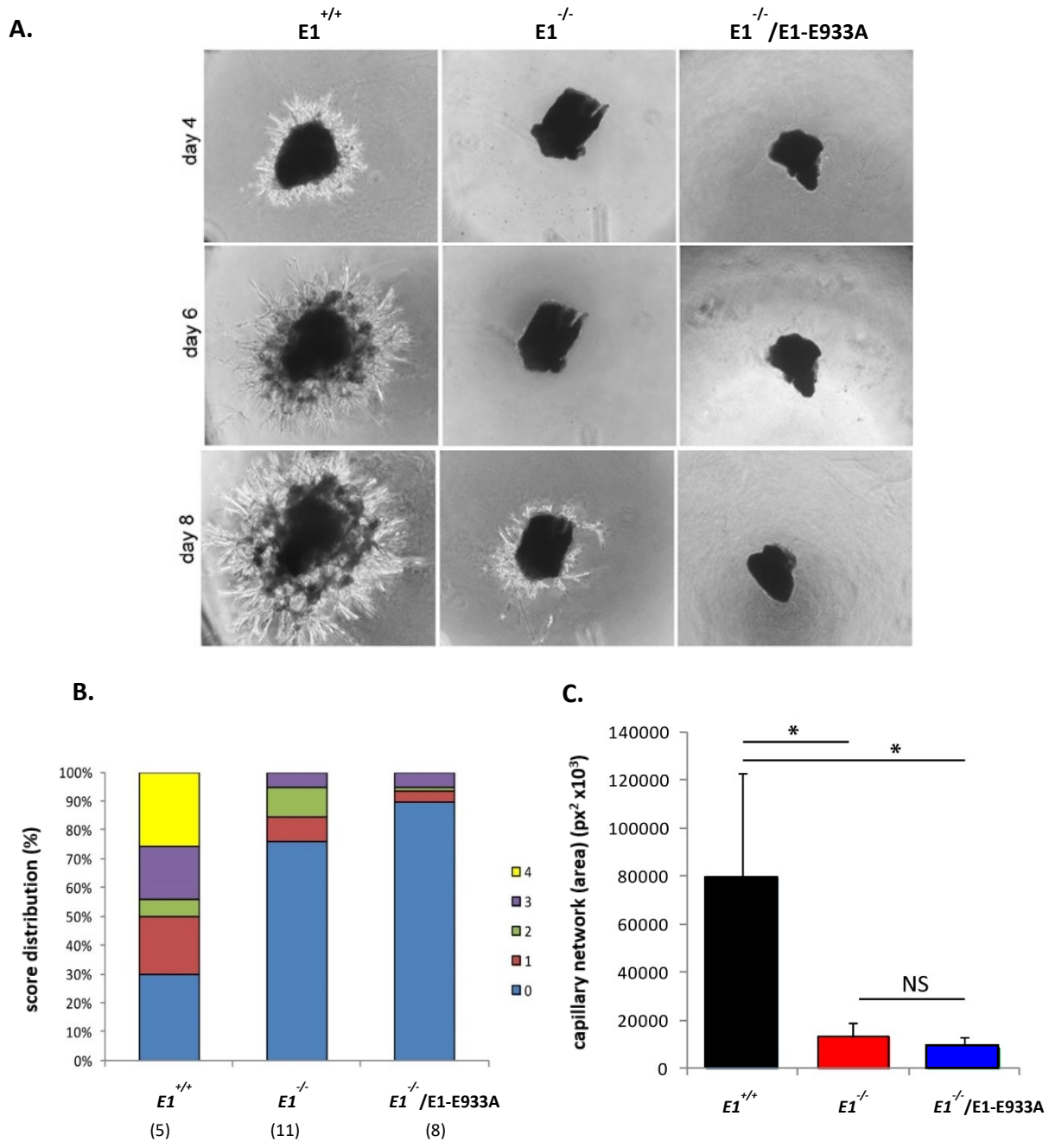

Figure 15: Limited sprouting capacity of E1$^{-/-}$/E933A LECs. **(A)** Representative images of thoracic duct (ring) explants from *E1*$^{+/+}$, *E1*$^{-/-}$ and *E1*$^{-/-}$/E1-E933A mice, embedded in 3D matrix (Cultrex) and cultured for 4, 6 and 8 days. The sprouting ability was very poor for both E1$^{-/-}$ and *E1*$^{-/-}$/E1-E933A rings. **(B)** Score distribution evaluated after 8 days of culture. The number of mice used for this analysis was reported between parentheses. For each thoracic duct, 10 fragments were scored for sprouting ability. For score 0 the difference between *E1*$^{+/+}$, *E1*$^{-/-}$ and *E1*$^{-/-}$/E1-E933A mice was statistically significant by one-way Anova test. **(C)** The area of capillary network of the samples examined in B, was calculated using ImageJ software (see Material and Methods, paragraph 5). *$P < 0.05$; NS, not significant (two-tailed unpaired Student's t test).

These results allowed us to indicate that the role played by EMILIN-1 in lymphatic sprouting was due to the gC1q domain and, more precisely, to the presence of E993 aminoacidic residue that allows the interaction with the integrin. To further confirm this, we isolated thoracic ducts only from *E1*$^{-/-}$ mice and cultured the corresponding rings in the presence of: **(I)** recombinant wt EMILIN-1, **(II)** wt gC1q and **(III)** mutant E993A gC1q. After 4 days of culture, we observed that *E1*$^{-/-}$ rings were able to sprout only in the presence of either wt EMILIN-1 or its wt gC1q domain reaching a score value of 3; on the other hand, only a small percentage of rings in the presence of the mutant E993A gC1q reached a score value of 1 as a maximum (Figure 16 A). Moreover, also the sprouting area of *E1*$^{-/-}$ rings cultured in the presence of both wt EMILIN-1 or wt gC1q was very similar at day 4 (Figure 16 B). After 8 days, even less pronounced than EMILIN-1, the effect of wt gC1q was maintained from both a qualitative and quantitative evaluation (Figure 16 C and D).

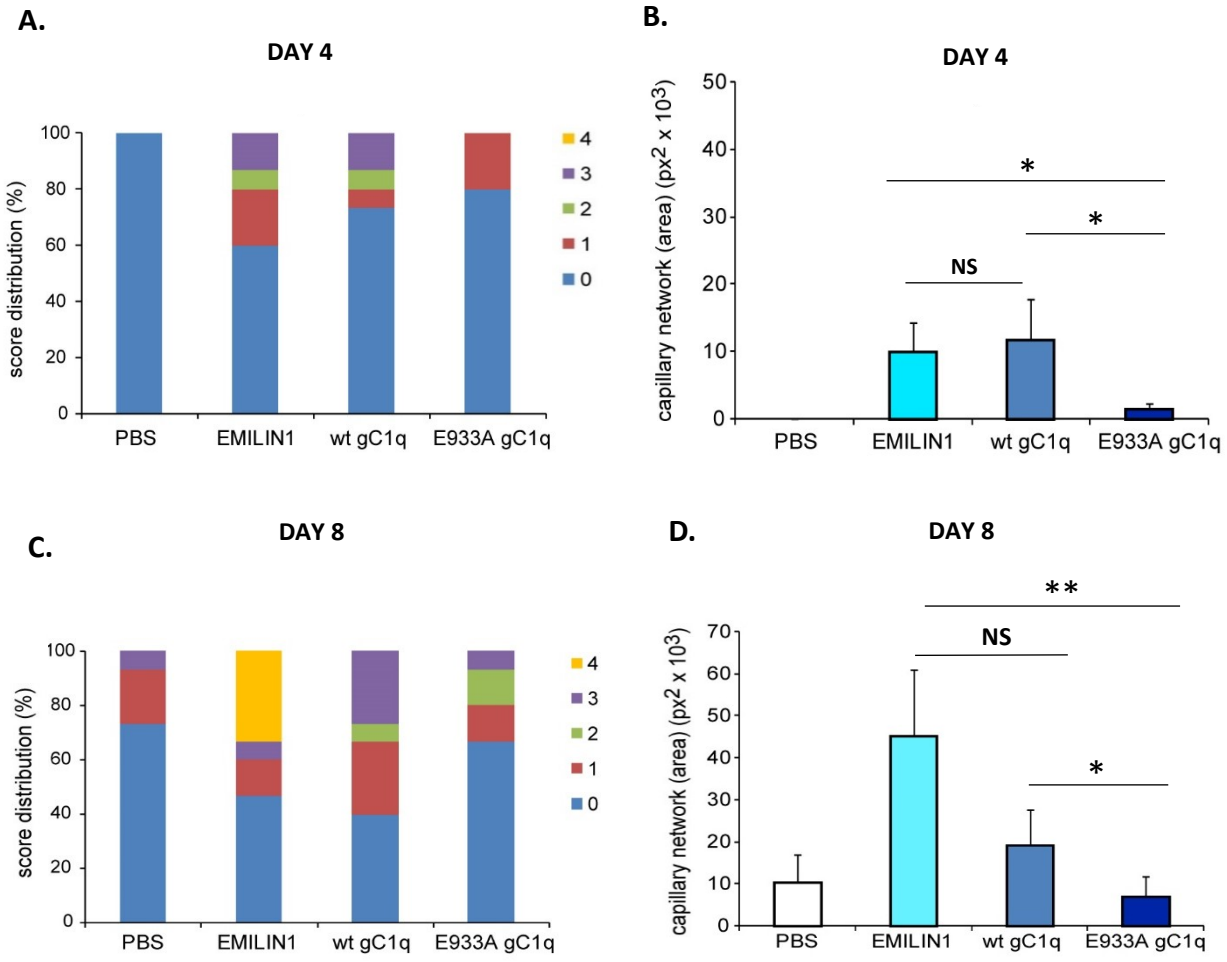

Figure 16: Evaluation of lymphangiogenic activity of recombinant fragments. Thoracic ducts from E1$^{-/-}$ mice (n = 5) were cultured in the presence of PBS, recombinant wt EMILIN-1, wt gC1q or E993A mutant gC1q (three fragments of the same duct for each condition). Score distribution **(A)** and capillary network area **(B)** calculated after 4 days of culture. Score distribution **(C)** and capillary network area **(D)** calculated after 8 days of culture. In **(B)** and **(D)**, growth area was calculated with ImageJ software; **P* < 0.05; NS, non-significant (Student's t test).

The score distribution determined by the sprouted structures that resulted podoplanin positive (Figure 17) and the calculation of the corresponding area at day 8, confirmed that the mutant fragment didn't display any effective sprouting capacity. These results confirmed that the binding site for $\alpha_4/\alpha_9\beta_1$ integrin was necessary for LEC activity.

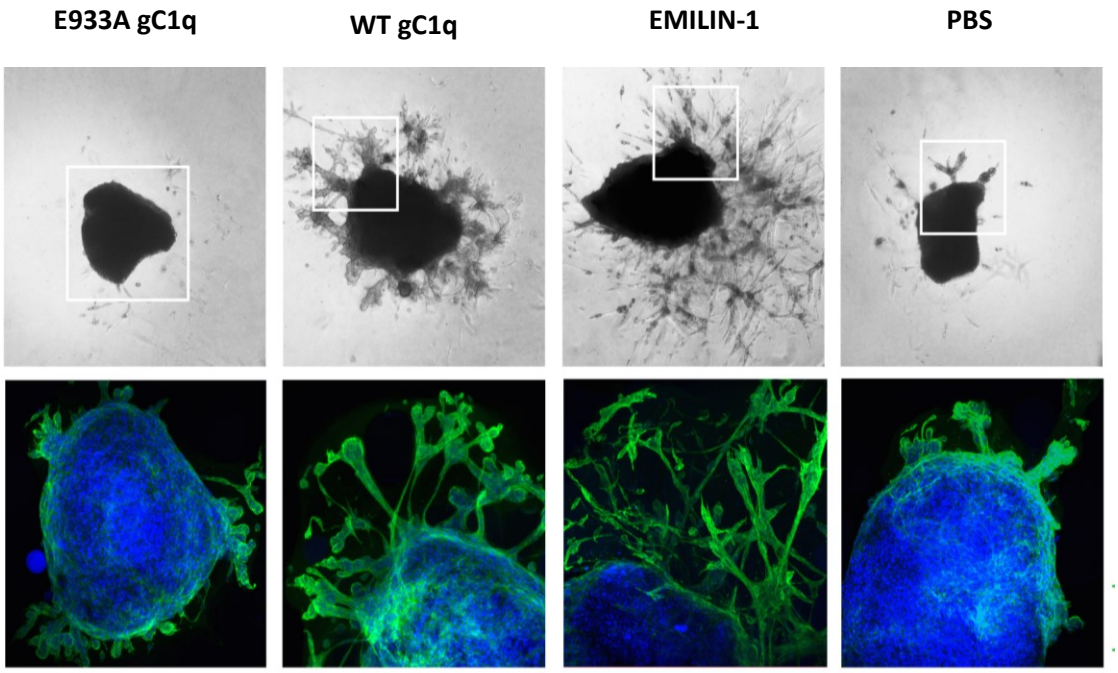

Figure 17. Immunofluorescence of *E1*$^{-/-}$ thoracic ducts in the presence of EMILIN-1 recombinant peptides. Representative images of the sprouts after 8 days of culture. Podoplanin (green) immunofluorescence of the whole mount ducts corresponding to the inset of contrast phase images is shown. LECs, positive to podoplanin, are able to induce an elevated sprouting capacity in the presence of EMILIN-1 and wt gC1q compared to the PBS and the mutated E933A gC1q.

1.4.2. Enhanced LN metastasis of transplanted tumors in E1$^{-/-}$/E1-E933A mice

To better demonstrate that the interaction between gc1q/$\alpha_4\beta_1$ was functionally crucial, we studied the dissemination of melanoma cells using an experimental approach where the preferential pathway of cancer cells to metastasize is the lymphatic system. We intrafootpad injected *E1*$^{+/+}$, *E1*$^{-/-}$ and *E1*$^{-/-}$/E1-E933A mice with B16F10*Luc* melanoma cells. When tumors growth was comparable in all three genotypes (Figure 18 A), popliteal (PL), inguinal (ING) and axillary (AX) LNs were excised and analyzed *ex vivo* for the presence of luciferase signal. AX LNs appeared negative in all genotypes. PL (100%) as well as ING (~30/40%) LNs were positive for luciferase signal in all *E1*$^{-/-}$ and *E1*$^{-/-}$/E1-E933A. Regarding *E1*$^{+/+}$ mice, only 50% of PL LNs were infiltrated by melanoma cells (Figure 18 B-D). No one ING LNs in *E1*$^{+/+}$ mice was positive for luciferase signal.

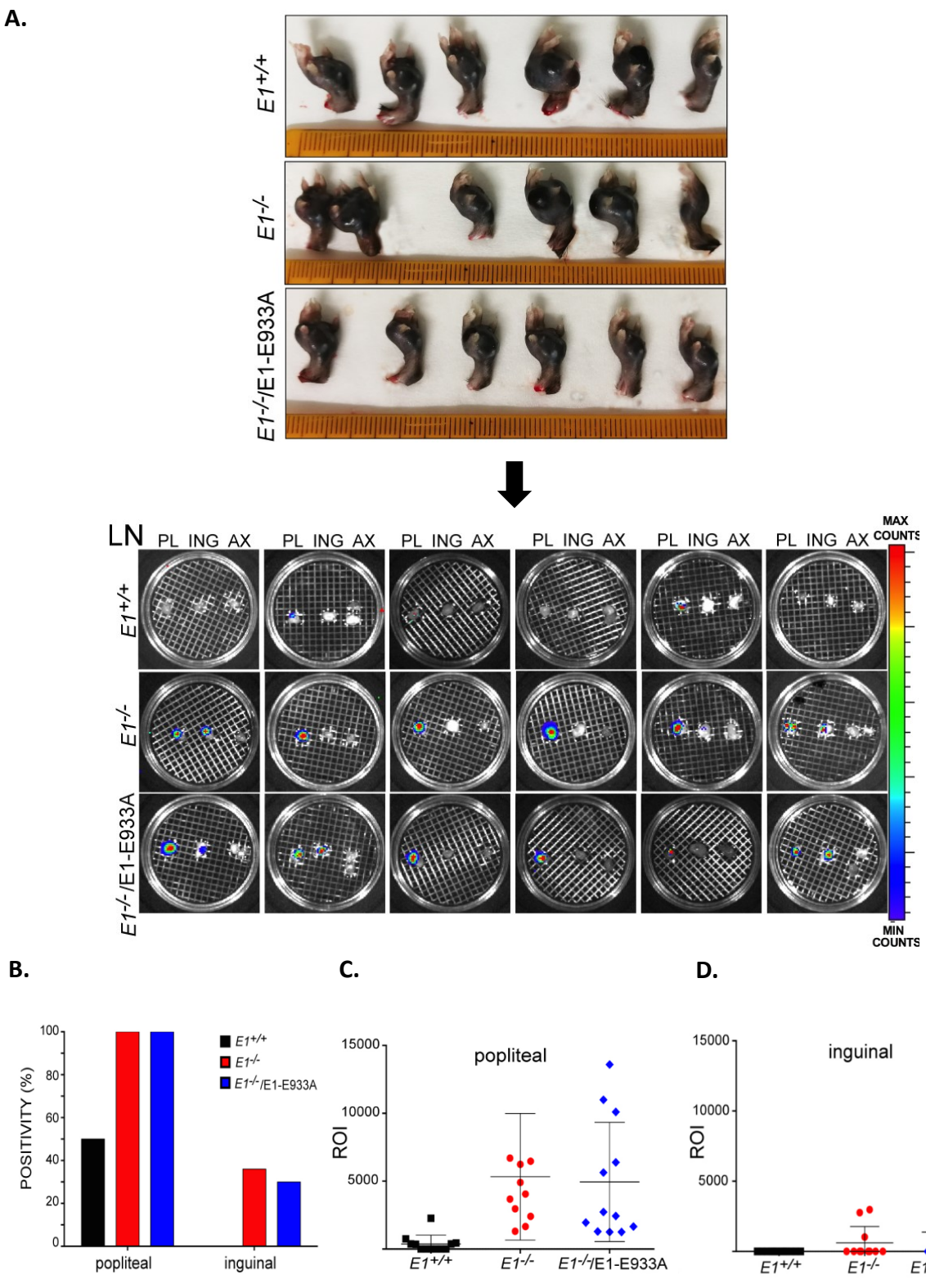

Figure 18: B16F10*Luc* metastases in $E1^{+/+}$, $E1^{-/-}$ and $E1^{-/-}$/E1-E933A LNs. **(A)** $E1^{+/+}$ (n = 12), $E1^{-/-}$ (n = 11) and $E1^{-/-}$/E1-E933A (n = 12) mice were intrafootpad implanted with $2x10^5$ B16F10*Luc* melanoma cells. Six tumors per genotype images and color scale of the luciferase signal emitted by LNs of the corresponding (upper) B16F10*Luc*-bearing mice (lower) are shown. **(B)** Percentage of B16F10*Luc* metastatic $E1^{+/+}$, $E1^{-/-}$ and $E1^{-/-}$/E1-E933A popliteal and inguinal LNs. (**C, D**) Mean ± SD luciferase signal detected by ex vivo optical imaging in the excised popliteal (**C**) and inguinal (**D**) LNs of B16F10*Luc*-bearing mice.

Interestingly, PL and ING LNs isolated from *E1*$^{-/-}$ and *E1*$^{-/-}$/E1-E933A mice, were significantly bigger than *E1*$^{+/+}$ counterpart (Figure 19 A-C). Furthermore, LYVE-1 positive vessel density was increased in both PL and ING LNs of *E1*$^{-/-}$ and *E1*$^{-/-}$/E1-E933A mice compared to those of *E1*$^{+/+}$ mice, even if in a significant way only in Ing LNs (Figure 19 D-F).

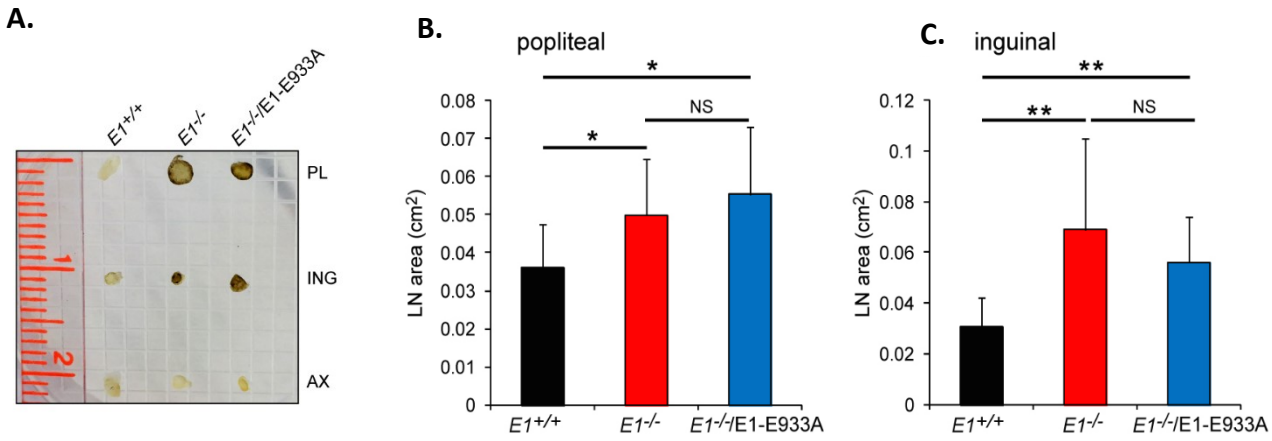

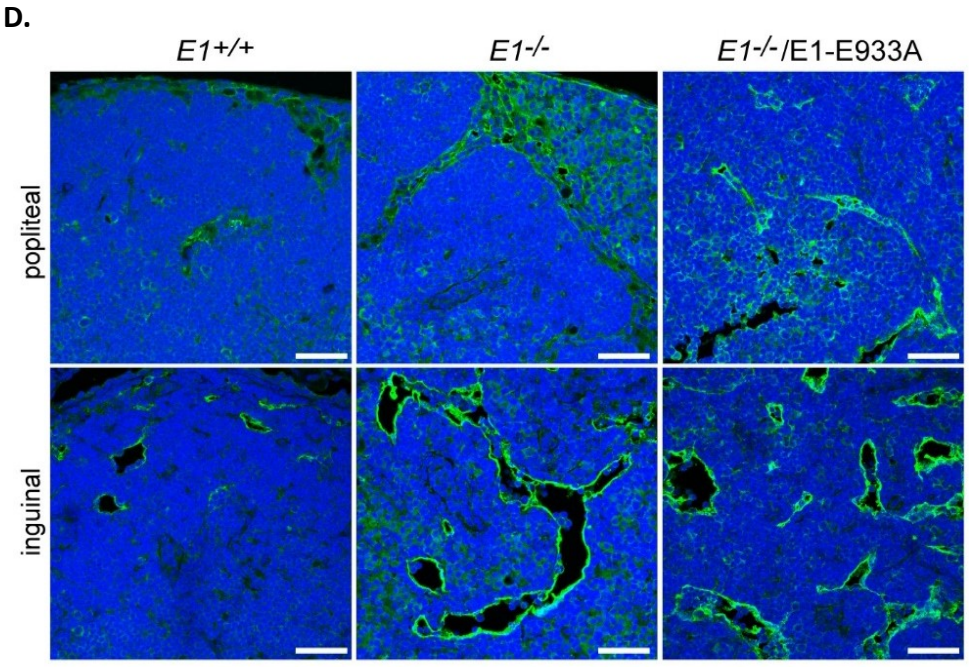

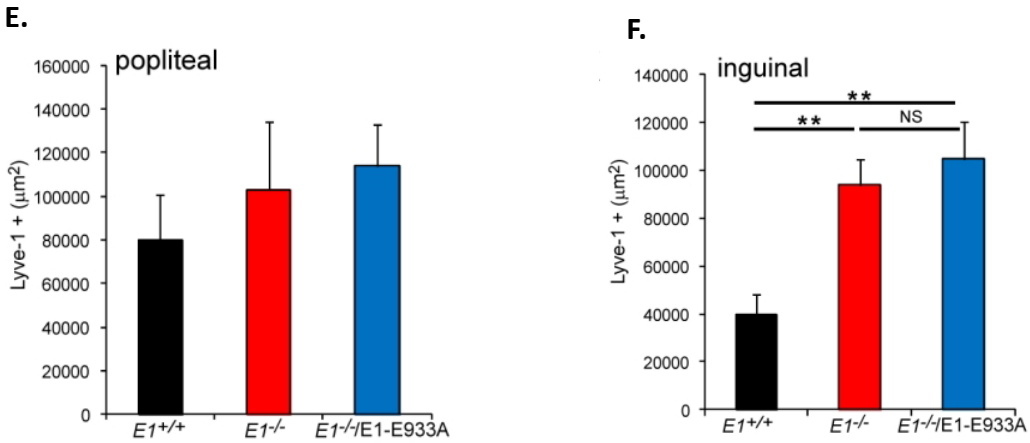

Figure 19: Analysis of PL an ING LN metastasis of *E1*$^{+/+}$, *E1*$^{-/-}$ and *E1*$^{-/-}$/E1-E933A B16F10*Luc* injected mice. (A) Representative images of LNs and size quantification of popliteal (**B**) and inguinal (**C**) LNs. **(D)** Representative LYVE-1 stained sections (green) of metastatic popliteal and inguinal LNs. Quantification of popliteal **(E)** and inguinal **(F)** LN area positive for LYVE-1 signal is reported. The analysis was performed on at least 4 fields (20x, original magnification) (n = 6 LNs per genotype; mean ± SEM). **P* < 0.05; ***P* < 0.005, NS, not significant. Scale bar: 50 µm.

These lymphatic structural and functional alterations observed in our transgenic model were closely related to the regulatory sequence of the gC1q domain. The fact that the *E1*$^{-/-}$/E1-E933A transgenic mouse displayed a lymphatic phenotype similar to the *E1*$^{-/-}$ mouse (**Danussi *et al.*, 2008 and 2013**), allowed us to conclude that the gC1q/integrin interaction is indispensable in the regulation of the lymphangiogenic process played by EMILIN-1. Thanks to these evidences, we can consider the gC1q as the key domain able to induce a correct lymphangiogenesis response.

2. AOM-DSS TUMORIGENESIS in DIFFERENT EMILIN1 BACKGROUNDS

The lack of EMILIN1 accelerates tumor development and increases the number and size of skin tumors in a two-step skin carcinogenesis protocol (**Danussi *et al.,* 2011 and 2012**). This evidence means that the EMILIN1/$\alpha_4\beta_1$ integrin interaction, as occurs in WT mice, is able to regulate proliferation, acting like an oncosoppressor. The basic hypothesis is that the presence of EMILIN1 can exert a contrasting role towards tumor growth and progression also in the colon microenvironment.

2.1. Tumour development

To demonstrate our hypothesis, colon tumors were induced in *E1*$^{+/+}$, *E1*$^{-/-}$ and *E1*$^{-/-}$/E1-E933A mice with a single intraperitoneal injection of AOM, followed by one-week exposure to 2% DSS in drinking water (Figure 20 A). This protocol represents the typical experimental procedure used to induced colon carcinogenesis and it is the most common documented in literature. Classically, AOM (a 1,2-dimethylhydrazine (DMH) metabolite) requires several metabolic activation steps (including N-oxidation and hydroxylation) to induce DNA-reactive adducts (**Laqueur 1964**)**.** We have chosen this model also because tumors induced in mice exposed to AOM/DSS treatment accurately recapitulate the pathogenesis observed in human CRC (**Tanaka *et al.,* 2003**).

Monitoring and evaluation of tumour growth were performed over time by endoscopy; at each time point, we established that *E1*$^{-/-}$ and *E1*$^{-/-}$/E1-E933A mice developed a higher number of tumours respect to *E1*$^{+/+}$ counterpart (Figure 20 B). At the end of the AOM/DSS treatment, colon samples were isolated from all mice and the part that goes from the cecum to the anus, was opportunely opened, washed and tumours counted (Figure 20 C). This macroscopic analysis confirmed what we had observed during endoscopy.

A.

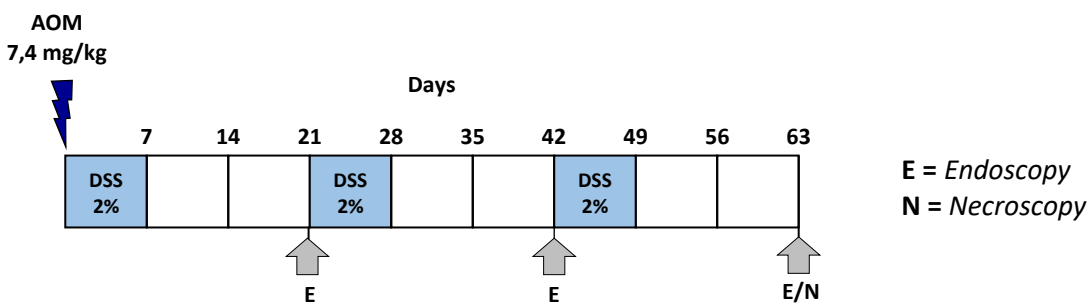

B.

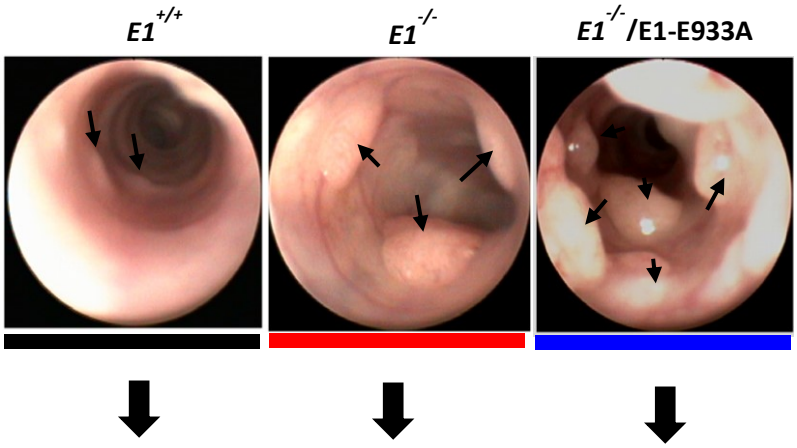

C.

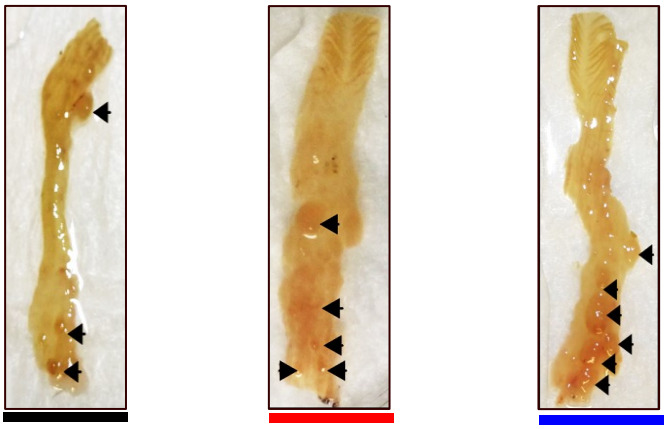

Figure 20: Tumour development in *E1*$^{+/+}$, *E1*$^{-/-}$ and *E1*$^{-/-}$/E1-E933A mice after AOM/DSS colon carcinogenesis induction. **(A)** Schematic representation of the regiment used to induce CAC, whereby a single AOM injection is followed by three cycles of 2% DSS in drinking water; tumour development was monitored by endoscopy at indicated times (denoted by E). Representative endoscopy panel made at day 63 **(B)** and opened colons recovered after necroscopy **(C)** indicating the presence (black arrows) of tumour lesions that are more in *E1*$^{-/-}$ and *E1*$^{-/-}$/E1-E933A mice compared to *E1*$^{+/+}$ counterpart. Black rectangle indicates ***E1***$^{+/+}$**,** blue rectangle ***E1***$^{-/-}$ and red rectangle ***E1***$^{-/-}$**/E1-E933A** mice.

2.2. Tumour scoring

We further analyzed tumours applying a "score" value (Figure 21). Tumour mass received a score of 1 to 5 depending on whether its size slightly, very or almost completely occupied the colonic mucosa. This analysis revealed that *E1*$^{-/-}$ and *E1*$^{-/-}$/E1-E933A mice developed not only more, but also bigger tumour than *E1*$^{+/+}$ littermates.

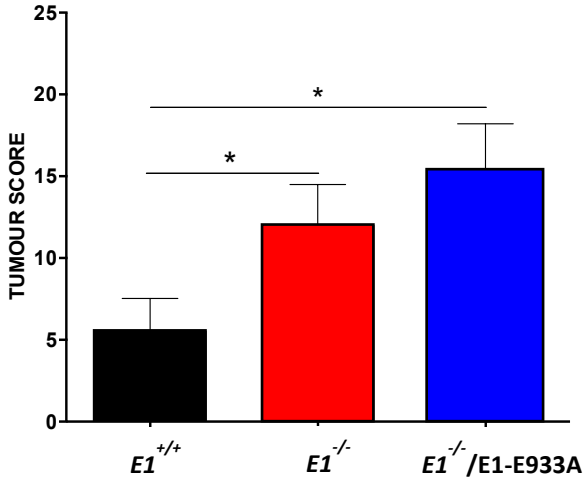

SIZE	SCORE
Just detectable	1
1/8	2
1/4	3
1/2	4
> 1/2	5

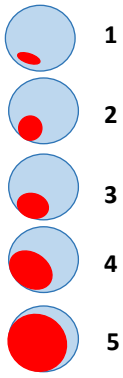

Figure 21: Tumour scoring. At the end of the treatment (day 63) all mice were sacrificed, and colon recovered, opened and washed in order to score the proliferative lesions founded within the mucosa. Both table and cartoon indicate the score (1 to 5) attributed to the tumour based on how its size occupied the mucosa. *E1*$^{-/-}$ and *E1*$^{-/-}$/E1-E933A mice presented bigger tumours compared to *E1*$^{+/+}$ littermates. **P* < 0.05 (Student's t test).

2.3. Classification of proliferative lesions

AOM/DSS-induced tumours showed differences depending on the mouse genotype. The graph in Figure 22, established that most of *E1*$^{+/+}$ treated mice didn't develop proliferative lesions; on the other hand, both *E1*$^{-/-}$ and *E1*$^{-/-}$/E1-E933A mice were prone to developed typical colonic tumours, particularly low and high-grade adenomas and also, in few cases, gastrointestinal intraepithelial neoplasia (GIN).

All these analyses led us to conclude that also in the colonic mucosa environment, as already demonstrated in skin (**Danussi *et al.*, 2012**), EMILIN-1 exerts an antiproliferative effect. Moreover, thanks to our transgenic mouse model, we were very confident that this EMILIN-1 property was strictly related to the gC1q domain and to its interaction with $\alpha_4\beta_1/\alpha_9\beta_1$ integrins.

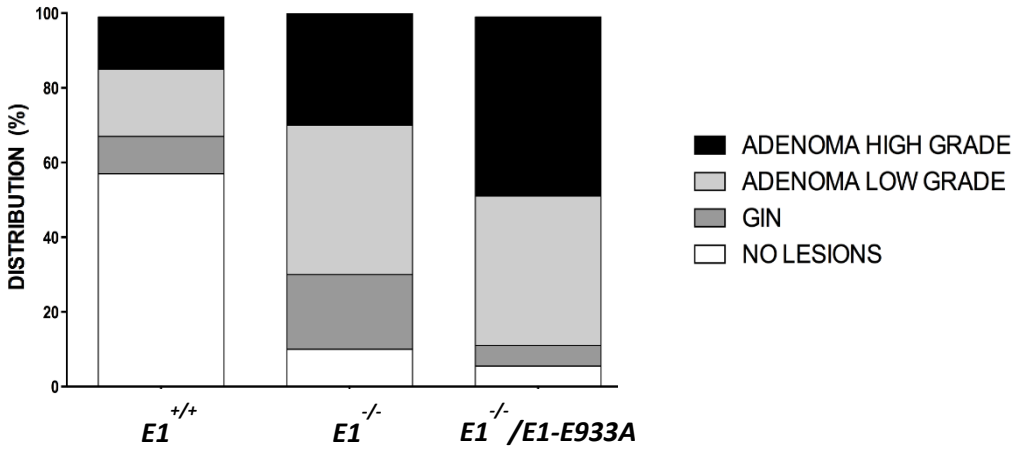

Figure 22: Classification of proliferative lesions within colonic mucosa of *E1*$^{+/+}$, *E1*$^{-/-}$ and *E1*$^{-/-}$/E1-E933A treated mice. Proliferative lesions were classified according to *Boivin et al.* using different types as reported in the legend. This histopathological analysis was performed on H&E colon section of all treated mice (14 for each genotype). *E1*$^{+/+}$ didn't develop a lot of proliferative lesions, on the contrary, *E1*$^{-/-}$ and *E1*$^{-/-}$/E1-E933A mice presented a lot of high- and low-grade adenomas and GIN.

2.4. Evaluation of inflammation within tumour lesions

The inflammatory microenvironment classically affects tumor promotion and progression (**Grivennikov *et al.*, 2010**). For this reason, we evaluated also the inflammatory extent in all EMILIN-1 different genetic background treated mice.

First of all, we considered two indexes that recapitulate the main characteristics of epithelial damage and inflammation; the first is the "DAI clinical index" that takes into consideration collectively three different parameters: weight loss, stool consistency and rectal bleeding. The second is the "MEICS endoscopy index" that allows to score the colitis severity considering five parameters: thickening of the colon wall, changes in the normal vascular pattern, presence of fibrin, mucosal granularity and stool consistency. All these parameters, as reported in Figure 23 A and B, demonstrated that *E1*$^{-/-}$ and *E1*$^{-/-}$/E1-E933A treated mice were characterized by the presence of signs of diffuse inflammation in the colonic mucosa respect to *E1*$^{+/+}$ counterpart.

A.

Disease Activity Index					
	0	**1**	**2**	**3**	**4**
Weight loss	0-2%	2-4%	4-6%	6-8%	>8%
Stool consistency	normal	soft and shaped	loose stools	between	diarrhoea
Rectal bleeding	negative	between	slight	between	gross

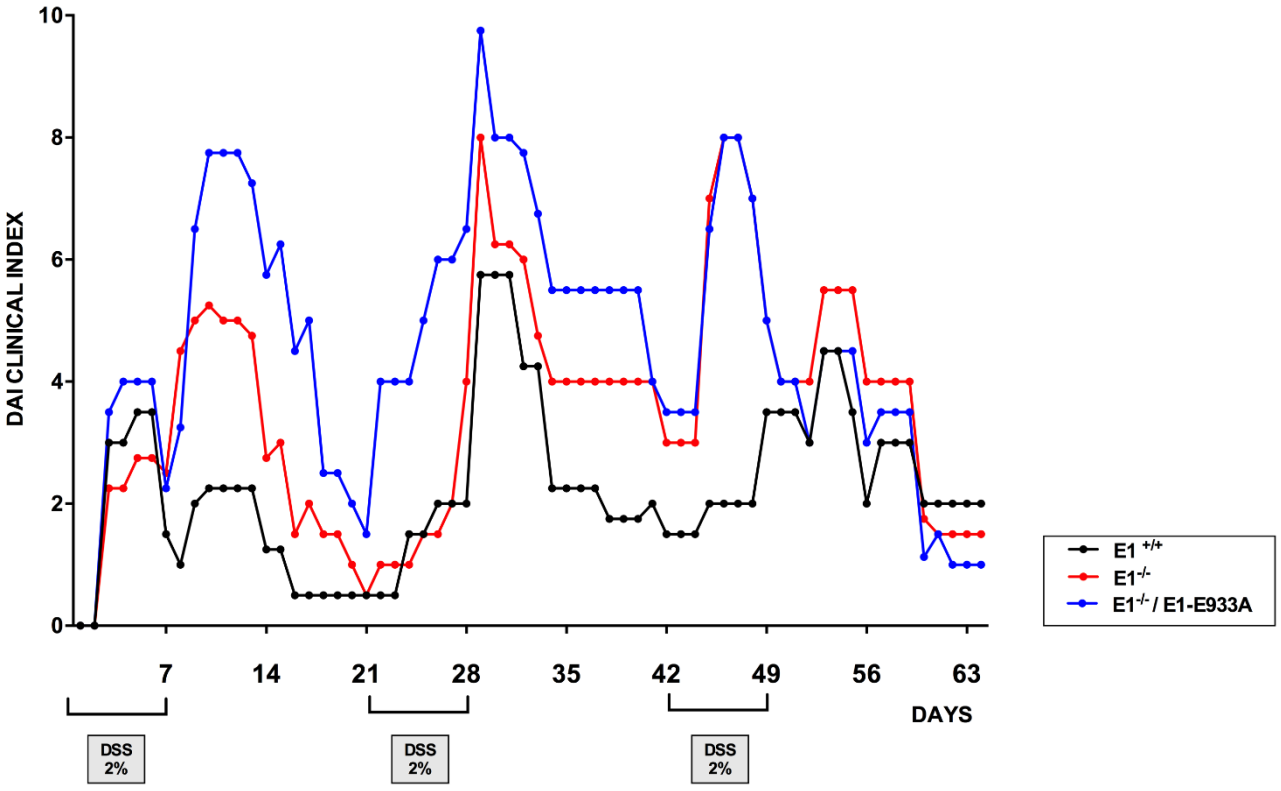

B.

Murine Endoscopic Index of Colitis Severity				
	0	**1**	**2**	**3**
Thickening	transparent	moderate	marked	non-transparent
Changes in the vascular pattern	normal	moderate	marked	bleeding
Fibrin visible	none	little	marked	extreme
Granularity	none	moderate	marked	extreme
Stool	Solid	Still shaped	unshaped	spread

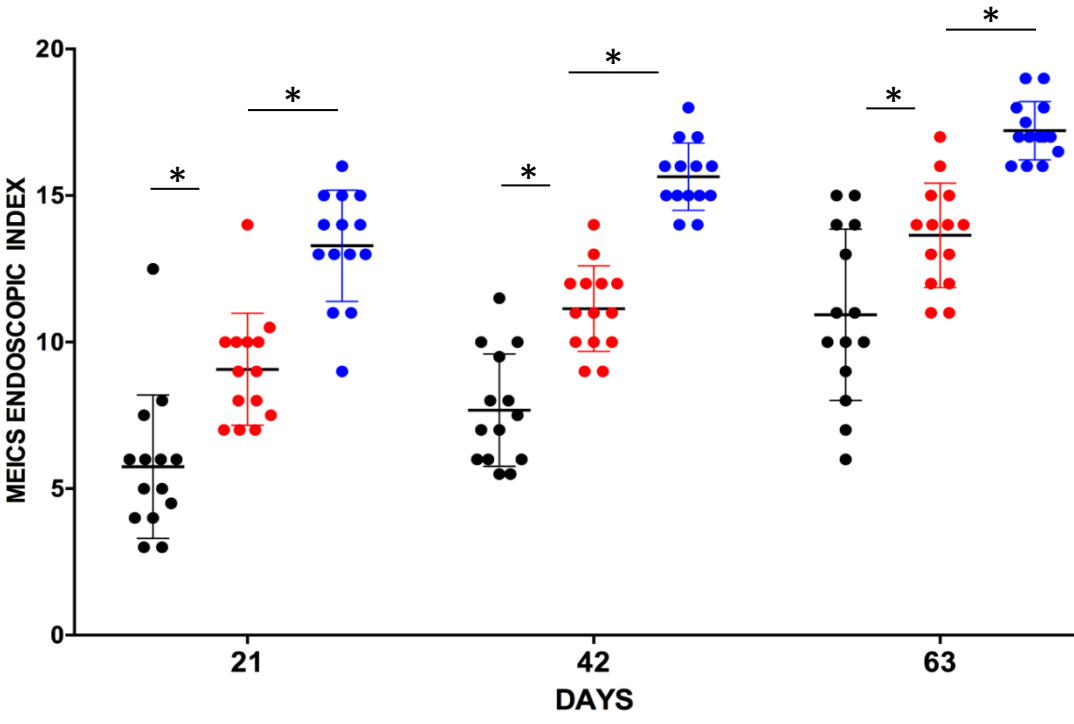

Figure 23: Clinical and Endoscopic Indexes for inflammatory extent evaluation. Clinical (DAI) **(A)** evaluated daily and Endoscopic (MEICS) **(B)** performed at day 21,42 and 63 during endoscopy are the two indexes that allow to score the inflammatory extent in the context of inflammatory colon cancer. In the two tables all the parameters taken into consideration are summarized. Both indicate that *E1*$^{-/-}$ and *E1*$^{-/-}$/E1-E933A mice appeared more inflamed during all treatment compared to *E1*$^{+/+}$ animals. **P* < 0.05 (Student's t test).

These results were confirmed after euthanasia with the measurements of the colon length, another important parameter of inflammation (**Wirtz *et al.*, 2007**) (Figure 24 A). These macroscopic analyses gave us the possibility to arbitrarily establish the inflammatory extent. To better characterize the inflammatory infiltrate we performed histopathological analysis; as reported in the panel of Figure 24 B, H&E stained colon sections presented typical signs of diffuse inflammation in the colonic mucosa of AOM/DSS-treated *E1*$^{-/-}$ and *E1*$^{-/-}$/E1-E933A mice. Moreover, epithelial crypts were distorted and irregularly distributed in the lamina propria, which contained high numbers of inflammatory cells (Figure 24 C).

A.

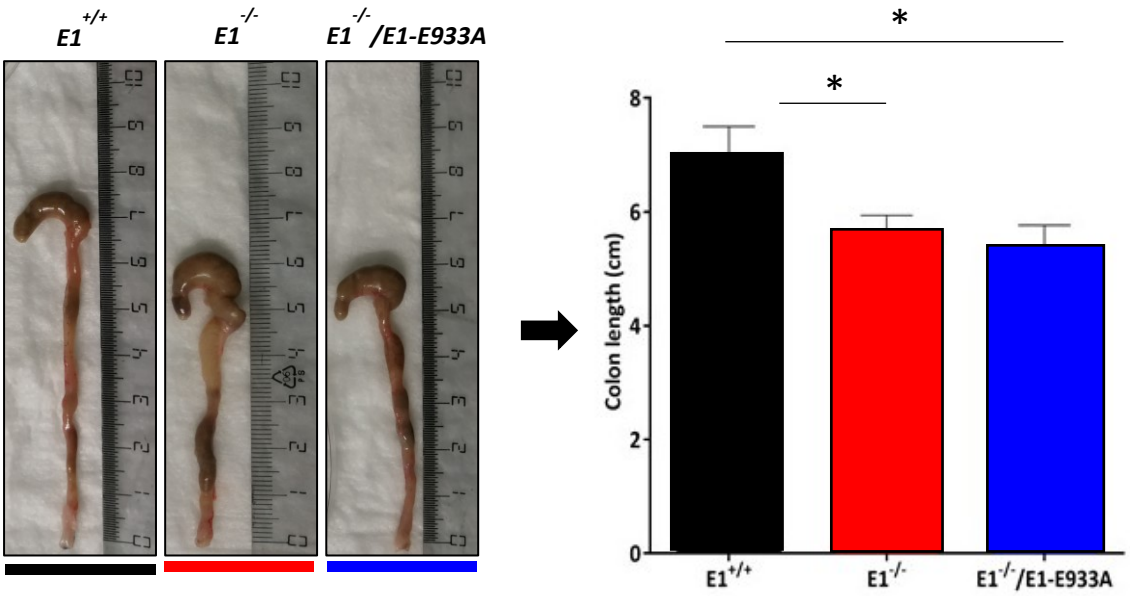

B.

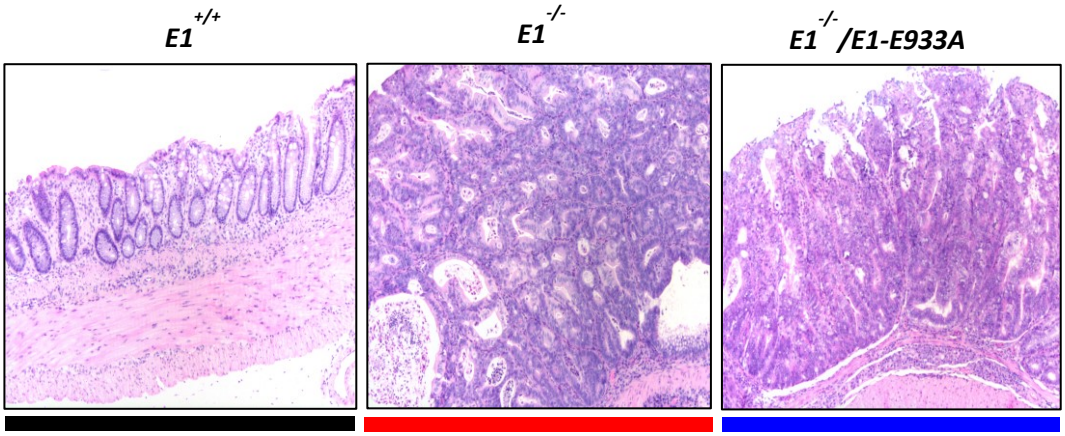

C.

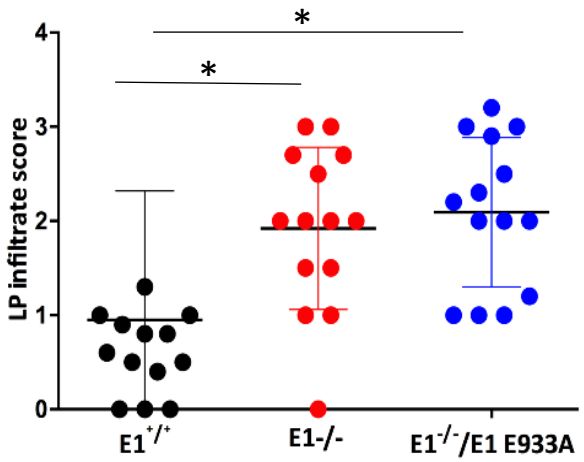

Figure 24: Parameter of inflammation extent. Immediately after necroscopy, colons were isolated and measured **(A)** to evaluate inflammatory extent. **(B)** Panel of representative images of H&E colon section of *E1*$^{+/+}$, *E1*$^{-/-}$ and *E1*$^{-/-}$/E1-E933A treated mice which represent the loss of the epithelial layer of the enteric mucosa. **(C)** Lamina propria (LP) score indicate the presence of inflammatory cells, counted as reported in Material&Methods section. (mean ± SD), *$P < 0.05$ (Student's t test). Original magnification 400x.

3. SCORE DISTRIBUTION of the DSS-INDUCED EXPERIMENTAL COLITIS in EMILIN1 GENETIC BACKGROUNDS

3.1. Assessment of inflammatory status in induced chronic colitis mice

Considering the results obtained in the two-steps colon carcinogenesis approach, in which inflammatory burden appeared really extensive, we decided to deeply investigate how EMILIN-1 with its functional properties works in this context. For this purpose, we applied an experimental approach based on repeated somministrations of DSS (Figure 25 A) that is toxic to colonic epithelial cells and causes defects in the epithelial barrier integrity, increasing mucosal permeability (**Chassaing *et al.,* 2014**). For this set of experiments, we used both FVB and C57BL/6J mice to avoid that the resulting effects could be strain specific.

During the treatment, the extent of inflammation was evaluated taking into consideration the clinical DAI and the endoscopic MEICS indexes. In both FVB and C57Bl/6J strains, DAI index was worst in *E1*$^{-/-}$ and *E1*$^{-/-}$/E1-E933A mice than in *E1*$^{+/+}$ mice (Figure 25 B); in fact, *E1*$^{-/-}$ and *E1*$^{-/-}$/E1-E933A mice lost more weight and presented more severe rectal bleeding. Also the evaluation on colon length confirmed a greater inflammatory extent in *E1*$^{-/-}$ and *E1*$^{-/-}$/E1-E933A samples, that appeared shorter and more thickened compared to the *E1*$^{+/+}$ counterpart. In fact, shorter was the colon, more pronounced was the inflammation (Figure 25 C).

A.

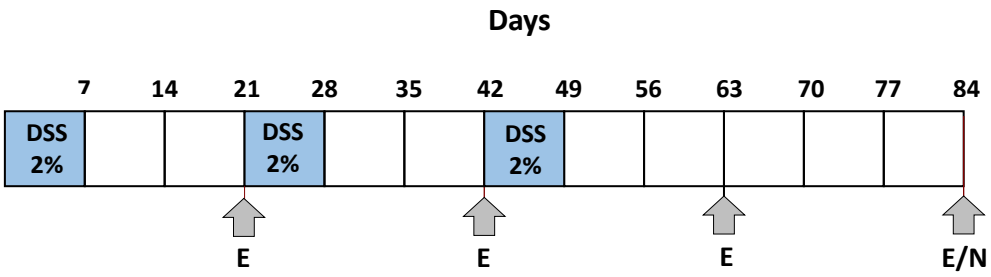

E = *Endoscopy*; **N** = *Necroscopy*

B.

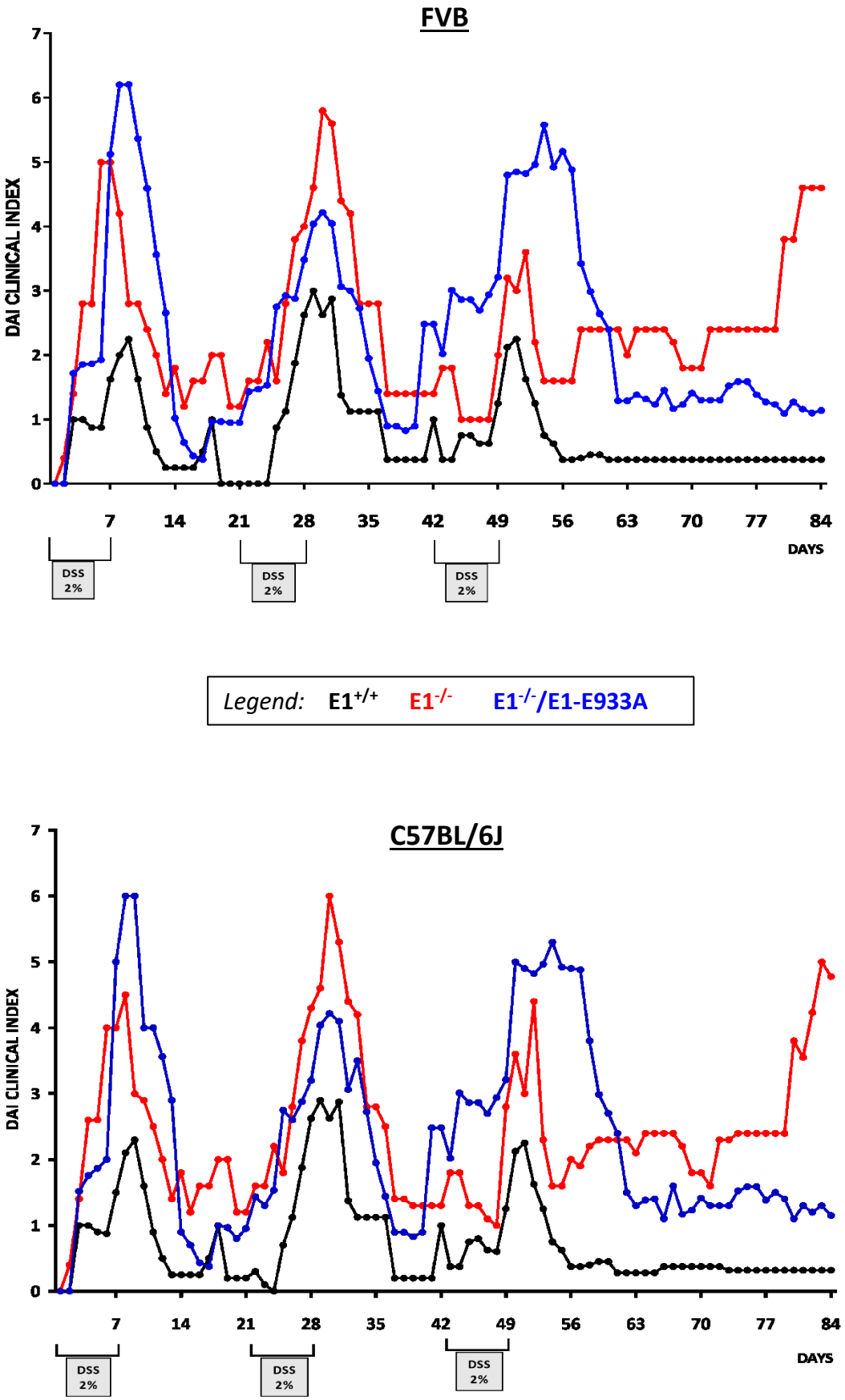
FVB
DAI CLINICAL INDEX
0
1
2
3
4
5
6
7
7
14
21
28
35
42
49
56
63
70
77
84
DAYS
DSS 2%
DSS 2%
DSS 2%
Legend: E1+/+ E1-/- E1-/-/E1-E933A
C57BL/6J
DAI CLINICAL INDEX
0
1
2
3
4
5
6
7
7
14
21
28
35
42
49
56
63
70
77
84
DAYS
DSS 2%
DSS 2%
DSS 2%

C.

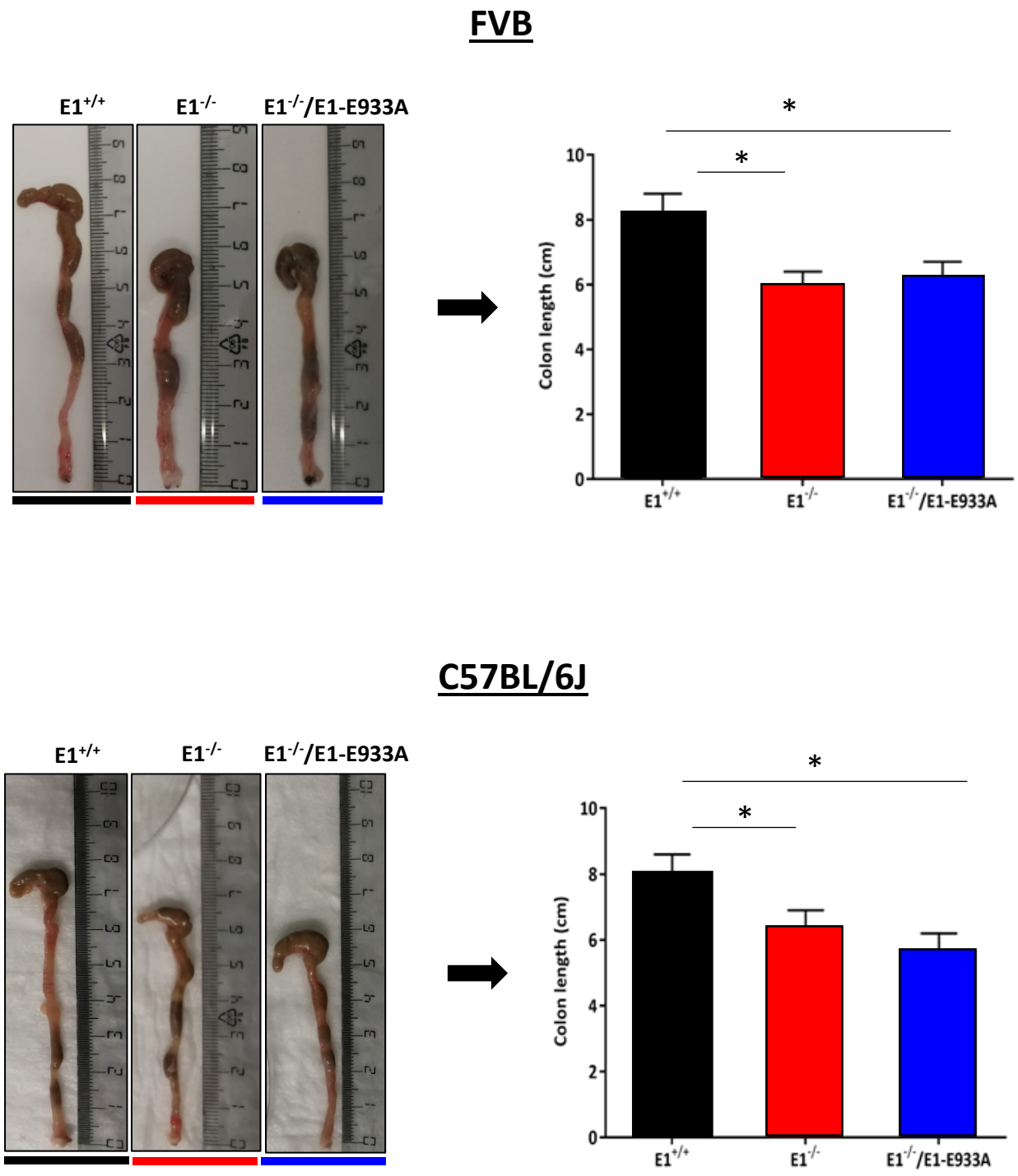

Figure 25: Clinical and macroscopic evaluation of inflammatory status. **(A)** Schematic representation of the regiment used to induce experimental chronic colitis characterized by three cycles of 2% DSS somministrations in drinking water; inflammatory status was daily evaluated by the DAI clinical index **(B)** and after necroscopy with the measurement of the colon length **(C)**. Both parameters indicate that *E1*$^{-/-}$ and *E1*$^{-/-}$/E1-E933A mice were more inflamed compared to *E1*$^{+/+}$ in both treated strains. (mean ± SD), **P* < 0.05 (Student's t test).

Regarding MEICS index, *E1*$^{-/-}$ and *E1*$^{-/-}$/E1-E933A mice presented more severe mucosal injury, fibrosis and higher colitis scores respect to *E1*$^{+/+}$ animals and these differences were statistically significant (Figure 26 A). As reported in Figure 26 B, also through endoscopy it was possible to appreciate the differences between mice with different genotypes; *E1*$^{-/-}$ and *E1*$^{-/-}$/E1-E933A mice presented thick mucosa with typical inflammatory granular pattern, a lot of fibrin accumulation, bleeding and changes in vascularization. On the contrary, *E1*$^{+/+}$ littermates had transparent mucosa, good vascular architecture and very moderate granularity.

A.

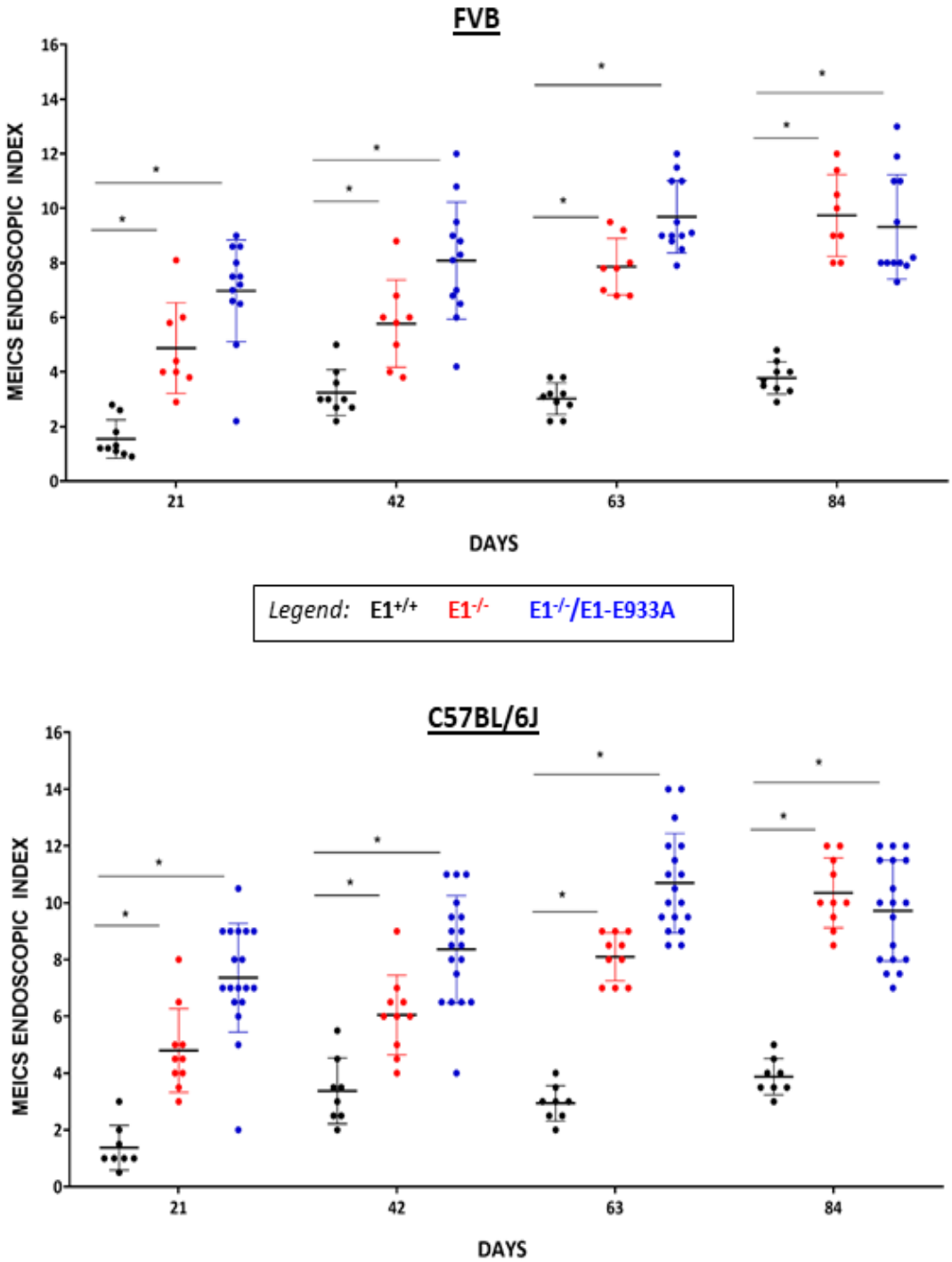

B.

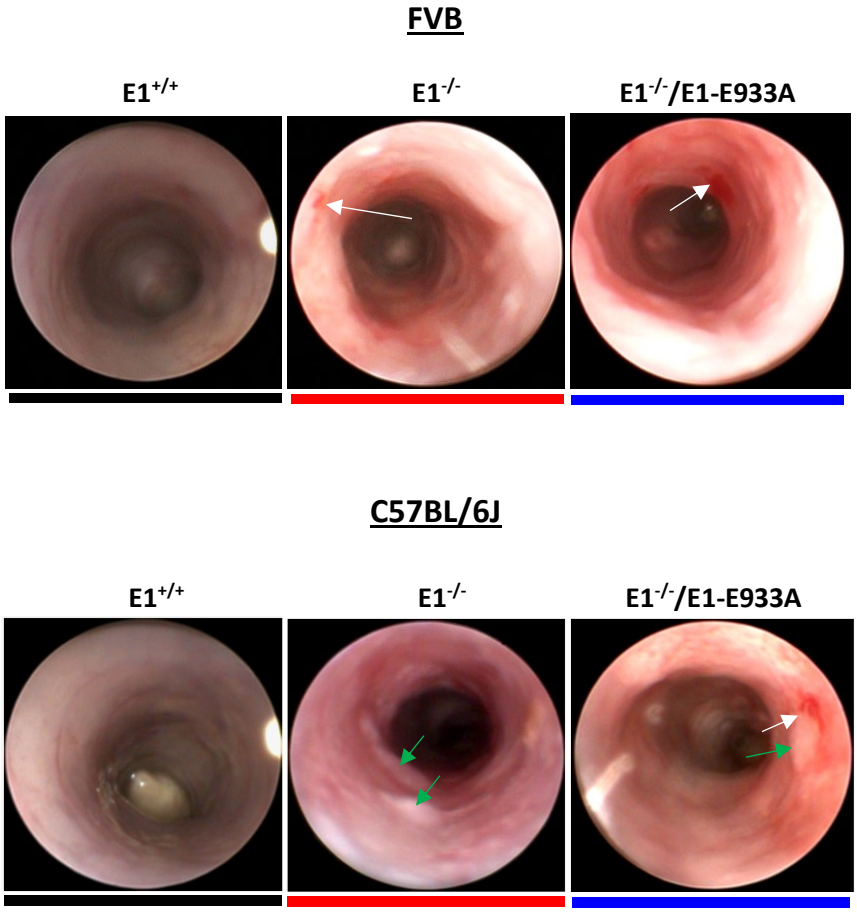

Figure 26: Endoscopic assessment of colitis severity. (A) MEICS endoscopic index was performed at specific time point: 21, 42, 63 and 84 days in order to evaluate the colitis severity. In **(B)** panel of endoscopy images performed at day 84 before sacrifice is reported. In both FVB and C57BL/6J mice the inflammatory extent was greater in *E1*$^{-/-}$ and *E1*$^{-/-}$/E1-E933A mice compared to *E1*$^{+/+}$ animals. Furthermore, *E1*$^{-/-}$ and *E1*$^{-/-}$/E1-E933A mice present typical signs of inflammation including bleeding (white arrows), fibrin accumulation (green arrows), thick mucosa and alterated vascular pattern. **P* < 0.05 (Student's t test).

3.2. Blood count evaluation

Blood samples, immediately collected after euthanasia from all treated mice, were analyzed in collaboration with the staff of the Immunopathology and Oncologic biomarker Division of Centro di Riferimento Oncologico (CRO), IRCCS, Aviano. By means of this analysis we aimed to better understand the inflammatory status and the differences in blood cell amount among EMILIN1 genetic backgrounds.

Hematology values included both the total amount of red blood cells (RBCs) and white blood cells (WBCs); RBCs decreased in all three genotypes compared to the normal basal values of untreated mice and, on the contrary, WBCs slightly increased. Among the genotypes analyzed, in *E1*$^{-/-}$ and *E1*$^{-/-}$/E1-E933A blood there was a general increase, even if not statistically significant, of inflammatory cells, corresponding positively to the clinical in vivo evaluation (DAI and MEICS) compared to *E1*$^{+/+}$ samples (Figure 27).

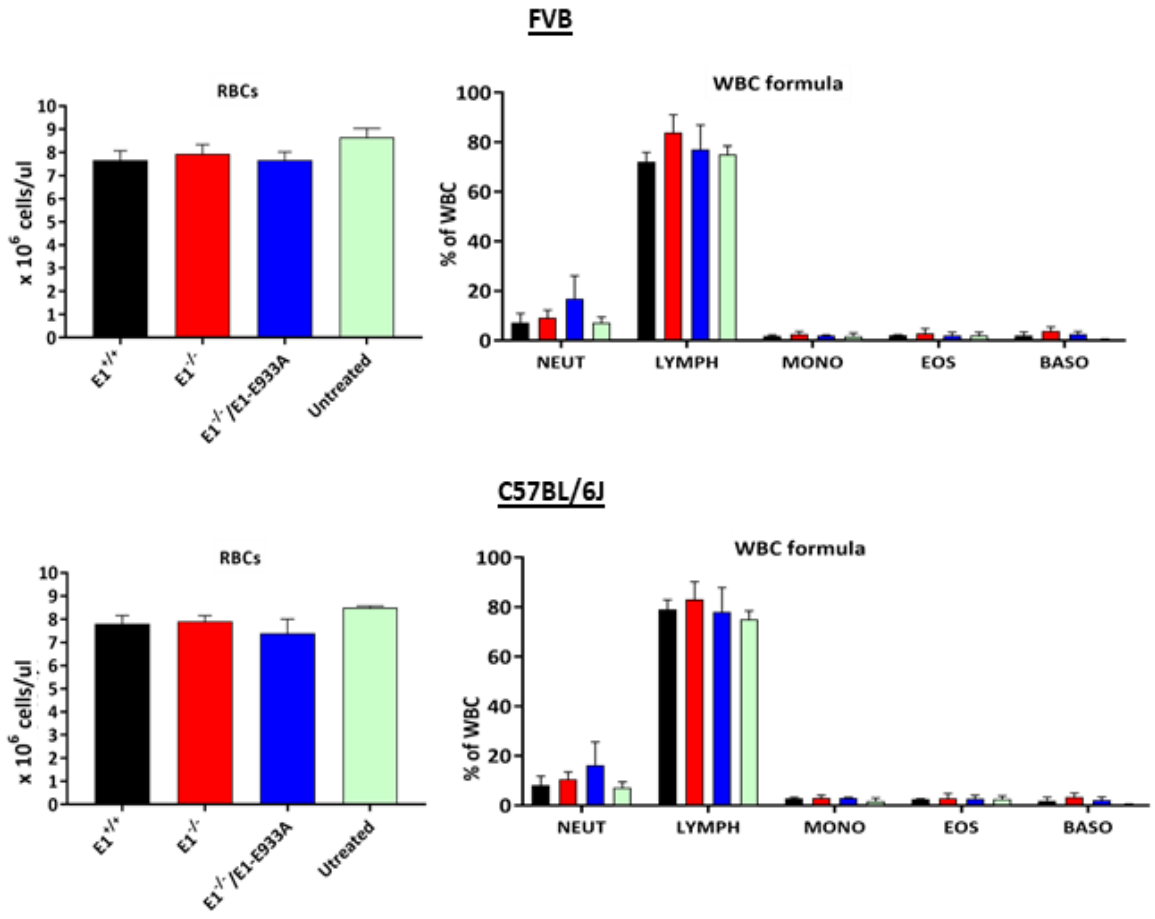

Figure 27: Differences in blood cell amounts between *E1*$^{+/+}$, *E1*$^{-/-}$ and *E1*$^{-/-}$/E1-E933A DSS treated mice. At the end of DSS treatments, blood from all treated mice was collected by intracardiac withdrawal. WBC formula represents the evaluation of each subpopulation which belongs to WBCs (neutrophils, lymphocytes, monocytes, eosinophils, basophils). There is a slight increase in WBCs in *E1*$^{-/-}$ and *E1*$^{-/-}$/E1-E933A mice respect to both *E1*$^{+/+}$ and untreated animals.

3.3. Histopathological evaluation of inflammation extent

Histopathological and immunohistochemical analyses were performed in collaboration with Prof. Scanziani at University of Milan, on paraffin embedded samples. For histopathology evaluation, colon samples were stained with H&E and then two specific parameters were evaluated. The first was the *epithelial damage* that consists in the loss of epithelial layer of the enteric mucosa; the second one was the *lamina propria infiltrate* that corresponds to the presence of infiltrating inflammatory cells within the lamina propria.

Both parameters allowed us to establish that *E1*$^{-/-}$ and *E1*$^{-/-}$/E1-E933A treated mice were more responsive to the colitis induction, with a worse histopathological status respect to the *E1*$^{+/+}$ counterparts. In fact, in both FVB (Figure 28 A) and C57BL/6J (Figure 28 B) strain, *E1*$^{-/-}$ and *E1*$^{-/-}$/E1-E933A mice had extensive epithelial damage, that in some cases led to squamous metaplasia. As reported in literature epithelial alteration takes part of the setting of UC, usually in the distal rectal mucosa, but its characteristic endoscopic appearance has been described rarely (**Fu et *al.*, 2008**). Moreover, *E1*$^{-/-}$ and *E1*$^{-/-}$/E1-E933A mice also lost their normal architecture, since the crypts were not well defined but appeared irregular. On the other hand, *E1*$^{+/+}$ mice displayed a normal mucosa architecture with defined unaffected crypts, which looked very similar to that of *E1*$^{+/+}$ untreated mice. Thanks to general quantitative analysis of the lamina propria infiltrates we also detected the presence of a greater number of inflammatory recruited cells in *E1*$^{-/-}$ and *E1*$^{-/-}$/E1-E933A treated mice compared to the *E1*$^{+/+}$ counterparts (Figure 28 C). We then performed immunohistochemical staining to characterize the infiltrates.

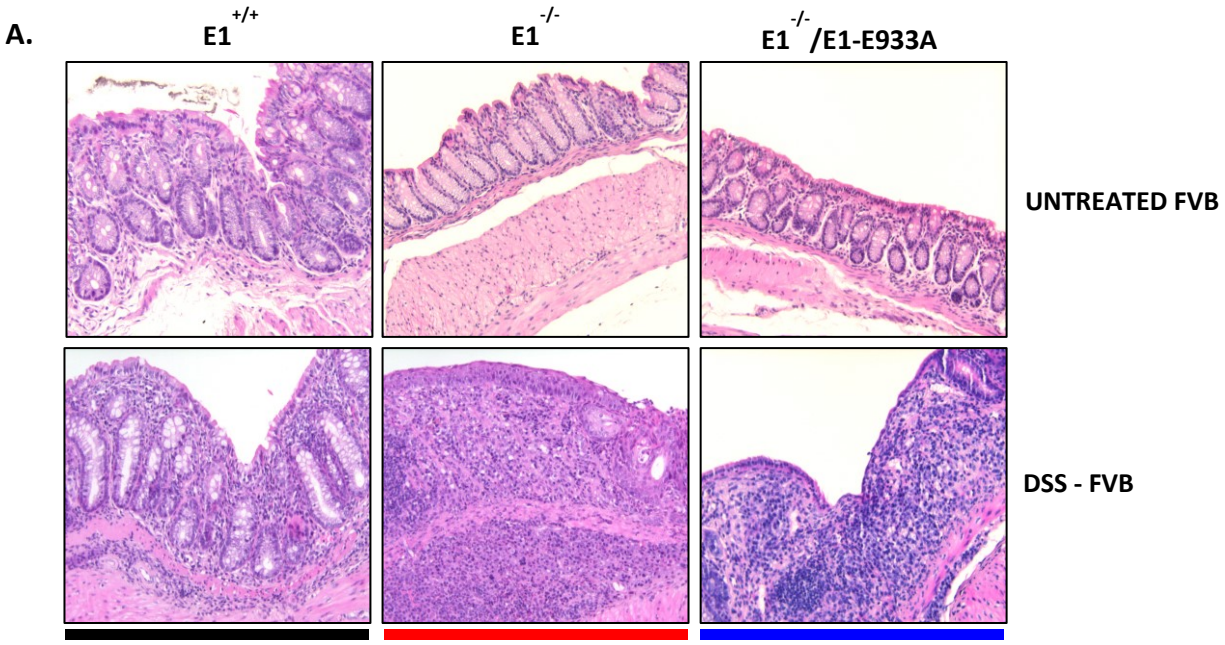

B.

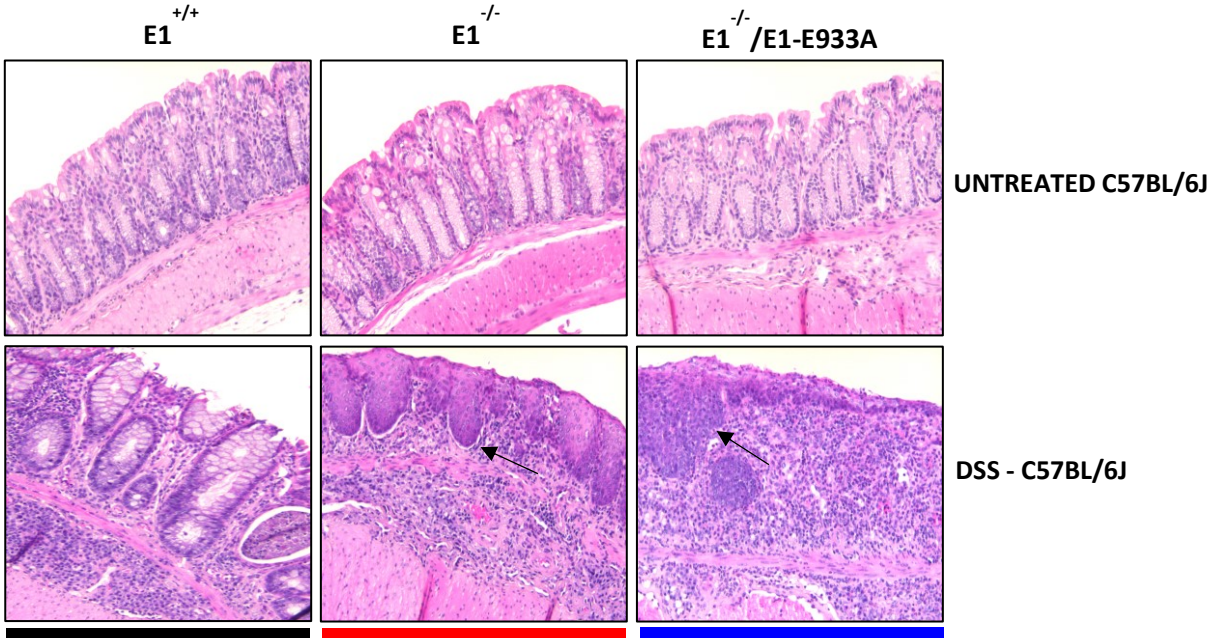

C.

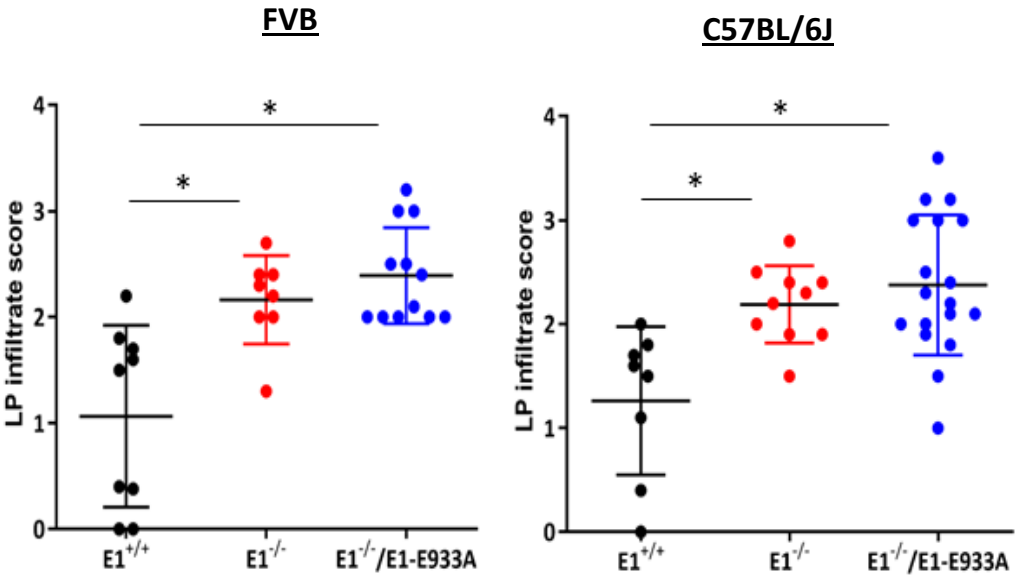

Figure 28: Histopathological analysis of colonic sections of both untreated and DSS *E1*$^{+/+}$, *E1*$^{-/-}$ and *E1*$^{-/-}$/E1-E933A treated mice. Epithelial damage **(A** and **B)** and lamina propria (LP) infiltrate **(C)** were evaluated as reported in Material&Methods. In both FVB and C57BL/6J strains there is an extensive epithelial damage and higher number of inflammatory recruited cells in *E1*$^{-/-}$ and *E1*$^{-/-}$/E1-E933A treated mice respect to *E1*$^{+/+}$ animals. Black arrows indicate cases of squamous metaplasia. **P* < 0.05 (Student's t test). Original magnification 400x.

3.4. Immunohistochemical evaluation of inflammatory infiltrates

Immunostaining with specific antibodies was performed on serial sections. As reported in both graphs and images of Figure 29, the global trend was characterized by an increase in inflammatory population. In fact, $CD3^+$ and $CD45/B220^+$ cells increased in *E1*$^{-/-}$ and *E1*$^{-/-}$/E1-E933A treated mice compared to the *E1*$^{+/+}$ counterparts (Figure 29 A and B); Ly6G staining revealed also a slight increase in granulocytes and neutrophil population in *E1*$^{-/-}$ and *E1*$^{-/-}$/E1-E933A treated mice (Figure 29 C) as well for macrophagic infiltrate revealed by Iba1 staining (Figure 29 D). In any case, no inflammatory population was statistically significantly increased in but not in *E1*$^{-/-}$ and *E1*$^{-/-}$/E1-E933A mice compared to *E1*$^{+/+}$ animals.

Thanks to this analysis, we concluded that there was a much more extensive inflammation in *E1*$^{-/-}$ and *E1*$^{-/-}$/E1-E933A treated mice compared to the *E1*$^{+/+}$ counterparts. However, we were not been able to discriminate a specific inflammatory cell population that could predominantly drive a major and consistent development of tumors in a two-steps colon carcinogenesis model.

A.

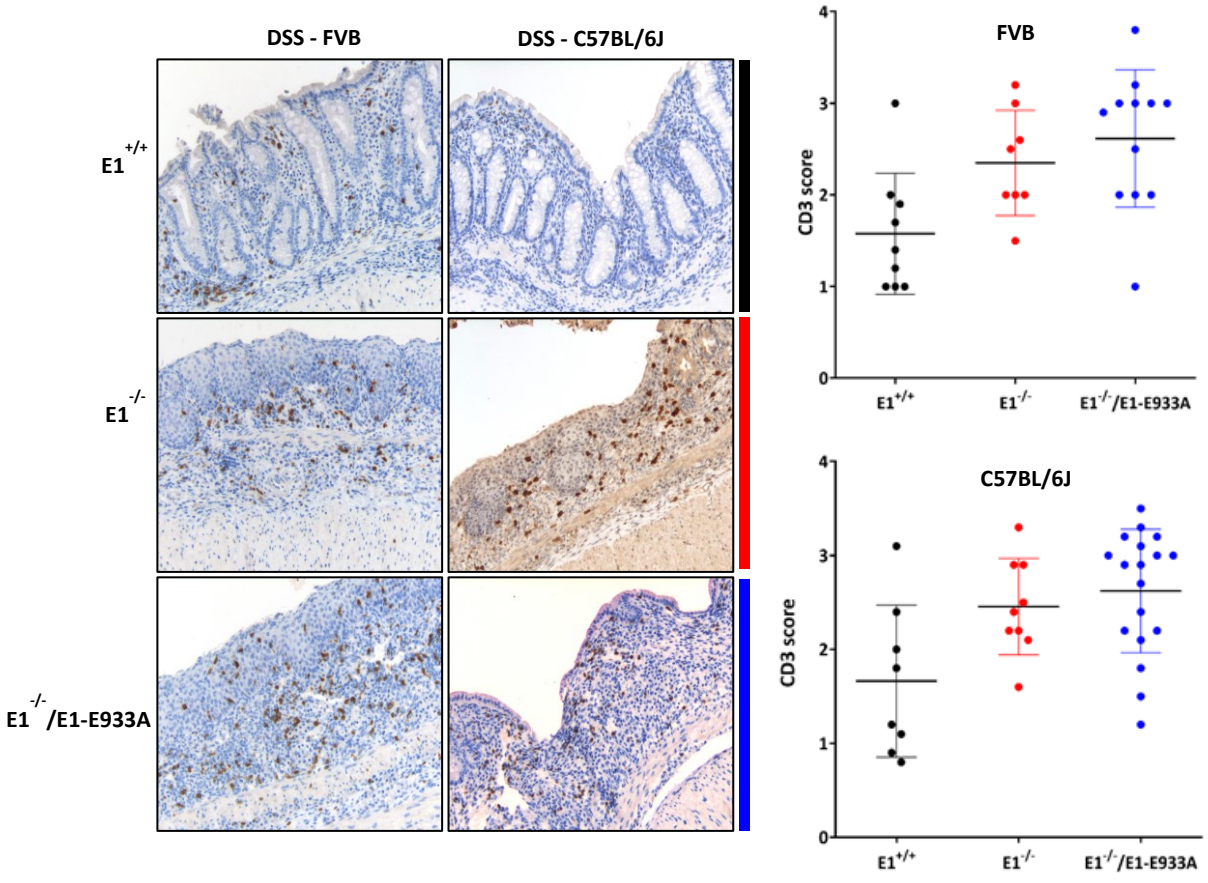

B.

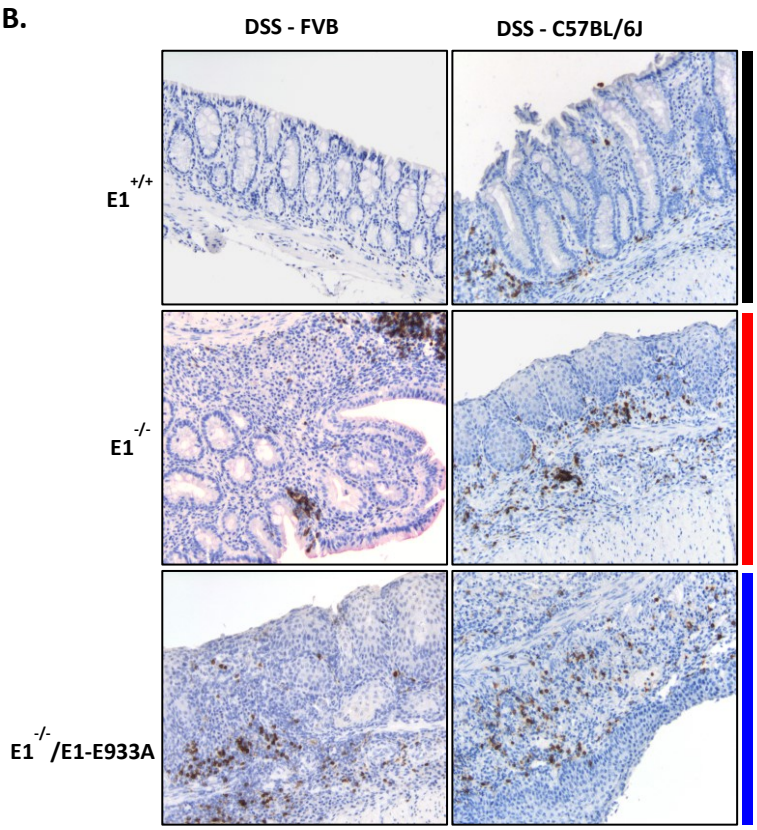
DSS - FVB
DSS - C57BL/6J
E1+/+
E1-/-
E1-/-/E1-E933A

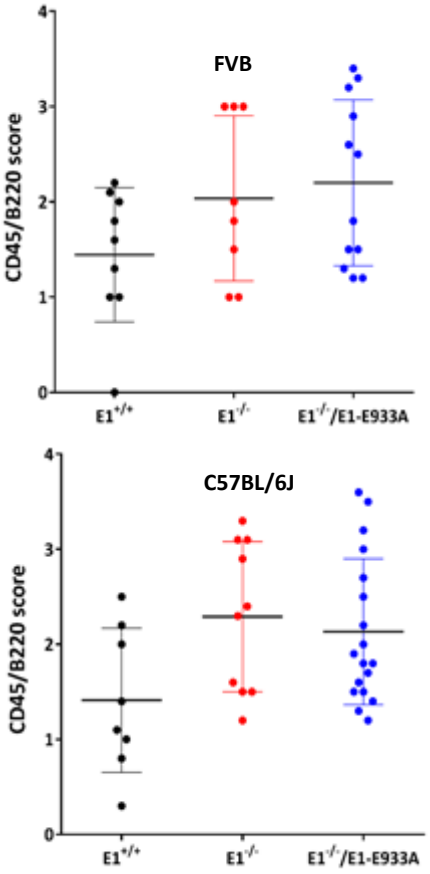
FVB
C57BL/6J
CD45/B220 score
E1+/+
E1-/-
E1-/-/E1-E933A

C.

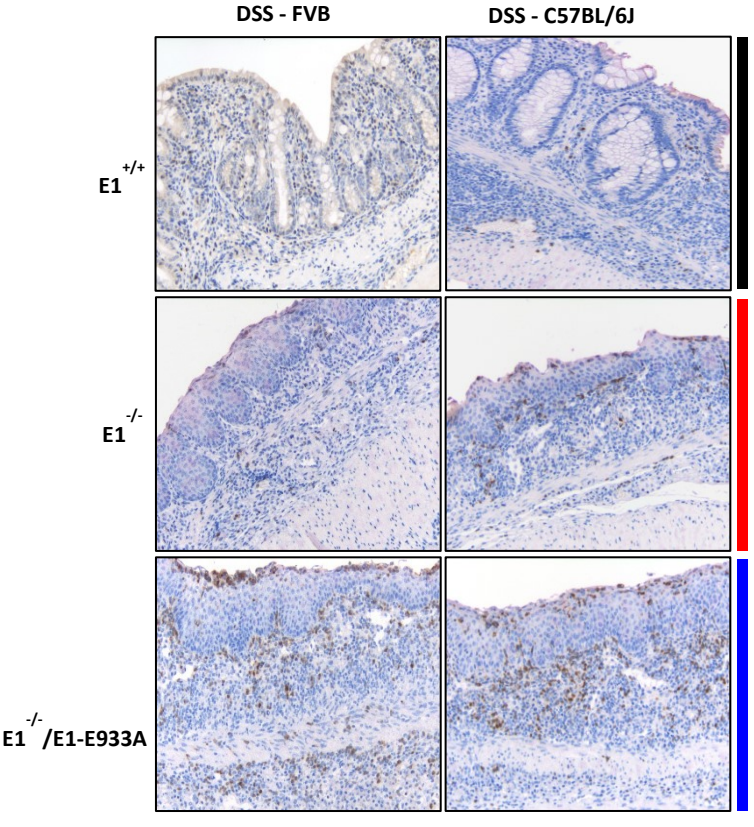
DSS - FVB
DSS - C57BL/6J
E1+/+
E1-/-
E1-/-/E1-E933A

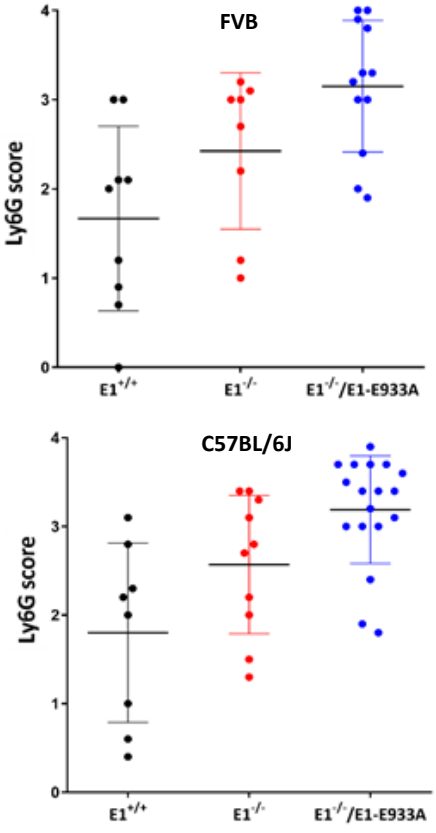
FVB
C57BL/6J
Ly6G score
E1+/+
E1-/-
E1-/-/E1-E933A

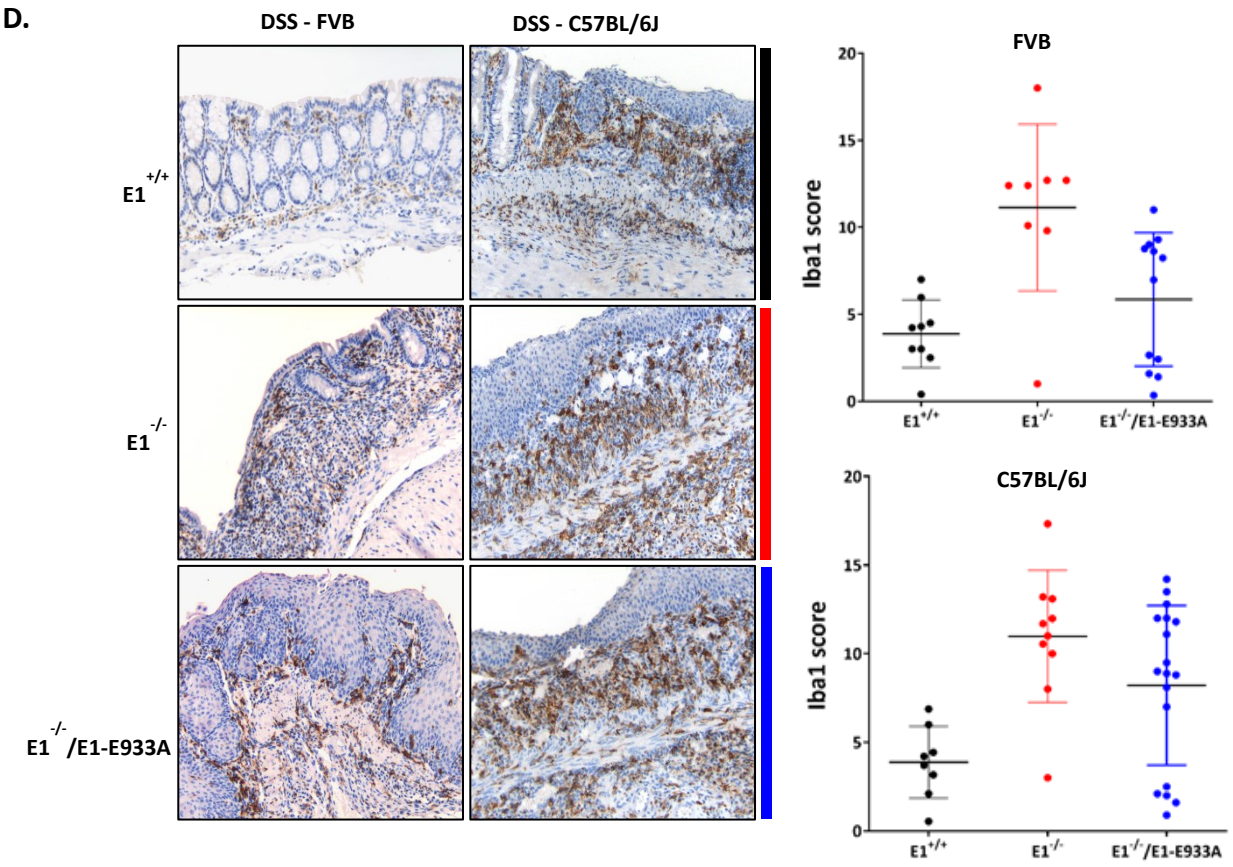

Figure 29: Immunohistochemical analysis using specific marker of inflammation. *E1*$^{+/+}$, *E1*$^{-/-}$ and *E1*$^{-/-}$/E1-E933A DSS colonic samples of DSS-treated mice were analyzed (as indicated in Material&Methods) with Ab anti CD3 **(A)**, anti CD45/B220 **(B)**, anti Ly6G **(C)** and anti Iba1 **(D)** in order to better evaluate the inflammatory infiltrate. In both analyzed strains, there is an increase of all population considered in *E1*$^{-/-}$ and *E1*$^{-/-}$/E1-E933A mice compared to *E1*$^{+/+}$animals. No inflammatory population was statistically significantly increased. Original magnification 400x.

3.5. RNA-sequencing and bioinformatic elaboration

Given the different outcome between *E1*$^{+/+}$ and *E1*$^{-/-}$/E1-E933A mice, we planned to investigate their gene expression profile with an NGS approach, after the DSS-induced colitis treatment. The RNA-sequencing analysis was performed at BMR Genomics and starting from the output of this analysis, in collaboration with the University of Padova, a list of 2100 differentially expressed genes (DEGs) was generated using the bioinformatic DeSeq package (Figure 30).

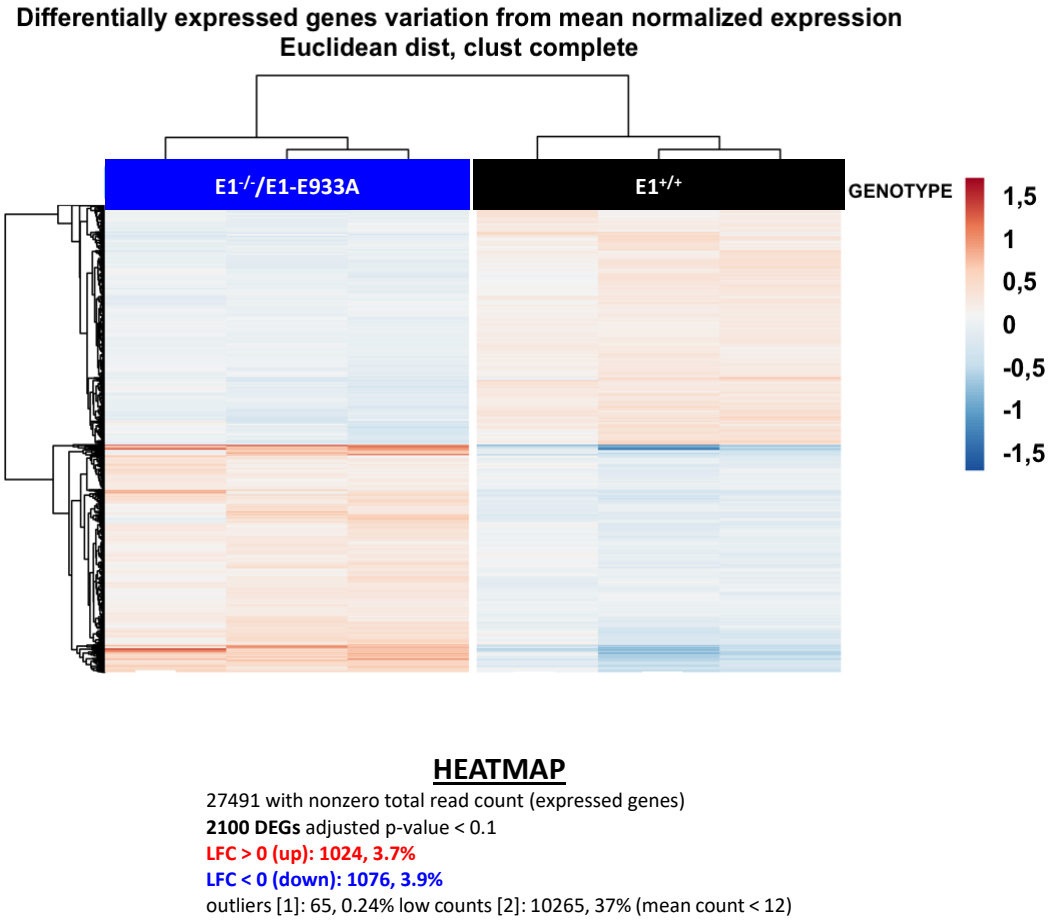

Figure 30. HeatMap of DEGs in *E1*$^{+/+}$ and *E1*$^{-/-}$/E1-E933A mice after DSS-induced experimental colitis. A planned comparison between *E1*$^{+/+}$ and *E1*$^{-/-}$/E1-E933A mice was performed in order to detect DEGs; the HeatMap, a graphical representation of data where the individual values contained in a matrix are represented as colors (red for up-regulation and blue for down-regulation). The list of 2100 DEGs was obtained with DeSeq2 program using an adjusted p-value < 0.1. LFC (log2 fold change).

On this list of DEGs, a first classical and functional enrichment using the David software was performed. Thanks to this tool, that is based on grouping in the same pathway all the genes that present common features, it was possible to identify several altered pathways. Among these, we discovered as up-regulated several inflammatory response genes and down-regulation of some cell-cell adhesion molecules in *E1*$^{-/-}$/E1-E933A (Figure 31 A).

All genes clustered in these pathways were then manually annotated and analyzed from a molecular point of view; as reported in the table of Figure 31 B and C, IL-1α and β, important inflammatory mediators, that we considered crucial and interesting genes in this context, were upregulated. This was in line with the trend of *E1*$^{-/-}$/E1-E933A mice that were more inflamed after DSS treatment respect to the *E1*$^{+/+}$ mice. Among the downregulated genes, we focused our attention on LYVE-1, a marker of lymphatic vessels, since lymphatic dysfunction is a well-established feature of human and experimental IBD.

A.

DAVID software

Annotation Cluster 1	Enrichment Score: 6.786422668688708			
Category	Term	Count	%	PValue
GOTERM_BP_FAT	GO:0007155~cell adhesion	94	5,040214477	1,78E-08
GOTERM_BP_FAT	GO:0022610~biological adhesion	94	5,040214477	1,96E-08
GOTERM_BP_FAT	GO:0016337~cell-cell adhesion	44	2,35924933	1,25E-05

Annotation Cluster 6	Enrichment Score: 3.8336180423490727			
Category	Term	Count	%	PValue
GOTERM_BP_FAT	GO:0009611~response to wounding	61	3,27077748	1,56E-06
GOTERM_BP_FAT	GO:0006954~inflammatory response	37	1,983914209	8,50E-04

B.

UP-REGULATED GENES

Response to wound - Inflammatory response (Annotation Cluster 6)

Symbol	log_2FC
ARG1	1,82
CXCL5	1,63
IL1A	1,12
CXCL3	0,77
IL1B	0,69

C.

DOWN-REGULATED GENES

Cell adhesion, Biological adhesion, cell-cell adhesion (Annotation Cluster 1)

Symbol	log_2FC
Lama2	-0,34
Cldn7	-0,49
Cldn3	-0,64
Cdh17	-0,64
Pcdh15	-0,68
➡ Lyve1	-0,70
Col14a1	-0,92

Figure 31: Important alterated pathways identified after functional enrichment with DAVID software. **(A)** Annotation Clusters 1 and 6 obtained with the functional enrichment DAVID that assembles genes with common features within same pathways. Tables of up-regulated genes **(B)** belonging to response to wound and inflammatory response pathways and down-regulated genes **(C)** of biological and cell-cell adhesion pathways. The black thick arrows highlight the up-regulated (IL-1α and β) and down-regulated (Lyve1) that we found interesting for this project.

3.6. Analysis of cytokines and chemokines

In order to determine and validate the levels of inflammatory response, proinflammatory cytokines and chemokines have been validated in the DSS-induced experimental colitis model.

The supernatant fluids obtained from the colon of each treated mouse was analyzed using a commercially available panel of Bio-Plex Multiplex System. The results coming from this analysis revealed that, among all the cytokines and chemokines considered, there were not statistically significant differences between *E1*$^{+/+}$ and *E1*$^{-/-}$/E1-E933A animals. Anyway, only IL-1α and β and IL-6 showed a slight increase in their expression levels (Figure 32). Considering that these ILs are all implicated as pro-inflammatory cytokines in chronic inflammation processing, these results are in line with all the others previously described, i.e. that the inflammatory status was worst and more extensive in *E1*$^{-/-}$/E1-E933A animals than in *E1*$^{+/+}$ counterpart.

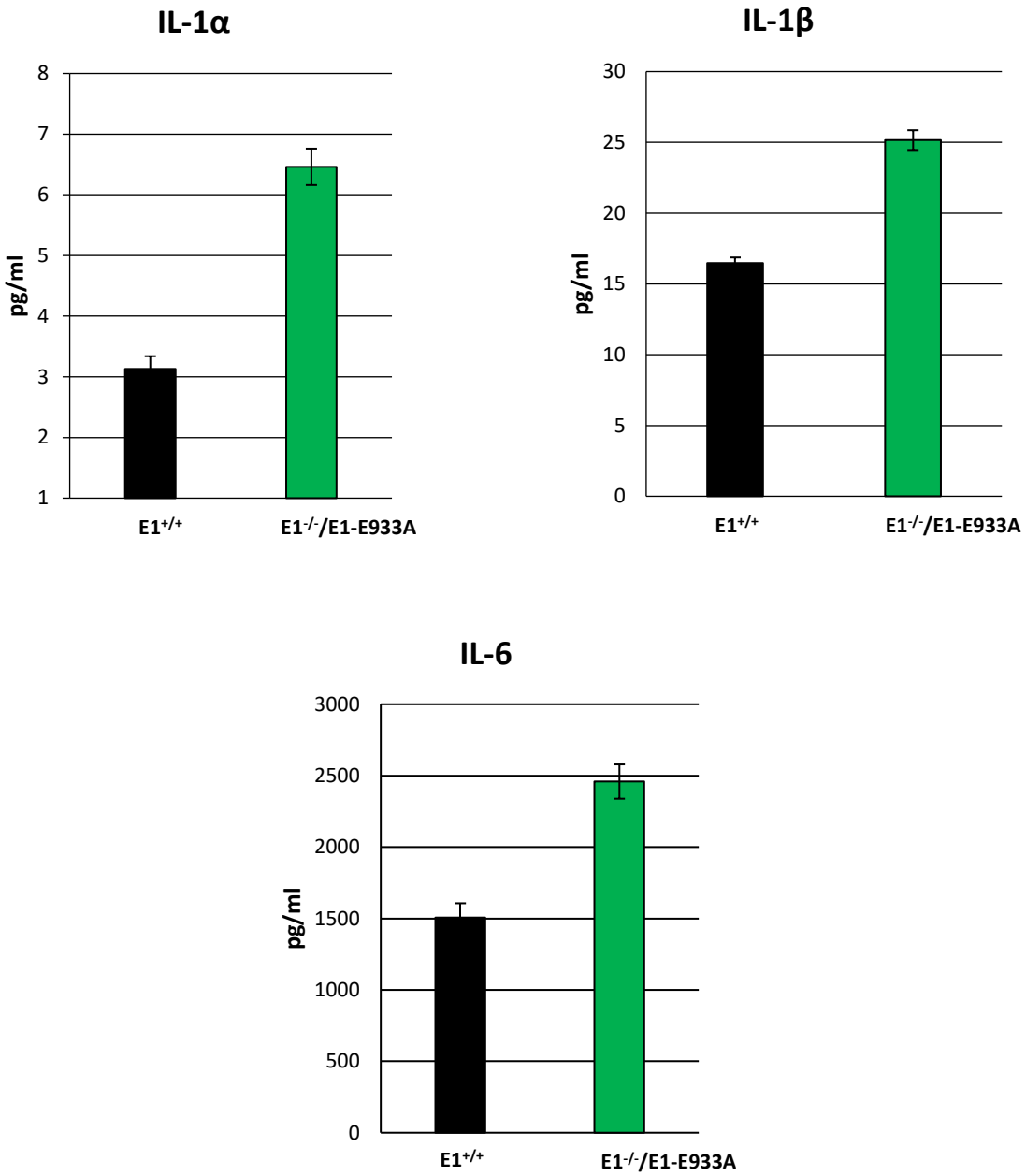

Figure 32: Cytokine expression levels after DSS treatment. Graphs showing the expression levels of some cytokines after treatment with DSS. Supernatant fluids of *E1*$^{+/+}$ and *E1*$^{-/-}$/E1-E933A treated colon were recovered at day 84 and then analyzed. Only IL-1α and β and interleukin 6 had a slight increase in their expression in *E1*$^{-/-}$/E1-E933A mice compared to *E1*$^{+/+}$ counterparts, although not statistically significant.

The cytokines dosage assay validated the results of RNA-seq for the upregulation of IL-1α and β cytokines. In general, all these results gave us information only about the quantity of the infiltrate rather than its specificity. Thus, we were not able to say why in *E1*$^{-/-}$ and *E1*$^{-/-}$/E1-E933A mice the inflammatory status was persistent and also more aggressive respect to *E1*$^{+/+}$. Considering that lymphatic alterations have been recently documented in human and experimental IBD, and that one of the downregulated genes in our RNA-seq analysis was the lymphatic marker LYVE-1, we decided to investigate if a correlation with lymphatic status and inflammation could exist in our model. More precisely, this evidence induced us to better investigate which mechanism regulates the lymphangiogenic role of EMILIN1 in the context of colon inflammation. In fact, as highlighted in the introduction, EMILIN-1 is the first ECM protein identified as structural modulator of lymphatic system.

4. EVALUATION of LYMPHATIC ALTERATIONS

4.1. Lymphatic phenotype in *E1*$^{-/-}$/E1-E933A mouse model

Whole mount immunostaining for podoplanin was performed on normal colon specimens and as shown in Figure 33 A, *E1*$^{+/+}$ LVs were well organized with a regular lumen. On the contrary, LVs of both *E1*$^{-/-}$ and *E1*$^{-/-}$/E1-E933A mice formed a dense network and appeared irregular and dilated. In all *E1*$^{-/-}$ and *E1*$^{-/-}$/E1-E933A colonic samples analyzed, we always detected dysmorphic structures and wide lacunae (with lymph leakage) were occasionally present as indicated by the asterisks in Figure 33 A. On the contrary, these structures were not detected in colonic LVs of *E1*$^{+/+}$ mice.

A further analysis on lymphatic collectors and their valves was performed. Whole mount specimens of ears skin were immunostained with anti-podoplanin antibodies. As shown in Figure 33 B, *E1*$^{-/-}$/E1-E933A collectors appeared tortuous and irregular and frequently displayed enlargements when compared with the regular *E1*$^{+/+}$ collectors. Moreover, *E1*$^{-/-}$ and *E1*$^{-/-}$/E1-E933A valves were detectable as narrowed structures, indicating a condition of immature formation. On the other hand, *E1*$^{+/+}$ mice presented well-formed valves with the typical v-shaped appearance (Figure 33 C).

A.

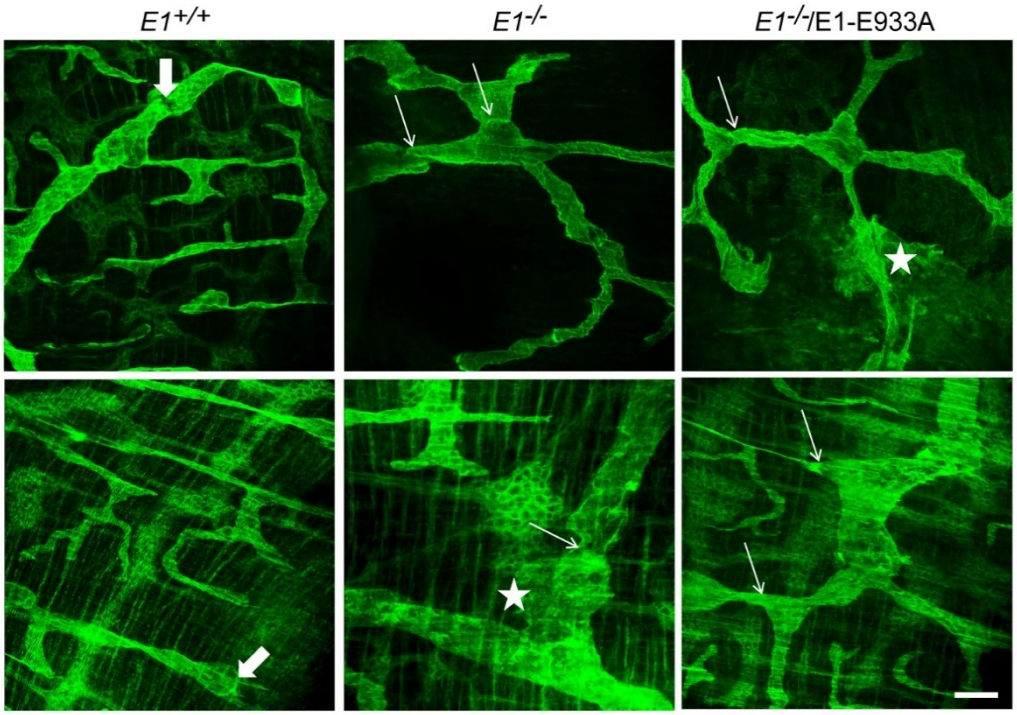

B.

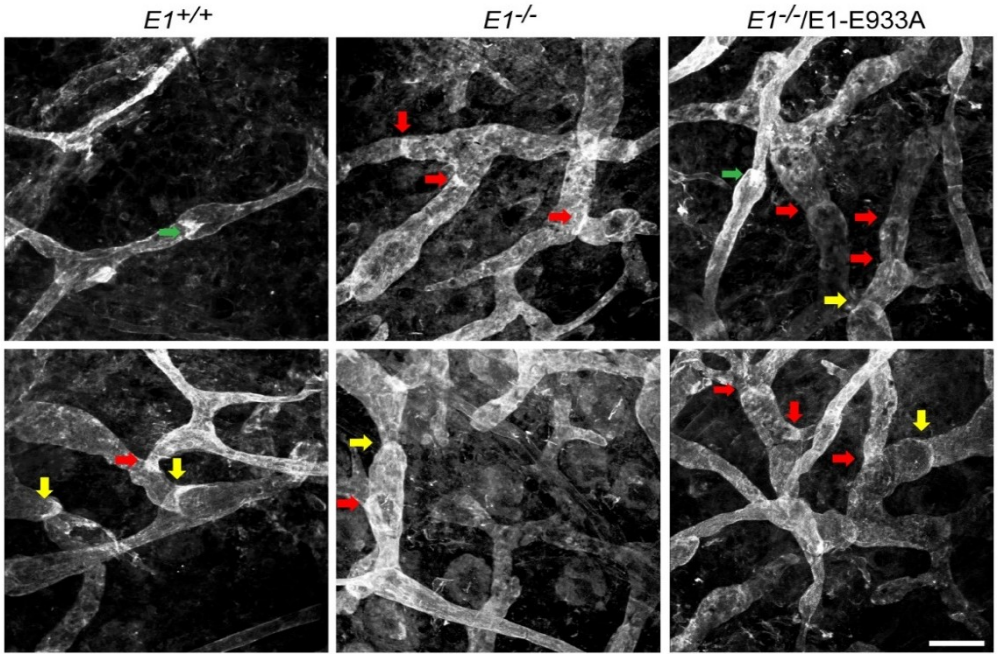

C.

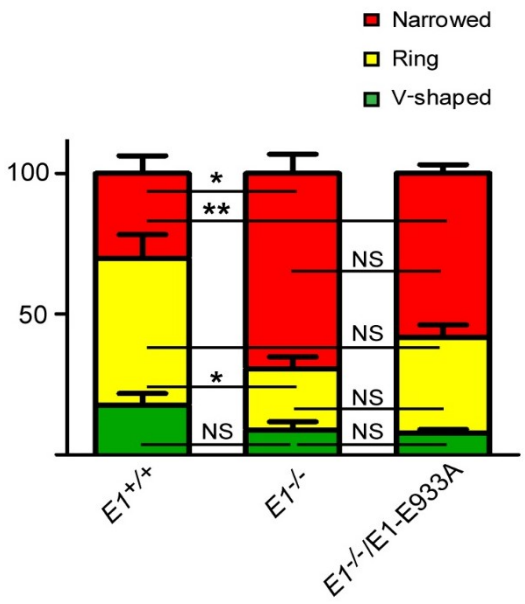

Figure 33. Evaluation of LV morphology. Representative panel of images from whole mount tissues stained with podoplanin. An irregular morphology is detectable in colonic submucosal **(A)** and ear skin **(B)** LVs on both *E1*$^{-/-}$ and *E1*$^{-/-}$ /E1-E933A mice. Thin and thick white arrows in A indicate narrowed /ring-shaped and v-shaped valves, respectively. **(C)** Morphological evaluation of valve shape of adult ear skin LVs. **Green bar**, V-shaped valves; **yellow bar**, ring-shaped valves; **red bar**, narrowed valves (mean ± SD, n=3 animals per genotype, *P < 0.01; **P < 0.001, NS, not significant, two-way ANOVA test). The colored arrows in B reflect the colored bars in C. Scale bar: 50 µm.

The situation was somewhat different when we observed lymphatics after DSS treatment. Whole mount analysis made on mesenteric LNs isolated from *E1*$^{+/+}$, *E1*$^{-/-}$ and *E1*$^{-/-}$/E1-E933A DSS treated mice revealed that *E1*$^{+/+}$ animals displayed a pro-lymphangiogenic capacity as evidenced by the high number of sprouting capillary structures (Figure 34, white thick arrows). This observation suggesting that the ability of *E1*$^{+/+}$ animals to react to an inflammatory insult could induce a proper lymphangiogenic response. The EMILIN-1 deposition, very close to budding structures (yellow signals), confirmed that the protein was important in structurally guiding new LVs. On the contrary, buddings structures were very rare and not well shaped in *E1*$^{-/-}$ and *E1*$^{-/-}$/E1-E933A counterpart indicating that anomalies on lymphatics led to an inability to react in the formation of competent LVs, probably due to the defects in lymphangiogenesis in these genetic backgrounds.

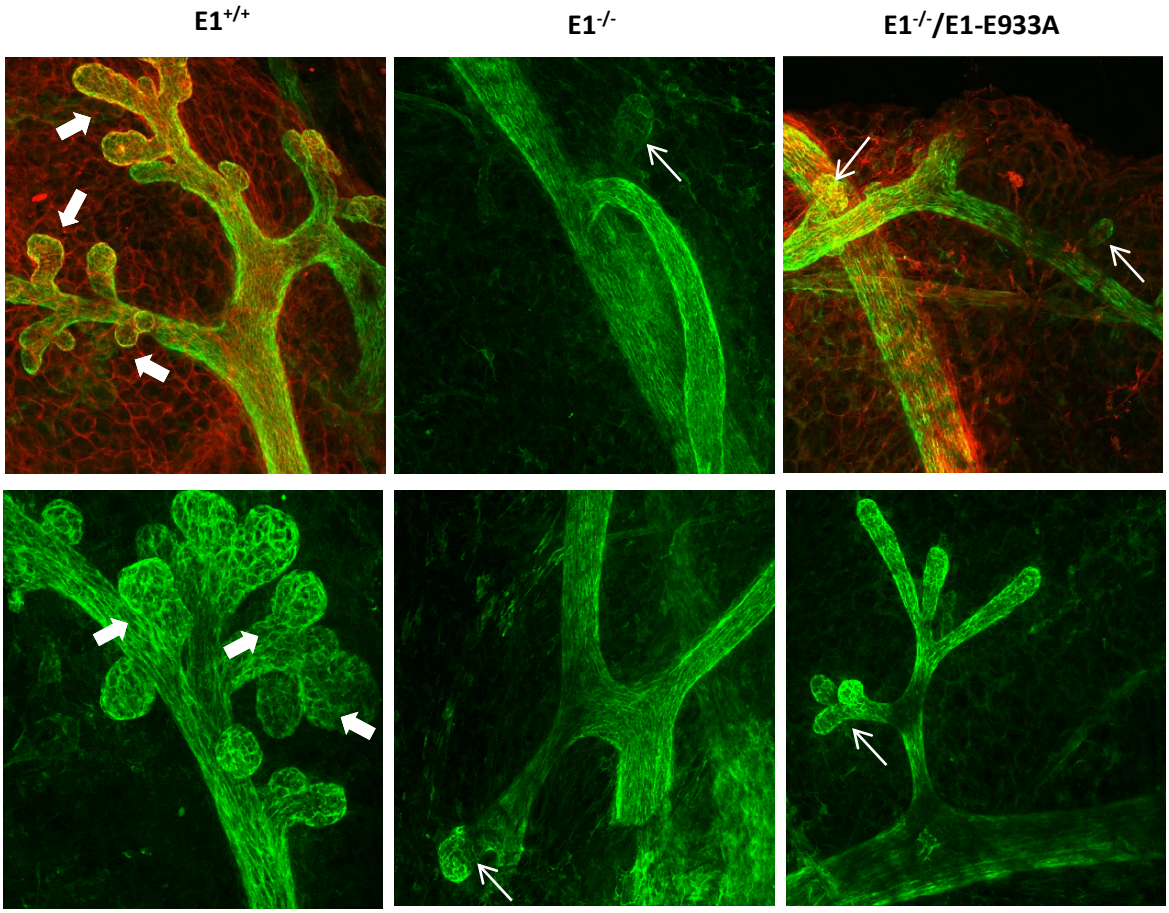

Figure 34: Structural anomalies in LVs after DSS-induced experimental colitis. Panel of DSS whole mount mesenteric LNs staining for podoplanin (green) and EMILIN-1 (red); a correct lymphangiogenesis is visible only in *E1*$^{+/+}$ animals, as represented by thick white arrows that indicate buddings structures where a clear EMILIN-1 localization (yellow signals) is evident. On the other hand, *E1*$^{-/-}$ and *E1*$^{-/-}$/E1-E933A mice show rare and not-well shaped buddings (thin arrows) and also a decrease number of sprouting capillaries. Original magnification 200x.

4.2. LVs density evaluation

The IF analysis on the colonic mucosae of *E1*$^{-/-}$ and *E1*$^{-/-}$/E1-E933A mice after DSS and AOM/DSS treatments, showed a several altered and abnormal condition (Figure 35), confirming the histopathological analysis and a reduced number of podoplanin positive colonic LVs. Again, as already described for mesenteric LNs, in a context of strong inflammatory stimulus, *E1*$^{+/+}$ mice were able to induce a lymphangiogenic response, whereas in *E1*$^{-/-}$ and *E1*$^{-/-}$/E1-E933A animals the presence of less LVs indicated a defect in the formation of a new lymphatic network. This incapacity and the consequent insufficient lymph drainage could explain why a massive inflammation persisted in *E1*$^{-/-}$ and *E1*$^{-/-}$/E1-E933A mice. These results also confirmed the data emerged from the RNA-seq analysis about the down-regulation of the lymphatic marker LYVE-1.

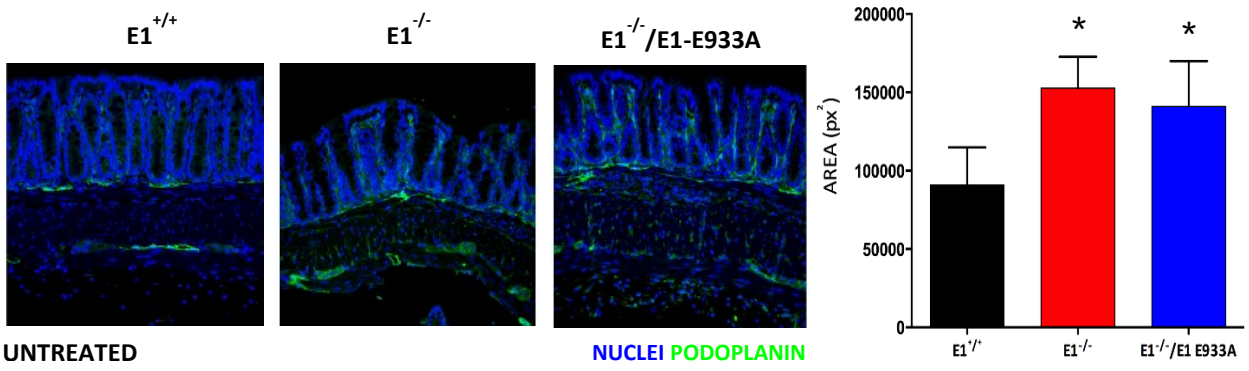

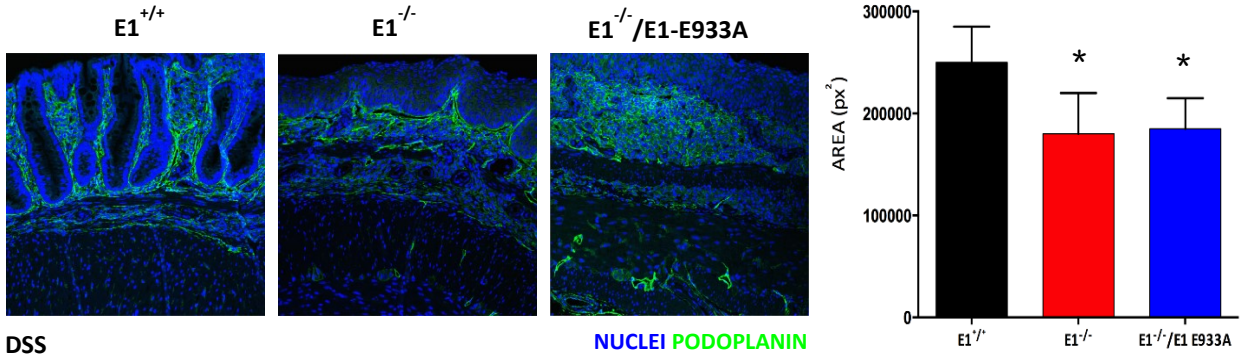

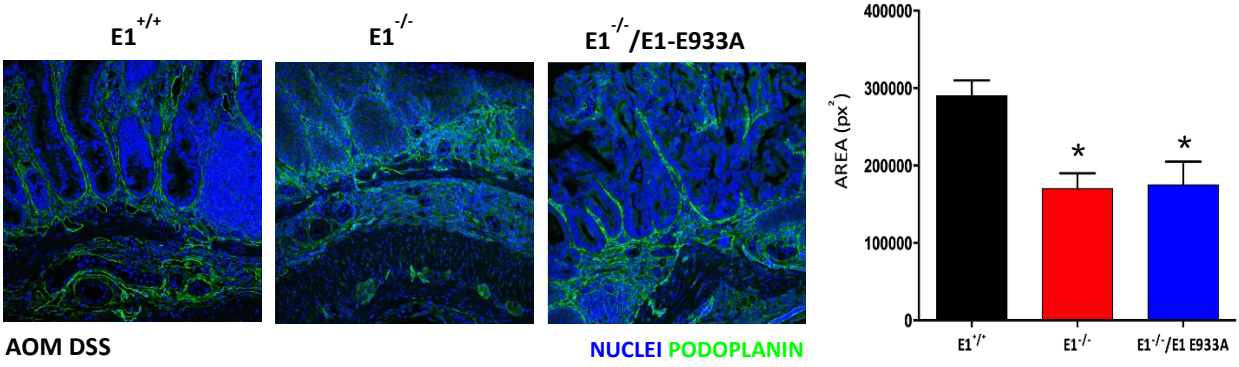

Figure 35. LV density alteration reflects the inability to induce a correct lymphangiogenesis in *E1*$^{-/-}$ and *E1*$^{-/-}$/E1-E933A mice. Representative panel of podoplanin staining of colonic LVs in normal condition and after induction of experimental colitis and colon carcinogenesis. In normal condition, *E1*$^{+/+}$ show less podoplanin positive LVs compared with *E1*$^{-/-}$ and *E1*$^{-/-}$/E1-E933A mice. After stimulus induction, the situation is the opposite: the density of LVs significantly decreased in *E1*$^{-/-}$ and *E1*$^{-/-}$/E1-E933A. **P* < 0.05 (Student's t test). Original magnification 400x.

4.3. Verification of LVs functionality

To evaluate if all these morphological LV alterations and valve defects could reduce the functionality of fluid movement in *E1*$^{-/-}$/E1-E933A mice, we investigated the drainage ability of mesenteric LVs in normal and DSS treated mice, after oral gavage administration of Bodipy-FL-C16, a fluorescently labeled 16-carbon chain fatty acid, used as a lipid tracer and then specific for visualizing lymphatic structures. In fact, it is packaged into chylomicrons and transported by LVs from the intestine through the mesenteric collecting vessels. Our data showed significantly fewer functional LV in the mesentery of *E1*$^{-/-}$ and *E1*$^{-/-}$/E1-E933A compared to untreated *E1*$^{+/+}$ littermates (Figure 36 A); in fact, we observed significantly fewer and also not well organized fluorescent mesenteric lymphatic vessels in *E1*$^{-/-}$ and *E1*$^{-/-}$/E1-E933A animals. This agreed with what already observed in previous studies that highlighted the presence of unfunctional iliac LNs in *E1*$^{-/-}$ mice (**Danussi *et al.*, 2013; Pivetta *et al.*, 2016**). After DSS-induced acute colitis, *E1*$^{-/-}$ and *E1*$^{-/-}$/E1-E933A (Figure 36 B) presented, an even more compromised situation than when untreated. These results indicated that, in normal conditions, lymphatics were already functionally altered when EMILIN-1 was absent or mutated in the E933 residue of gC1q domain and that the situation got considerably worst, after induction of experimental colitis. The fluorescent dye labeled weakly and faintly the mesenteric LNs (as visible in broken circles) and also collectors were difficult to visualize in both *E1*$^{-/-}$ and *E1*$^{-/-}$/E1-

E933A mice, suggesting that valve morphological anomalies contributed to the reduced mesenteric lymphatic functionality that appeared completely impaired after inflammatory-induced condition.

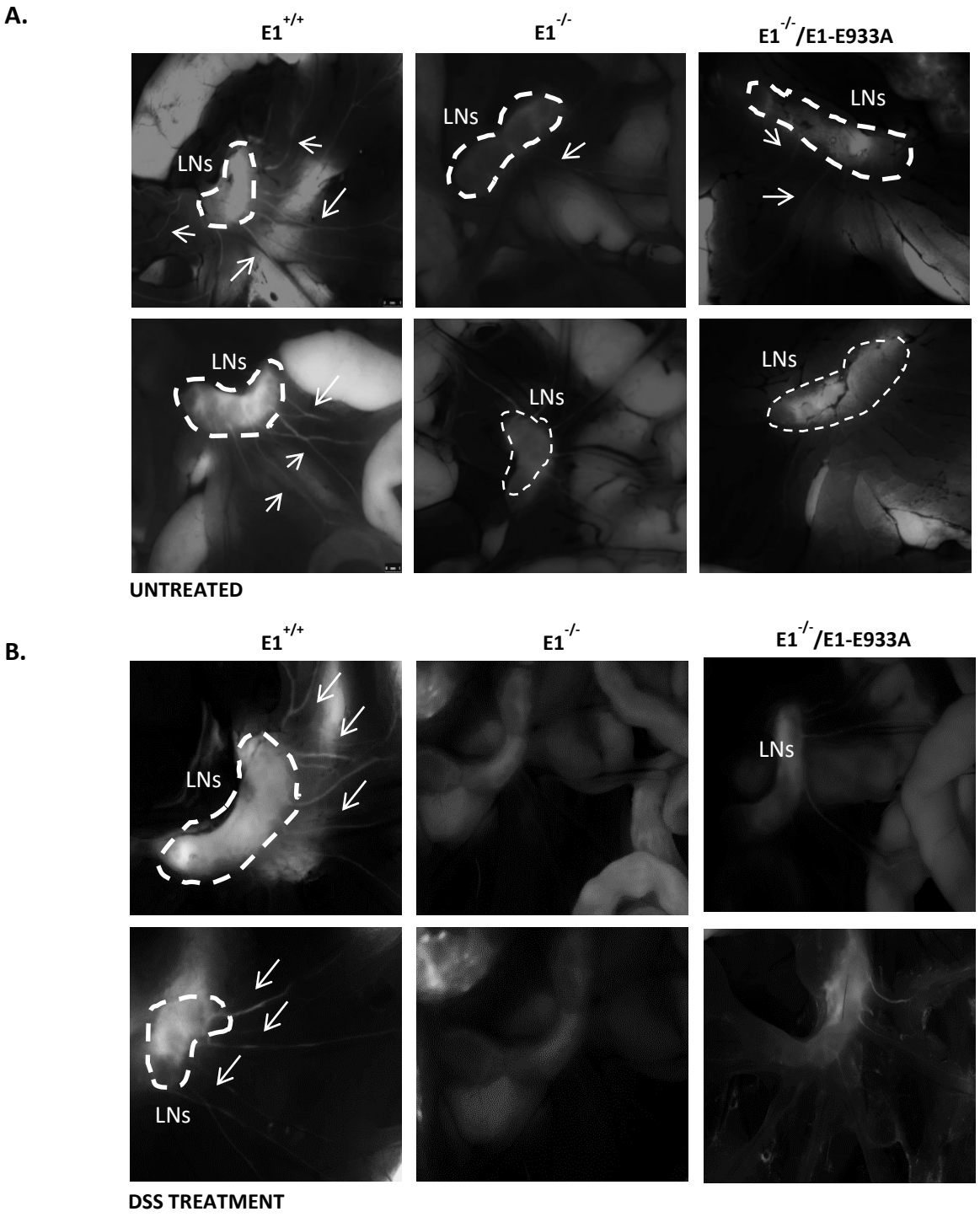

Figure 36. LV structural alterations lead to an unfunctional lymphatic system in *E1*$^{-/-}$ and *E1*$^{-/-}$/E1-E933A. Representative panel of untreated **(A)** and DSS-treated **(B)** mesenteric LNs after oral gavage administration of the fluorescent dye Bodipy-FL-C16. Broken circles indicate LNs and white thin arrows collector vessels. Lymphatics are normal and well-functioning in *E1*$^{+/+}$ mice. On the contrary *E1*$^{-/-}$ and *E1*$^{-/-}$/E1-E933A animals appear not well organized in normal conditions and, after DSS treatment, anomalies seem to be worse, contributing to a completely impaired functionality. Original magnification 10x.

DISCUSSION

During my PhD program, I focused the attention on the importance of structural and functional properties exerted by the ECM glycoprotein EMILIN-1; in particular, I investigated how EMILIN-1 is crucial to control proliferation and to guarantee the regeneration of a competent and well-functioning lymphatic vasculature in the context of inflammatory colon cancer.

To demonstrate that EMILIN-1 represents a structural regulator of a competent vasculature and that it is located in the context of the development and progression on inflammatory colon cancer, we took advantage, in addition to the *E1*$^{-/-}$ mouse model, to the new *E1*$^{-/-}$/E1-E933A transgenic mouse model, in which a mutant human EMILIN-1, unable to be engaged by $\alpha_4/\alpha_9\beta_1$, was expressed. This transgenic mouse represents a strong model compared to that used in the previous studies which were based on the inactivation of the entire protein; in *E1*$^{-/-}$/E1-E933A transgenic mouse, in fact, all the other structural and functional properties of the protein were maintained: *E1*$^{-/-}$/E1-E933A transgenic mice displayed normal TGF-β levels, similar to those of *E1*$^{+/+}$ mice, allowing us to separate the possible effects linked to the regulation of TGF-β from those dependent on EMILIN-1 $\alpha_4/\alpha_9\beta_1$ integrin interaction. Thus, our results on lymphatics alterations were not absolutely consequences of TGF-β mediated effects. Within the characterization approach of the transgenic mouse model we demonstrated the structural and functional importance of the interaction between gC1q and integrin in the regulation of a competent vasculature (**Capuano *et al.,* in press**). The use of this transgenic mouse model also provided evidence that the gC1q/$\alpha_4\beta_1$ interaction was functionally crucial also in a metastatic context, since melanoma cells disseminated more rapidly into *E1*$^{-/-}$/E1-E933A LNs. These results indicated that the E933 residue at the apex of each monomer of gC1q domain was sufficient to favor the dissemination of melanoma cells through its interaction with the integrin, independently from other EMILIN-1 domains.

Only few ECM proteins exert a tumour suppressor function, such as fibulin-2 (**Law *et al.,* 2012**) and EMILIN-1 (**Danussi *et al.,* 2012**). Previous studies demonstrated that, in a skin carcinogenesis model, a target inactivation of *Emilin1* gene, caused an increase of dermal and epidermal proliferation (**Danussi *et al.,* 2011**) and an increase of the number and size of skin tumours (**Danussi *et al.,* 2012**). Thanks to the transgenic model, we first verify if the EMILIN1/$\alpha_4\beta_1$ integrin interaction was able to

exert an antiproliferative and oncosoppressor role also in the colon microenvironment, as occurs in skin. Interestingly, endoscopic analysis as well as post mortem histopathologic evaluation indicated that both *E1*$^{-/-}$ and *E1*$^{-/-}$/E1-E933A mice displayed an increased in tumour burden. In fact, they developed a higher number of tumour (specially high-grade adenoma and GIN) that appeared also bigger and with a more severe phenotype respect to *E1*$^{+/+}$. Thus, these results confirmed the contrasting role of EMILIN-1 towards tumour growth and progression also in the colonic mucosa microenvironment. Furthermore, considering that in *E1*$^{-/-}$/E1-E933A mice the pathological response was the same observed in *E1*$^{-/-}$ mice, we were very confident that the oncosoppressive role of EMILIN-1 was strictly related to the gC1q domain and its interaction with $\alpha_4\beta_1$ or $\alpha_9\beta_1$ integrin, without any interference exerted by TGF-β, whose maturation process is finely regulated by the EMI domain (**Zacchigna et *al.,* 2006**). The most interesting observation coming from the AOM/DSS colon carcinogenesis approach was that *E1*$^{-/-}$ and *E1*$^{-/-}$/E1-E933A treated mice displayed signs of diffuse inflammation in the colonic mucosa respect to *E1*$^{+/+}$ counterpart.

In this scenario, we aimed to understand how the functional and structural properties of EMILIN-1 might be crucial during inflammatory process. As it is known, during the pathogenesis of IBD, both the lamina propria and the epithelial layer are infiltrates by different types of immune cells, which create an inflammatory microenvironment (**Neurath *et al.,* 2014**). Our immunohistochemical analysis actually revealed an increase infiltration of T and B cells, granulocytes and neutrophils population and a slight but not statistically significant increase of macrophages in both *E1*$^{-/-}$ and *E1*$^{-/-}$/E1-E933A mice respect to *E1*$^{+/+}$ counterpart, but there was not the prevalence of a specific cell population. Cytokines are able to induce extensive inflammatory status in the colon (**Francescone *et al.,* 2015**) and this was confirmed also by our RNA-seq analysis, where we found, as up-regulated genes in *E1*$^{-/-}$/E1-E933A mice respect to *E1*$^{+/+}$ counterpart, several inflammatory response genes such us IL-1α and β, that are generally secreted into the inflamed mucosa of IBD by lamina propria dendritic cells and macrophages (**Ng *et al.,* 2011**). These data were important to establish the quantity (rather that the quality) of the infiltrate, indicating that more inflammatory cells probably are the cause that generates higher levels of cytokines and chemokines which, in turn, activate the recruitment of other inflammatory cells, causing maybe a non-resolving chronic inflammatory situation (that is part of the tumor microenvironment in gastrointestinal as well as other tumors, **Danese *et al.,* 2010**) in *E1*$^{-/-}$ and *E1*$^{-/-}$/E1-E933A treated mice. Among genes differentially expressed, we individuated not only genes related to inflammatory pathways, but also several down-regulated

cells-cell adhesion molecules in our transgenic treated mice. Among these, we identified the well-known lymphatic marker LYVE-1. Thus, the contribution of EMILIN-1 in the interplay between lymphatics and inflammation could have a rational base.

This interestingly result induced us to focus our attention on another hot topic: the inflammation-associated lymphangiogenesis. Given that EMILIN-1 is responsible of the maintenance of a correct lymphatic structure and that its gC1q domain is able to induce a correct lymphangiogenesis response, it has become fundamental to understand if the aberrant lymphangiogenesis is only drive by DSS-induced inflammation or if lymphatic dysfunction could contribute to disease exacerbation. To do this, we took advantage to the use of our animal models and whole mount staining of colon specimen indicated that *E1*$^{-/-}$ and *E1*$^{-/-}$/E1-E933A mice displayed an aberrant lymphatic phenotype already in normal conditions. In fact, even before colitis induction, their intestinal LVs presented several lymphatic alterations that were absent in *E1*$^{+/+}$ mice. After inflammatory-induced conditions by DSS treatment we found that only *E1*$^{+/+}$ animals displayed pro-lymphangiogenic capacity and that the functionality of LVs monitored by mesenteric lymphangiography was completely compromised in both *E1*$^{-/-}$ and *E1*$^{-/-}$/E1-E933A mice. It is well known that an expanded lymphatic vasculature is necessary for the resolution of inflammation. This is the situation that we observed for *E1*$^{+/+}$ mice in which the strong stimulus induced by DSS let very likely to the formation of new competent and functional vasculature that in turn could restore the situation to a pre-inflammatory state. On the contrary, *E1*$^{-/-}$ and *E1*$^{-/-}$/E1-E933A animals that, as demonstrated, are characterized by the development of a defective vasculature due to the lack of gC1q/$\alpha_4\beta_1$, when subjected to an inflammatory insult, are not able to induce the formation of new draining vessels. The consequence of this already compromised situation is that *E1*$^{-/-}$ and *E1*$^{-/-}$/E1-E933A mice developed a much more severe inflammatory pattern than *E1*$^{+/+}$ mice. Thus, it is reasonable to think that the massive inflammatory extent observed in *E1*$^{-/-}$ and *E1*$^{-/-}$/E1-E933A models was the consequence of structural and functional lymphatic dysregulation associated with a lack of the functional domain of EMILIN-1.

These results are very important and innovative; the use of these adult models, that to our knowledge are the only ones with an altered lymphatic phenotype, could help to explain how lymphatics anomalies are responsible of the non-resolution of inflammatory state. Thus, overall these data suggest that EMILIN-1, by its multifaceted functions, may be centrally located in the context of the development and progression of inflammatory colon cancer. Our previous study

demonstrated that, in an inflammatory context, EMILIN-1 was subject to degradation by NE released by neutrophils (**Pivetta *et al.,* 2016**); moreover, there are lot of evidences that reported that CRC is characterized by the presence of consistent inflammatory infiltrates, consisting of a lot of immune cells including macrophages and neutrophils that colonized the lamina propria and submucosa (**Shang *et al.,* 2012**). This indicates that during CRC pathogenesis EMILIN-1 and above all its gC1q domain, could be degraded by NE. More importantly, NE is the only enzyme able to fully impair the interaction of gC1q with integrin by cleaving this domain close to the E933 binding site (**Maiorani *et al.,* 2017**). Given that, we hypothesize that local inflammatory response and related gC1q degradation could be important events favoring colon cancer initiation acting in different ways: (I) the degradation would abolish EMILIN1/gC1q oncosoppressor properties; (II) the lack of functional EMILIN1/gC1q domain would favour lymphatic dysfunction and lymphatic spread; (III) lymphatic dysfunction, in turn, would be crucial in increasing inflammatory cascade through the impairment of inflammatory cells drainage. The attempts to block or prevent gC1q degradation could represent the basis for a novel ECM-based pharmacological approach aimed to rescue the control of proliferation and LV normalization.

MATERIAL AND METHODS

1. LIST OF ANTIBODIES

Antibody	Specificity	Target	Manufacturer, Dilution and Application
Primary Rabbit polyclonal AS556	Human (cross-reaction also with murine)	EMILIN-1	Product in our laboratories 1:200 (IF)
Primary Rat monoclonal C11A8	Mouse	*EMILIN-1*	Product in our laboratories 1:100 (IF)
Primary Hamster monoclonal Podoplanin	Mouse	Podoplanin	Abcam 1:400 (IF)
Primary Rabbit polyclonal LYVE-1	Mouse	LYVE-1	Abcam 1:1000 (IF)
Primary Goat polyclonal Vinculin	Mouse	Vinculin	Santa Cruz Biotechnologies 1:500 (WB)
Primary Rabbit polyclonal TGFβ1	Mouse	TGFβ1	Santa Cruz Biotechnologies 1:500 (WB)
Primary Rat monoclonal CD45/B220	Mouse	B cells	BD Pharmigen 1:500 (IHC)
Primary Goat polyclonal CD3 epsilon	Mouse	T cells	Santa Cruz Biotechnologies 1:2000 (IHC)
Primary Rat monoclonal Ly6G	Mouse	Granulocytes	BD Bioscience 1:1000 (IHC)
Primary Rabbit polyclonal Iba1	Mouse	Histiocytes/macrophages	Wako 1:2000 (IHC)
TO-Pro3	Mouse	Nuclei	Invitrogen S.r.l., Milan, Italy 1:5000 (IF)
Secondary HRP-conjugated	-	-	Amersham, GE-Healthcare Various dilution (WB)
Secondary conjugated with Alexa Fluor 568 and 488	-	-	Invitrogen S.r.l., Milan, Italy 1:200 (IF)

Table 1: List of antibodies used for the analyses performed in this PhD Thesis.

2. *E1*$^{-/-}$/E1-E933A TRANSGENIC MOUSE MODEL

Through the strategy of pronuclear microinjection of DNA into fertilized eggs, the *E1*$^{-/-}$/E1-E933A transgenic mouse model was generated using the construct described below. Founders obtained in FVB strain, were mated with C57BL/6J mice (more than 10 backcrossing) to obtain a transgene also in C57Bl/6J background. Successive matings with *E1*$^{-/-}$ mice (C57Bl/6J background) were designed to derive newborns expressing a transgenic human EMILIN-1 in an *Emilin1* null background. Thanks to this strategy we are able to analyze the phenotype related to the expression of the exogenous mutated EMILIN1 without interference about the endogenous murine protein. I took part not in the generation process, but in the characterization analyses of the transgenic mouse.

2.1. DNA construct to produce *E1*$^{-/-}$/E1-E933A transgenic mice

The DNA construct used to generate the *E1*$^{-/-}$/E1-E933A mouse model was an 8 kb genomic fragment that included all the mouse *Emilin1* gene promoter elements (**Fabbro *et al.,* 2005**) fused to the sequence coding for human EMILIN1-E933A mutant cDNA. The cDNA was obtained through the overlapping polymerase chain reaction (PCR) method using primers carrying the E933A mutation and as template the human pCEPu-EMILIN1 construct (**Mongiat *et al.,* 2000**). After PCR, the amplification products were treated with the restriction enzymes NcoI and NotI and the resulting fragment (1301 pb) carrying the E933A point mutation instead ligated to the NcoI/NotI restricted pCEPu-EMILIN1 construct. The result was a 2984 pb long sequence coding for the mature human EMILIN1 E933A that was then amplified via PCR with NotI restriction site adaptor primers and cloned in a NotI restricted pBlueScript clone carrying a BAC derived mouse genomic sequence spanning 8 kb of EMILIN1 mouse promoter gene (**Zanetti et al., 2004**). The resulting plasmid was digested with KpnI restriction enzyme to avoid unwanted plasmid DNA sequences, and the purified fragment was employed for transgenesis procedures.

2.2. Staining of transgenic human E933A EMILIN-1

Different mouse tissues and organs (colon, lung, heart, and kidney) were isolated, embedded in OCT (Kaltek, Padova, Italy), snap frozen and stored at -80°C wrapped in aluminium foil. Before using, 5 µm sections were equilibrated at room temperature (RT), rehydrated in PBS for 5 min and then fixed with a solution of PBS-PFA 4% for 20 min. After fixation, sections were permeabilized with a PBS solution containing 1% BSA, 0.1% TRITON X-100 for 5 min and saturated with blocking buffer of PBS-1% BSA and finally incubated with the rabbit polyclonal anti human EMILIN-1 AS556, rat monoclonal

or anti mouse EMILIN-1 C11A8, and TO-pro3 for nuclear counterstaining (see dilution in the table of the first paragraph of this section).

2.3. DNA extraction and PCR to genotype transgenic mice

To genotype animals, DNA was extracted from mice tails using Maxwell mouse tail purification kit (Promega, Italia) according to the manufacturer's protocol. PCR reaction were performed with 1:400 (the optimum dilution that we discovered to obtain a good reaction) of total extracted DNA using goTAQ polymerase (Promega). The primers for the amplification of wild type (WT), knock out (KO), specific transgene sequence (TG) and β-actin sequence were:

***Emilin1* WT primers** → Forward (**5'**): **5'**-GAGGAGAGCGGAAGGAACTGAGG-**3'**;
Reverse (**3'**): **5'**-GAGGGAACAGAGCAGGAGGAGTG-**3'**;

***Emilin1* KO primers** → Forward (**5'**): **5'**-CGCCTTCTTGACGAGTTCTTCTGAG-**3'**;
Reverse (**3'**): **5'**-GAGGGAACAGAGCAGGAGGAGTG-**3'**;

EMILIN1 TG primers → Forward (**5'**): **5'**-CACCTCGCAGGGCTGGCGGTG-**3'**;
Reverse (**3'**): **5'**-AGGAGCCCCAGGCCAGCTCTC-**3'**;

β-actin primers → Forward (**5'**) primer: **5'**-GATGACGATATCGCTGCGCTGGTCG-**3';**
Reverse (**3'**) primer: **5'**-GCCTGTGGTACGACCAGAGGCATACAG-**3'**

The PCR samples were run on a 1.5% agarose gel with ethidium bromide. The hEMILIN1 PCR product was identified as a band corresponding to a length of 300 bp; the βactin PCR produced a band of 1kb.

3. CELL ADHESION ASSAY (CAFCA)

Recombinant proteins (EMILIN-1 wt gC1q and E933A gC1q) were functionally examined using a cell adhesion assay known as CAFCA (Centrifugal Assay for Fluorescence-based Cell Adhesion) (**Spessotto *et al.,* 2001**), that is based on two centrifugation steps: the first one to guarantee a synchronized cell-substratum contact and the second one (in the reverse direction) to allow for removal of the unbound/weakly bound cells under controlled condition. The "coating preoteins" were aliquoted in each well of the bottom CAFCA miniplates that were incubated at 4°C for 8-16 h. After removing the coating solution from the wells, they were filled with 1% (w/v) BSA blocking solution and incubated at room temperature for at least 2 h. Murine B16F10 melanoma cells to be assayed for their binding capability to molecular substrates were detached from the culture dishes with PBS containing 5 mM EDTA. Cells were washed by centrifugation to remove EDTA, resuspended in DMEM and then incubated at 37°C for 10-20 minutes in the presence of 1-10 µM calcein (AM) to allow fluorescent labelling. The blocking agent were then removed from the wells, which were washed at least twice with cell-adhesion medium containing PVP (poly-vinyl pyrrolidone). The wells were filled with the cell-adhesion medium containing 2% (v/v) India Ink. Aliquots of the labelled cells were added in each well. The bottom CAFCA miniplates were placed in the apposite bottom black holder and centrifuged at 142g for 5 min, followed by incubation 37°C for 20 min. The top CAFCA miniplate wells were fill with the same PVP-and India ink-containing medium as used for the bottom CAFCA miniplates. The CAFCA miniplates were assembled to form a unique chamber, the fluorescence signal emitted by cells in wells of the top (unbound cells) and bottom (substrate-bound cells) sides were measured independently, using a microplate fluorometer (Infinitem1000, Tecan Group, Maennedorf, Switzerland). The percentage bound cells, out of the total amount of cells introduced into the system, can be calculated as: bottom fluorescence value/bottom fluorescence + top fluorescence values.

4. EVALUATION of TGFβ-1 EXPRESSION LEVELS

4.1. Sample preparation

Colon tissue samples were collected from *E1*$^{+/+}$, *E1*$^{-/-}$ and *E1*$^{-/-}$/E1-E933A mice and tissue extracts were prepared using the gentleMACS dissociator (Miltenyi Biotec). An appropriate volume of tissue protein extraction lysis buffer supplemented with protease inhibitor cocktail (Roche, Basilea, Switzerland) was pipetted into gentleMACS M Tubes and then samples added. The homogenization procedure was performed in a closed system, thus avoiding cross-contamination and facilitating sterile handling. Tissue extracts were then buffered on ice for 30 minutes and centrifuged at 13.200g at 4°C for 20 minutes. After centrifugation, supernatants were recovered and quantified with Bradford reagent (Bio-Rad Laboratories) for subsequent analysis.

4.2. Western Blotting Analysis

Samples were subjected to a 4-12% SDS Page electrophoresis (using Criterion Precast Gel, BioRad) and then blotted on nitrocellulose membranes (Amersham Hybond-ECL, Amersham Pharmacia Biotech). Membranes were blocked (5% not fat milk, 0.1% Tween-20 in TBS) and incubated with anti TGF-β1 and anti vinculin (as loading control) primary antibodies (Santa Cruz Biotechnology). HRP-tagged secondary (GE Healthcare) antibodies were used at proper dilutions. Signals were detected using ECL reagents (Amersham Western Blotting Detection System and HyperFilm ECL, Amersham Pharmacia Biotech). Membranes were analyzed on Biorad Chemidoc Touch Imaging System and quantified by Quantity One Software densitometry or by Biorad ImageLab.

5. THORACIC DUCT SPROUTING ASSAY

Thoracic ducts of *E1*$^{+/+}$, *E1*$^{-/-}$ and *E1*$^{-/-}$/E1-E933A mice were precisely dissected and culture as described for the first time, by *Bruyère et al.* Precisely, after euthanasia, we cut the skin with sterile scissors along the abdominal midline; then we opened the sternal plate and cut ribs, leaving the diaphragm intact. Esophagus and vena cava were removed and the periaortic fibro-adipose tissue dissected carefully. When ducts were clean from fat, were cut into 1-mm-long rings, embedded in Cultrex® BME (Trevigen) gels and cultured in µ-plates angiogenesis 96-well (Ibidi) for 4-8 days with Endothelial Cell Medium MV2 (PromoCell) containing 20% FBS (Figure 37 A). In some experiments recombinant EMILIN-1 (20 µg/ml) or WT/E933A gC1q (40 µg/ml) were added to the culture media as soluble stimuli. The lymphatic ring cultures exhibited an outgrowth of cells that organized into capillary-like structures. Hamster anti-mouse podoplanin was used to identify the sprouting structures as LECs. Sprouting area was measured using ImageJ software (http://rsb.info.nih.gov) on the optical acquired images. The ability to produce a capillary network (Figure 37 B) was also qualitatively evaluated using an arbitrary score ranging from 0 (total absence of sprouts) to 4 (well organized and dense capillary area).

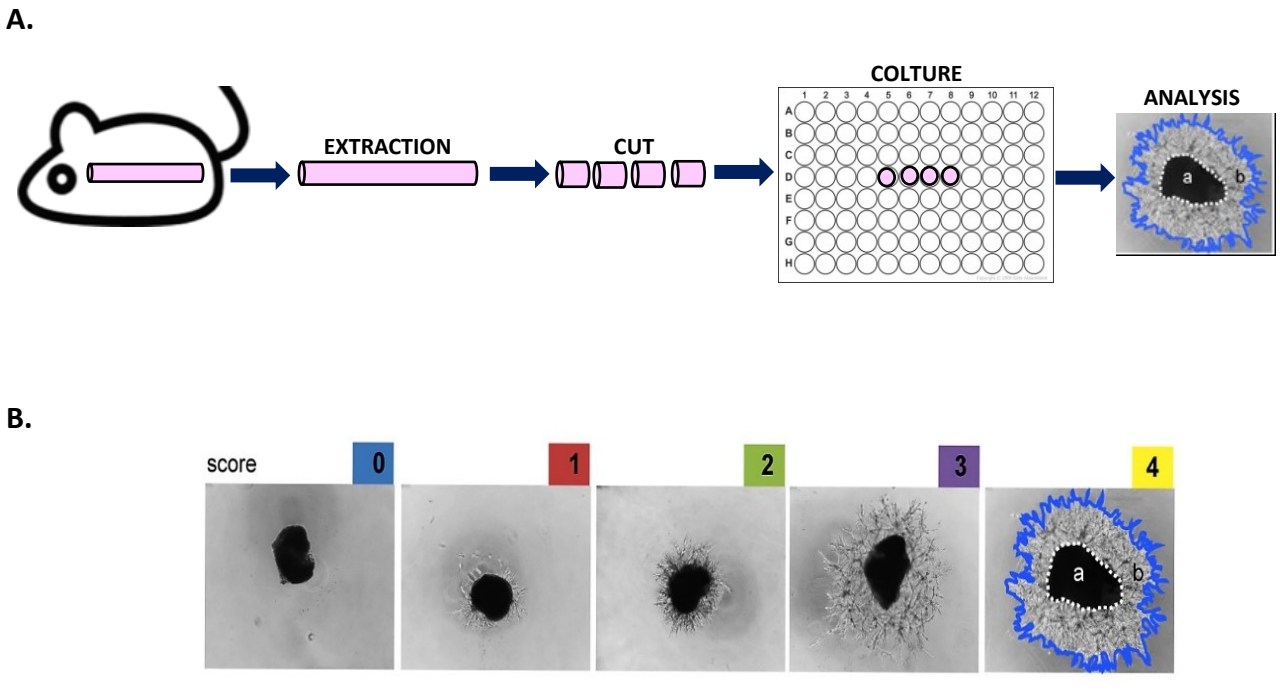

Figure 37: Representative scheme of thoracic duct sprouting assay. (A) Ducts were dissected, cut into 1-mm-long rings and cultured in Cultrex® BME (Trevigen); after 4-8 days of culture, the sprouting area was measured with ImageJ software. **(B)**. Representative images of the arbitrary score used to qualitatively evaluate the ability to produce a capillary network: the range of score values varied from 0 (total absence of sprouts) to 4 (well organized and dense capillary area).

6. MODELS OF LYMPH NODES DISSEMINATION

Intrafootpad injections of $2x10^5$ firefly-expressing B16F10*Luc* were applied to 6-8- week-old $E1^{+/+}$, $E1^{-/-}$ and $E1^{-/-}$/E1-E933A mice. The tumour growth was daily monitored and measured with the caliber until the tumour size were comparable between the three genotypes. Mice were then sacrificed for subsequent analyses. B16F10*Luc* derived-LN metastases were evaluated *ex vivo* by excising the draining popliteal, inguinal and axillary LNs (Figure 38); bioluminescence was quantified by means of an *in vivo imaging* system (Xenogen IVIS-100) at different time intervals (1 minute or 3 minutes exposures).

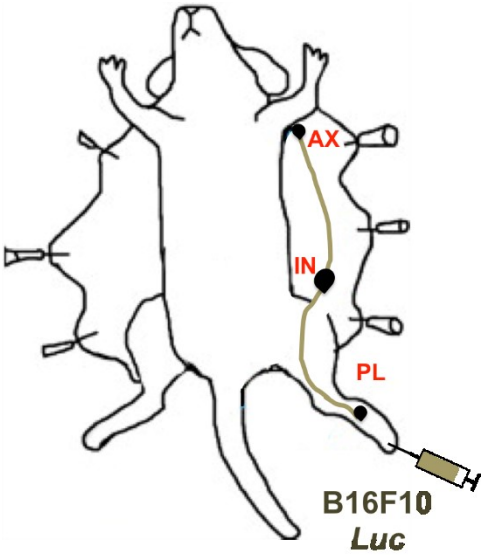

Figure 38: Scheme for intrafootpad injection model. $2x10^5$ firefly-expressing B16F10*Luc* were intrafootpad injected to evaluate LN dissemination; when tumour size were comparable, mice were sacrificed and popliteal (PL), inguinal (ING) and axillar (AX) LNs collected for in vivo imaging (Xenogen IVIS-100).

We performed also another set of experiments in which $5x10^5$ B16F10*Luc* cells were injected subcutaneously. To evaluate LV density in metastatic LNs, we stained paraffin-embedded LN sections with anti LYVE-1 antibodies and counterstained nuclei with To-pro3. Images were acquired using a Leica TCS SP8 confocal system and the series obtained were processed with Volocity 3D Image Analysis Software (PerkinElmer).

7. *IN VIVO* and *EX VIVO* ANALYSES FOR INDUCED EXPERIMENTAL COLITIS AND COLON CARCINOGENESIS

C57Bl/6J and FVB mice were purchased from Charles River Laboratories. *Emilin1*$^{-/-}$ (*E1*$^{-/-}$) FVB and C57Bl/6J background mice and *E1*$^{-/-}$/E1-E933A transgenic mice were generated and maintained at the CRO-IRCCS mouse facility. All animal procedures and their care were performed according to the institutional guidelines in compliance with national laws and with the authorization by the Italian Ministry of Health to Dr. Spessotto (n. 248/2015). Both for DSS-induced chronic colitis and AOM/DSS colon carcinogenesis treatments, we used 6/8 weeks aged female mice of each genotype (*E1*$^{+/+}$, *E1*$^{-/-}$ and *E1*$^{-/-}$/E1-E933A).

7.1. Two-steps colon carcinogenesis (AOM/DSS)

Mice were treated with a single intraperitoneal injection of Azoxymethane (AOM, 7,4 mg/kg body weight, Sigma-Aldrich) followed by 1-week exposures (for a total of three times) to 2% Dextran Sulphate Sodium Salt (DSS, Sigma-Aldrich) in the drinking water. During treatment the tumor growth was observed over time by endoscopy and at the end of the observation period (that was established when tumors in the colon lumen reach grade 5, occupying it almost entirely) mice were sacrificed. Differences in tumor number and volume between groups were first evaluated and then tumor tissue was examined by immunohistochemistry (IHC) and immunofluorescence (IF) analysis. Colonic mucosa dysplasia (low and high grade) was diagnosed according to the criteria described by *Cooper et al.* (**Cooper *et al.,* 2000**).

7.2. DSS-induced experimental colitis

Chronic colitis was induced with several 1-week exposures to 2% DSS in the drinking water. During treatment, the impact of intestinal inflammation was performed applying the clinical Disease Activity Index (DAI) and Murine Endoscopy Index of Colitis Severity (MEICS) (**Becker *et al.,* 2005**). At the end of each cycle of treatment, mice were monitored by endoscopy and at the end of the whole process, they were sacrificed. Colon tissue samples were then collected, recovering the part that goes from the cecum to the anus. As first analysis, colons of all mice were measured using ImageJ software applied on acquired images, and then cut longitudinally to obtain sampling for Western Blot, RNA-sequencing, dosage for cytokines expression analysis and paraffin embedding.

7.3. Endoscopy assessment

In order to evaluate colonic mucosal injury, during both DSS induced experimental colitis and AOM/DSS treatments, mice were monitored by endoscopy using the Coloview apparatus (Karl Storz Veterinary Endoscopy, Tuttlingen, Germany) (Figure 39). Before endoscopy mice were anesthetized with an intraperitoneal injection of ketamine (Imalgene, Merial) (100 mg/Kg) and xylazine (Rompun, Bayer) (10 mg/Kg) and the colon appropriately washed with a physiologic solution. Two cm of the colon proximal to the anus was visualized after inflation with air and endoscopic damage score was determined using the MEICS scoring methods. Based on this method introduced by *Beker et al.,* assessment of colon translucency (0-3 points), presence of fibrin in the bowel wall (0-3 points), granularity of the mucosa (0-3 points), morphology of vascular pattern (0-3 points), and stool consistency (normal to diarrhea, 0-3 points) were evaluated.

Figure 39: Specific strumentation use to perform endoscopy. This coloview endoscopy system endoscopy allows to perform a video-controlled direct analysis into the colon of living mice; the endoscopic tower is fiber optic light transmission incorporated and provides a bright and magnified view of the colon mucosa into the monitor.

7.4. Blood samples collection

At the end of whole DSS induced experimental colitis and two-steps colon carcinogenesis treatments, a blood sample was collected by intracardiac sampling from all groups of previously anesthetized mice. Blood was recovered with 27 G (Becton, Dickinson and Co.), transferred in special tubes BD Microtrainer® MAP K2EDTA 1.0 mg (Becton, Dickinson and Co.) to avoid blood coagulation and then analyzed to obtain the leucocyte formula using the Complete Blood Count (CBC) program.

8. HISTOPATHOLOGICAL AND IMMUNOHISTOCHEMICAL ANALYSES

8.1. Samples recovering and processing

After necroscopy, 1 cm of the distant colon was recovered, fixed in 10% neutral buffered formalin for 48 hours and transferred in 70% ethanol. Samples were then processed for paraffin embedding. For *histopathological examination* 5 µm thick sections were obtained at the microtome and stained with hematoxylin and eosin (H&E) and examined with a light microscope for the detection and quantification of histological lesions. Regarding *immunohistochemical analysis*, serial sections were immunostained with different primary antibodies: CD45/B220, CD3 epsilon, Ly6G and Iba1. After primary Ab incubation, sections were incubated with biotinylated secondary (rabbit anti-rat or rabbit anti goat or goat anti-rabbit) antibodies. Sections were labelled by avidin-biotin-peroxidase system, using a commercial immunoperoxidase kit (Santa Cruz Biotechnology). Finally, immunoreaction was visualized with 3,3'-diaminobenzidine (DAB) substrate and sections counterstained with Mayer's hematoxylin.

8.2. Examination procedures

Histopathology → all evaluation procedures were made in blind fashion. Thanks to this analysis different findings were detected and scored as follows:

1. **Epithelial damage:** loss of the epithelial layer of the enteric mucosa.
    - **- (0)** = absence of epithelial damage;
    - **+ (1)** = mild epithelial damage;
    - **++ (2)** = moderate epithelial damage;
    - **+++ (3)** = severe epithelial damage;
    - **N.B:** in some cases, squamous metaplasia of the epithelial layer was observed. This finding was scored as epithelial damage with the indication of metaplasia.

2. **Inflammatory infiltrate:** presence of infiltrating inflammatory cells within *lamina propria* (in the case of DSS induce experimental colitis approach), or within the *proliferative lesions* (in the case of two steps colon carcinogenesis approach).
    - **- (0)** = absence of infiltrating cells;
    - **+ (1)** = slight presence of infiltrating cells;
    - **++ (2)** = moderate presence of infiltrating cells;
    - **+++ (3)** = sever presence of infiltrating cells.

3. **Proliferative lesions:** specific for all C57Bl/6J mice with different genetic background treated with the two steps colon carcinogenesis (AOM/DSS) approach and classified according to *Boivin et al., 2003.*

    - Gastrointestinal intraepithelial neoplasia (GIN);
    - Adenoma (low or high grade);
    - Adenocarcinoma.

Immunohistochemistry → also in this case, all evaluation procedures were made in blind fashion, without knowledge about treatment or control groups.

1. **CD45/B220, CD3 epsilon** and **Ly6G** inflammatory cell positivity was scored as follow:

    - **-** = 0;
    - **+** = 1 to 5 cells;
    - **++** = 6 to 15 cells;
    - **+++** = 16 to 30 cells;
    - **++++** = > 30 cells.

    Counts were made at 400x and areas to be examined were chosen on the basis of more positive areas (hot spots areas).

    2. Iba1 positive cells: this analysis was evaluated through digital image analyses using ImageJ software (http://rbs.info.nih.gov/ij/).

9. RNA EXTRACTION USING TRIZOL REAGENT

RNA was extracted from *E1*$^{+/+}$ and *E1*$^{-/-}$/E1-E933A colon samples using TRIzol RNA Isolation Reagent (Thermo Fisher Scientific). Samples were recovered and maintained in TRIzol reagent (the volume of the tissue did not exceed 10% of the volume of the reagent). Colon samples were then homogenized and centrifuged at 13.200 rpm for 15 minutes at 4 °C to remove the insoluble material (extracellular membranes, polysaccharides, and high molecular mass DNA). The supernatant, that contained RNA and protein, was transferred to a fresh tube and an isovolume of 2-propanol was added. After 10 minutes at 4 °C, samples were centrifuged at 13.200 rpm and the RNA precipitate washed twice with 75% ethanol. RNA pellet was then briefly dried for 5–10 minutes by air-drying and resuspended in an appropriate volume of water. After isolation, RNA was clean up thanks to the RNeasy Mini Kit for subsequently sequencing.

9.1. RNA-sequencing and bioinformatics analysis

The total murine RNA-seq NGS analysis was performed at BMR Genomics of Padua on *E1*$^{+/+}$ and *E1*$^{-/-}$/E1-E933A RNA extracted from treated colon samples. RNA libraries were produced using the Illumina kit “TruSeq Stranded Total RNA with Ribo Zero gold” and then loaded on a run-sequencing program of Illumina NextSeq 500. Sequences, directly provided by the sequencer as file FASTQ, were subsequently aligned through the Burrows-Wheeler Aligner (BWA) program (Version 0.7.10-r789) against the murine genome (GRCm38). For the count it has been used the Ensemble annotation (Mus_musculus. GRCm38.81.gtf) referred to the genome used for the alignment (GRCm38). The differential expression gene (DEG) analysis was performed with “edgeR”.

10. CYTOKINE and CHEMOKINE EXPRESSION ANALYSIS

To determine the levels of the inflammatory responses of chronically DSS-induced tissue damages the expression of chemokine and cytokines was determined. At the end of the DSS treatment, mice were sacrificed, colons excised, opened and cut longitudinally. Samples were incubated in medium supplemented with penicillin and streptomycin and 0.1% FBS. After 24 h, the content of cytokines and chemokines in the supernatant fluids was analyzed by using commercially available panels of Bio-Plex Multiplex System (ThermoFisher Scientific) that allowed to quantify multiple biomarkers in a single well of 96-well plate, using a principle similar to that of ELISA assay. The ProcartaPlex Mix&Mattch Mouse 10-plex that we used for our experiments allows to quantify 10 targets of interest including ENA-78/CXCL5, IFN-γ, IL-1 α and β, IL-17, IL-21, IL-22, IL-23, IL-6 and TNF-α. Detection and quantitation of multiple secreted proteins was then performed thanks to the Luminex xMAP (multi-analyte profiling) technology.

11. STAINING of WHOLE MOUNT COLON and LYMPH NODE SPECIMENS

Colon and LNs were isolated, dissected and fixed in 4% PFA for 2 hours at room temperature. After hydration for at least 48 hours and permeabilization with PBS, 0.5% Triton X-100 buffer for 2 hours, samples were incubated for 2 hours with the blocking solution (PBS, BSA 1.5%). Later, an overnight incubation at 4°C with anti podoplanin primary antibody was performed. After 5 washes with PBS 0.3% Triton X-100, the secondary Alexa Fluor® conjugated antibody was added for a 3 hours incubation at room temperature. Samples were washed and mounted with Mowiol-2,5% DABCO; images were acquired with a true confocal scanner system (TCS SP8 FSU AOBS, Leica Microsystems), using Leica confocal LAS AF SP8 software.

12. IN SITU MESENTERIC LYMPHANGIOGRAPHY

To visualize mesenteric LVs and to evaluate lymph node draining capacity, 1 mL of long-chain fatty acid, Bodipy-FL-C16 (Life Technologies) was orally administered to *E1*$^{+/+}$, *E1*$^{-/-}$ and *E1*$^{-/-}$/E1-E933A C57Bl/6J DSS-treated and untreated mice (Figure 40). After 1,5 hours from oral administration, mice were euthanized, and fluorescence imaging was performed in order to visualize labelled LVs and

LNs in the mesentery, using a Leica M205 FA stereomicroscope (excitation light at 493 nm and emission light at 503 nm) equipped with a Leica DFC310 digital camera (Leica Microsystems).

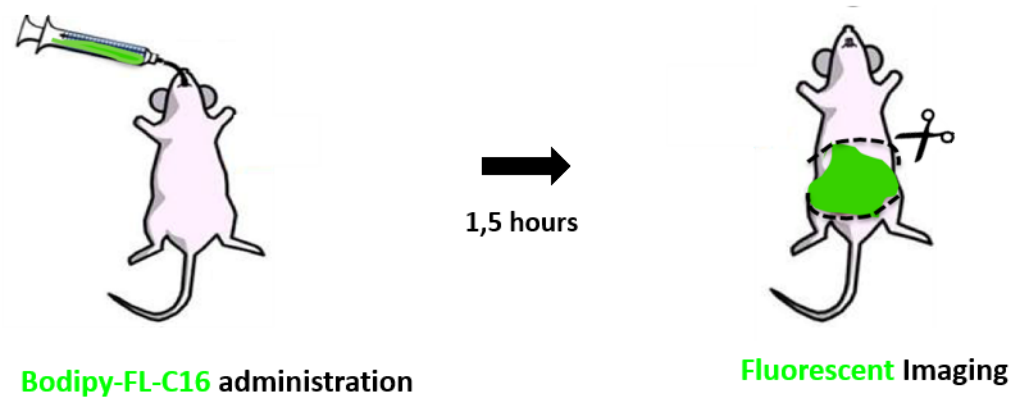

Figure 40: Schematic representation of the in situ mesenteric lymphangiography. Bodipy-FL-C16 was administrated with oral gavage, after 1,5 hours mice were euthanized and visualized using a Leica M205 FA stereomicroscope.

13. STATISTICAL ANALYSIS AND DATA ELABORATION

In order to quantitatively evaluate LV density, samples were analyzed using a Leica TCS SP8 confocal system detecting positivity for antibodies of interest and subsequently processed with Volocity 3D Image Analysis Software (PerkinElmer). On the optical acquired images, computer-assisted morphometric analyses were performed using the ImageJ software (http://rsb.info.nih.gov). Statistical significance of the results was determined by using the two-tailed unpaired Student's t test to determine whether two datasets were significantly different. To compare more than two datasets, we additionally performed a one-way analysis of variance followed by Tukey's post-hoc test. χ^2 test was used in some analyses, as indicated. A value of $P < 0.05$ was considered significant.

REFERENCES

- **Aebischer D, Iolyeva M, Halin C**. The inflammatory response of lymphatic endothelium. *Angiogenesis.* 17 (2014) 383–393. doi:10.1007/s10456-013-9404-3.
- **Aggarwal BB, Gupta SC, Kim JH.** Historical perspectives on tumor necrosis factor and its superfamily: 25 years later, a golden journey. *Blood.* (2012); 119:651–65.
- **Alitalo K, Tammela T, Petrova TV**. Lymphangiogenesis in development and human disease. *Nature*. (2005); 438:946–53.
- **Angeli V, Randolph GJ**. Inflammation, lymphatic function, and dendritic cell migration. *Lymphat Res Biol (*2006); 4: 217-228 [PMID:17394405 DOI: 10.1089/lrb.2006.4406].
- **Arnold M, Karim-Kos HE, Coebergh JW, Byrnes G, Antilla A, Ferlay J, Renehan AG, Forman D, Soerjomataram I.** Recent trends in incidence of five common cancers in 26 European countries since 1988. *Anal. Eur. Cancer Obs. Eur. J. Cancer 51* (2015). 1164–1187.
- **Asquith M, Powrie F.** An innately dangerous balancing act: intestinal homeostasis, inflammation and colitis-associated cancer. The *JEM*, (2010) http://doi.org/10.1084/jem.20101330.
- **Bazigou E, Xie S, Chen C, Weston A, Miura N, Sorokin L, Adams R, Muro AF, Sheppard D and Makinen T.** *Integrin-α9 is required for fibronectin matrix assembly during lymphatic valve morphogenesis*. *Dev. Cell* **17**, (2009) 175–186.
- **Becker C, Fantini MC, Wirtz S, Nikolaev A, Kiesslich R, Lehr HA, et al**. In vivo imaging of colitis and colon cancer development in mice using high resolution chromoendoscopy. *Gut.* (2005); 54:950–4.
- **Berg DJ, Davidson N, K¨uhn R et al.,** Enterocolitis and colon cancer in interleukin-10-deficient mice are associated with aberrant cytokine production and CD4+ Th1-like responses. *Journal of Clinical Investigation*, (1996) vol. 98, no. 4, pp. 1010–1020.
- Boivin **GP, Washington K, Yang K, Ward JM, Pretlow TP, Russell R, Besselsen DG, Godfrey VL, Doetschman T, Dove WF, Pitot HC, Halberg RB, Itzkowitz SH, Groden J, Coffey RJ.** Pathology of mouse models of intestinal cancer: consensus report and recommendations. (2003) *Gastroenterology*, 124: 762-777.
- **Bouma G, Strober W.** The immunological and genetic basis of inflammatory bowel disease. *Nature Reviews Immunology***,** (2003) volume3, pages521–533.
- **Braghetta P, Ferrari A, De Gemmis P, Zanetti M, Volpin D, Bonaldo P, Bressan GM**. Overlapping, complementary and site-specific expression pattern of genes of the EMILIN/Multimerin family. *Matrix Biol*. (2004) Jan;22(7):549-56.
- **Braghetta P, Ferrari A, de Gemmis P, Zanetti M, Volpin D, Bonaldo P, Bressan GM**. Expression of the EMILIN-1 gene during mouse development. *Matrix Biol*. (2002) Nov;21(7):603-9.
- **Bressan GM, Castellani I, Colombatti A, Volpin D.** Isolation and characterization of a 115,000-dalton matrix-associated glycoprotein from chick aorta. *J Biol. Chem*., (1983) vol. 258, no. 21, pp. 13262–13267.

- **Bressan GM, Daga-Gordini D, Colombatti A, Castellani I, Marigo V, Volpin D**. Emilin, a component of elastic fibers preferentially located at the elastin-microfibrils interface. *J Cell Biol*. (1993) Apr;121(1):201-12.
- **Bruyere F, Melen-Lamalle L, Blacher S, Roland G, Thiry M, Moons L, Frankenne F, Carmeliet P, Alitalo P, Libert C, Sleeman JP, Foidart JM, Noel A.** Modeling lymphangiogenesis in a threedimensional culture system, *Nat.Methods.* 5 (2008) 431–437. doi:10.1038/nmeth.1205.
- **Burt R**. Inheritance of colorectal cancer. *Drug Discov* (2007) Today Dis Mech 4: 293-300.
- **Campbell ID**. Studies of focal adhesion assembly. *Biochem. Soc. Trans*. (2008) 36, 263–26610.1042/BST0360263.
- **Capuano A, Fogolari F, Bucciotti F, Spessotto P, Nicolosi PA, Mucignat MT, Cervi M, Esposito G, Colombatti A, Doliana R**. The $\alpha_4\beta_1$/EMILIN1 interaction discloses a novel and unique integrin-ligand type of engagement. *Matrix Biol*. (2018) 66, 50-66.
- **Capuano A, Pivetta E, Baldissera F, Bosisio G, Wassermann B, Bucciotti F, Colombatti A, Doliana R, and Spessotto P.** Integrin binding site within the gC1q domain orchestrates EMILIN-1 induced lymphangiogenesis. *Matrix Biology* (2018) (under revision).
- **Carethers JM, Jung BH**. Genetics and Genetic Biomarkers in Sporadic Colorectal Cancer. *Gastroenterology* (2015); 149:1177-90. e3.
- **Chassaing B, Aitken JD, Malleshappa M and Vijay-Kumar M.** Dextran Sulfate Sodium (DSS)-induced Colitis in Mice. *Curr Protoc Immunol.* (2014) Feb 4; 104: Unit–15.25. 10.1002/0471142735.im1525s104.
- **Chen R, Rabinovitch PS, Crispin DA, Emond MJ, Bronner MP, Brentnall TA.** The initiation of colon cancer in a chronic inflammatory setting. *Carcinogenesis*, (2005) vol. 26, no. 9, pp. 1513–1519.
- **Christian S, Ahorn H, Novatchkova M, Garin-Chesa P, Park JE, Weber G,Eisenhaber F, Rettig WJ, Lenter MC**. Molecular cloning and characterization of EndoGlyx-1, an EMILIN-like multisubunit glycoprotein of vascular endothelium. *J Biol Chem*. (2001) Dec 21;276(51):48588-95.
- **Colombatti A, Bressan GM, Castellani I, Volpin D.** Glycoprotein 115, a glycoprotein isolated from chick blood vessels, is widely distributed in connective tissue. *J Cell Biol* (1985) 100(1):18-26.
- **Colombatti A, Doliana R, Bot S, Canton A, Mongiat M, Mungiguerra G, Paron-Cilli S, Spessotto P**. The EMILIN protein family. *Matrix Biol*. (2000) Aug;19(4):289-301.
- **Cooper HS, Murthy S, Kido K, Yoshitake H, Flanigan A**. Dysplasia and cancer in the dextran sulfate sodium mouse colitis model. Relevance to colitis-associated neoplasia in the human: a study of histopathology, B-catenin and p53 expression and the role of inflammation. *Carcinogenesis*. (2000); 21:757–68.
- **Danese S, Malesci A, Vetrano S.** Colitis-associated cancer: the dark side of inflammatory bowel disease. *Gut Journals* (2011). doi.org/10.1136/gutjnl-2011-300953.
- **Danese S, Mantovani A.** Inflammatory bowel disease and intestinal cancer: a paradigm of the Yin-Yang interplay between inflammation and cancer. *Oncogene*, (2010) 29, 3313–3323.

- **Danussi C, Del Bel Belluz L, Pivetta E, Modica TME, Muro A, Wassermann B, Doliana R, Sabatelli P, Colombatti A, and Spessotto P**. EMILIN1/α9β1 integrin interaction is crucial in lymphatic valve formation and maintenance. *Mol. Cell. Biol.,* (2013) vol. 33, no. 22, pp. 4381–94.
- **Danussi C, Petrucco A, Wassermann B, Modica TME, Pivetta E, Del Bel Belluz L, Colombatti A, and Spessotto P.** An EMILIN1-negative microenvironment promotes tumor cell proliferation and lymph node invasion. *Cancer Prev. Res*., (2012) vol. 5, no. 9, pp. 1131–1143.
- **Danussi C, Petrucco A, Wassermann B, Pivetta E, Modica TM, Belluz LB, et al.** EMILIN1-α4/α9 integrin interaction inhibits dermal fibroblast and keratinocyte proliferation. *JCell Biol*. (2011); 195:131–45.
- **Danussi C, Spessotto P, Petrucco A, Wassermann B, Sabatelli P, Montesi M, Doliana R, Bressan GM, Colombatti A.** Emilin1 deficiency causes structural and functional defects of lymphatic vasculature. *Mol Cell Biol*. (2008) Jun;28(12):4026-39.
- **Dieterich LC, Ducoli L, Shin JW, Detmar M.** Distinct transcriptional responses of lymphatic endothelial cells to VEGFR-3 and VEGFR-2 stimulation. *Sci. Data. 4* (2017) 170106. doi:10.1038/sdata.2017.106.
- **Doliana R, Bot S, Bonaldo P, and Colombatti A.** EMI, a novel cysteine-rich domain of EMILINs and other extracellular proteins, interacts with the gC1q domains and participates in multimerization. *FEBS Lett.,* (2000) vol. 484, no. 2, pp. 164–168.
- **Doliana R, Bot S, Mungiguerra G, Canton A, Cilli SP, Colombatti A**. Isolation and characterization of EMILIN-2, a new component of the growing EMILINs family and a member of the EMI domain-containing superfamily. *J Biol Chem*. (2001) Apr 13;276(15):12003-11.
- **Doliana R, Canton A, Bucciotti F, Mongiat M, Bonaldo P, Colombatti A**. Structure, chromosomal localization, and promoter analysis of the human elastin microfibril interface located proteIN (EMILIN) gene. *J Biol Chem*. (2000) Jan 14;275(2):785-92.
- **Doliana R, Mongiat M, Bucciotti F, Giacomello E, Deutzmann R, Volpin D, Bressan GM, Colombatti A**. EMILIN, a component of the elastic fiber and a new member of the C1q/tumor necrosis factor superfamily of proteins. *J Biol Chem*. (1999) Jun 11;274(24):16773-81.
- **Duplaa´ C, Couffinhal T, Dufourcq P, Llanas B, Moreau C and Bonnet J.** The integrin VLA-4 is expressed in human smooth muscle cell. Involvement of a4 and VCAM-1 during smooth muscle cell differentiation. *Circ. Res.* (1997) 80, 159-169.
- **Fabbro C, De GP, Braghetta P, Colombatti A, Volpin D, Bonaldo P, Bressan GM**. Analysis of regulatory regions of Emilin1 gene and their combinatorial contribution to tissue-specific transcription. *J.Biol.Chem*. 280 (2005) 15749–15760. doi:10.1074/jbc.M412548200.
- **Feagins LA, Souza RF, Spechler SJ.** Carcinogenesis in IBD: potential targets for the prevention of colorectal cancer. *Nat Rev Gastroenterol Hepatol. (*2009); 6(5):297-305.
- **Ford AC, Sandborn WJ, Khan KJ, et al.** Efficacy of biological therapies in inflammatory bowel disease: systematic review and meta-analysis. *Am J Gastroenterol*. (2011); 106:644–59. quiz 660.
- **Francescone R, Hou V, Grivennikov SI.** Cytokines, IBD, and Colitis-associated Cancer. *Inflamm Bowel Dis.* (2015). Volume 21, Number 2.
- **Fu K** et al. NBI diagnosis of squamous metaplasia of the rectum and ulcerative colitis. *Endoscopy* (2008); 40: E45-E46.

- **Gerli R, Ibba L and Fruschelli C.** Ultrastructural cytochemistry of anchoring filaments of human lymphatics capillaries and their relation to elastic fiber. *Lymphology* (1991) 24,105-112.
- **Gorrini C, Harris IS, Mak TW**. Modulation of oxidative stress as an anticancer strategy. *Nat Rev Drug Discov* (2013); 12:931–947.
- **Grady WM and Pritchard CC.** Molecular alterations and biomarkers in colorectal cancer. *Toxicol Pathol* (2014) 42: 124-139.
- **Grivennikov SI, Greten FR, Karin M**. Immunity, inflammation, and cancer. *Cell*. (2010); 140:883–99.
- **Grivennikov SI, Karin E, Terzic J, et al.** IL-6 and Stat3 are required for survival of intestinal epithelial cells and development of colitis-associated cancer. *Cancer Cell.* (2009); 15:103–13.
- **Grivennikov SI.** Inflammation and colorectal cancer: colitis-associated neoplasia. *Semin Immunopathology*. (2013); 35:229–244.
- **Hanahan D, Weinberg RA.** Hallmarks of cancer: the next generation. *Cell (*2011); 144: 646-674.
- **Hayward CP, Warkentin TE, Horsewood P, Kelton JG.** Multimerin: a series of large disulfide-linked multimeric proteins within platelets. *Blood*. (1991) 77(12):2556-60.
- **Herbeuval JP, Lelievre E, Lambert C, et al.** Recruitment of STAT3 for production of IL-10 by colon carcinoma cells induced by macrophage-derived IL-6*. J Immunol*. (2004); 172:4630–6.
- **Huang C, Chen Y.** Lymphangiogenesis and colorectal cancer. *Saudi Med J* (2017); Vol. 38 (3): 237-244 doi: 10.15537/smj.2017.3.16245.
- **Ihara S, Hirata Y, Koike K.** TGF-b in inflammatory bowel disease: a key regulator of immune cells, epithelium, and the intestinal microbiota. *J Gastroenterol* (2017) 52:777–787 DOI 10.1007/s00535-017-1350-1.
- **Iida J, Meijne AM, Spiro RC, Roos E, Furcht LT and McCarthy JB.** Spreading and focal contact formation of human melanoma cells in response to the stimulation of both melanoma-associated proteoglycan (NG2) and α4β1 integrin. *Cancer Res.* (1995) 55, 2177–2185.
- **Innamorati G, Bianchi E, Whang MI**. An intracellular role for the C1q-globular domain. *Cell Signal*. (2006) Jun;18(6):761-70.
- **Itzkowitz SH, et al.** Inflammation and cancer IV. Colorectal cancer in inflammatory bowel disease: the role of inflammation. *Am. J. Physiol. Gastrointest. Liver Physiol.*, (2004), vol. 287 (pg. G7-G17).
- **Jiang X, Nicolls MR, Tian W and Rockson SG**. Lymphatic dysfunction, leukotrienes, and lymphedema. *Annu Rev Physiol* (2018). https://doi.org/10.1146/annurev-physiol-022516-034008.
- **Jostins L, Ripke S, Weersma RK, et al.** Host-microbe interactions have shaped the genetic architecture of inflammatory bowel disease*. Nature*. (2012); 491:119–24.
- **Kai Y, Takahashi I, Ishikawa H, et al.** Colitis in mice lacking the common cytokine receptor gamma chain is mediated by IL-6-producing CD4+ T cells. *Gastroenterology. (*2005); 128:922–34.
- **Kanneganti M, Kenudson MM, Mizoguchi E.** Animal Models of Colitis-Associated Carcinogenesis. *Journal of Biomedicine and Biotechnology*. **(**2011), Article ID 342637, 23 pages doi: 10.1155/2011/342637.

- **Karpanen T, Egeblad M, Karkkainen MJ, Kubo H, Yla-Herttuala S, Jaattela M, and Alitalo K.** Vascular Endothelial Growth Factor C promotes tumor lymphangiogenesis and intralymphatic tumor growth. *Cancer Research* (2001) 61, 1786–1790.
- **Kim ER, Chang DK.** Colorectal cancer in inflammatory bowel disease: The risk, pathogenesis, prevention and diagnosis. *World J Gastroenterol*. (2014); 20:9872–9881.
- **Kim H, Kataru RP, Koh GY**. Inflammation-associated lymphangiogenesis: a double-edged sword? *J.Clin.Invest.* 124 (2014) 936–942. doi:10.1172/JCI71607.
- **Kishore U, Gaboriaud C, Waters P, Shrive AK, Greenhough TJ, Reid KB, Sim RB, Arlaud GJ**. C1q and tumor necrosis factor superfamily: modularity and versatility. *Trends Immunol*. (2004) Oct;25(10):551-61.
- **Lakatos PL, Burisch.** Environment and invironment in IBDs: partners in crime. http://dx.doi.org/10.1136/gutjnl-(2014)-308460.
- **Laqueur GL.** Carcinogenic effects of cycad meal and cycasin, methylazoxymethanol glycoside, in rats and effects of cycasin in germfree rats. *Fed Proc.* (1964); 23:1386–8.
- **Law EW, Cheung AK, Kashuba VI, Pavlova TV, Zabarovsky ER, Lung HL, Cheng Y, Chua D, Lai-Wan Kwong D, Tsao SW, et al**. Antiangiogenic and tumor-suppressive roles of candidate tumor-suppressor gene, Fibulin-2, in nasopharyngeal carcinoma. *Oncogene* (2012) 31: 728–738.
- **Leahy DJ, Aukhil I, and Erickson HP**. 2.0 A° crystal structure of a four-domain segment of human fibronectin encompassing the RGD loop and synergy region. *Cell,* (1996) vol. 84, no. 1, pp. 155–164.
- **Leimeister C, Steidl C, Schumacher N, Erhard S, Gessler M.** Developmental Expression and Biochemical Characterization of Emu Family Members. *Dev Biol*. (2002) 249: 204–218.
- **Lobb RR and Hemler ME.** The pathophysiologic role of a4 integrins *in vivo*. *J. Clin. Invest.* (1994) 94, 1722-1728.
- **Maiorani O, Pivetta E, Capuano A, Modica TME, Wassermann B, Bucciotti F, Colombatti A, Doliana R, Spessotto P**. Neutrophil elastase cleavage of the gC1q domain impairs the EMILIN1-alpha4beta1 integrin interaction, cell adhesion and anti-proliferative activity. *Sci.Rep*. 7 (2017) 39974. doi:10.1038/srep39974.
- **Masumoto A, Hemler ME**. Multiple activation states of VLA-4. Mechanistic differences between adhesion to CS1/fibronectin and to vascular cell adhesion molecule-1. *J Biol Chem*. (1993) Jan 5;268(1):228-34.
- **Mazmanian SK, Round JL, Kasper DL.** A microbial symbiosis factor prevents intestinal inflammatory disease. *Nature.* (2008); 453:620–625.
- **Molodecky NA** et al. Increasing incidence and prevalence of the inflammatory bowel diseases with time, based on systematic review. *Gastroenterology* (2012), 142, 46–54.
- **Mongiat M, Mungiguerra G, Bot S, Mucignat MT, Giacomello E, Doliana R, Colombatti A**. Self-assembly and supramolecular organization of EMILIN. *J Biol Chem*. (2000) Aug 18;275(33):25471-80.
- **Munkholm P.** Review article: the incidence and prevalence of colorectal cancer in inflammatory bowel disease. *Aliment Pharmacol Ther.* (2003); 18(Suppl 2):1–5.

- **Neurath MF.** Cytokines in inflammatory bowel disease. *Nature Reviews Immunology* (2014) volume 14, pages329–342.
- **Ng SC, Benjamin JL, McCarthy NE, et al.** Relationship between human intestinal dendritic cells, gut microbiota, and disease activity in Crohn's disease. *Inflamm Bowel Dis*. (2011); 17:2027–37.
- **Olszewski WL.** The lymphatic system in body homeostasis: physiological conditions. *Lymphat Res Biol (*2003); 1: 11-21; 21-24 [PMID: 15624317]10.
- **Palmer EL, Ru¨egg C, Ferrando R, Pytela R, Sheppard D.** Sequence and tissue distribution of the integrin alpha 9 subunit, a novel partner of beta 1 that is widely distributed in epithelia and muscle. *J. Cell Biol.* (1993) 123**:**1289–1297.
- **Piller NB.** Macrophage and tissue changes in the developmental phases of secondary lymphoedema and during conservative therapy with benzopyrone. *ArchHistolCytol*. (1990); 53 Suppl:209–18.
- **Pinco KA, He W, Yang JT**. alpha4beta1 integrin regulates lamellipodia protrusion via a focal complex/focal adhesion-independent mechanism. *Mol Biol Cell*. (2002) Sep;13(9):3203-17.
- **Pivetta E, Wassermann B, Del Bel Belluz L, Danussi C, Modica TME, Maiorani O, Bosisio G, Boccardo F, Canzonieri V, Colombatti A, and Spessotto P.** Local inhibition of elastase reduces EMILIN1 cleavage reactivating lymphatic vessel function in a mouse lymphoedema model.," *Clin. Sci. (Lond).,* (2016) vol. 130, no. 14, pp. 1221–36.
- **Podgrabinska S, Braun P, Velasco P, Kloos B, Pepper MS, Skobe M.** Molecular characterization of lymphatic endothelial cells. *Proc Natl Acad Sci U S A*. (2002) Dec 10;99(25):16069-74.
- **Qian F, Vaux DL and Weissman IL.** Expression of the integrin a4b1 on melanoma cells can inhibit the invasive stage of metastasis formation. *Cell* (1994) 77, 335-347.
- **Rakoff-Nahoum S, Paglino J, Eslami-Varzaneh F, et al.** Recognition of commensal microflora by toll-like receptors is required for intestinal homeostasis. *Cell*. (2004); 118:229–41.
- **Raman M, Cobb MH.** TGF-beta regulation by Emilin1: new links in the etiology of hypertension. *Cell.* (2006) Mar 10;124(5):893-5.
- **Round JL, Mazmanian SK.** The gut microbiota shapes intestinal immune responses during health and disease. *Nature reviews Immunology*. (2009); 9:313–323.
- **Rustgi AK**. The genetics of hereditary colon cancer. *Genes Dev.* (2007); 21:2525–2538.
- **Saharinen P, Tammela T, Karkkainen MJ, Alitalo K.** Lymphatic vasculature: development, molecular regulation and role in tumor metastasis and inflammation. *Trends Immunol (*2004); 25:387-395.
- **Schulte-Merker S, Sabine A, Petrova TV.** Lymphatic vascular morphogenesis in development, physiology, and disease. *J Cell Biol* (2011) 193: 607–618.
- **Shang K, Bai YP, Wang C, Wang Z, Gu HY, Du X, Zhou XY, Zheng CL, Chi YY, Mukaida N, Li YY.** *Crucial involvement of tumor-associated neutrophils in the regulation of chronic colitis-associated carcinogenesis in mice*. *PLoS ONE* **7**, (2012) e51848.
- **Shimaoka M, Springer TA**. Therapeutic antagonists and conformational regulation of integrin function. *Nat Rev Drug Discov (*2003), 2**:**703-716.

- **Smith LL, Cheung HK, Ling LE, Chen J, Sheppard D, Pytela R, Giachelli CM.** Osteopontin N-terminal domain contains a cryptic adhesive sequence recognized by a9b1 integrin. *J. Biol. Chem.* (1996) 271**:**28485– 28491.
- **Somayeh JS, Masoud A, Sharareh M, Hamed AA, Hajieh GS.** Role of gut microbiota in the pathogenesis of colorectal cancer. *Gastroenterol Hepatol Bed Bench* (2018); 11(2):101-109.
- **Spessotto P, Bulla R, Danussi C, Radillo O, Cervi M, Monami G, Bossi F, Tedesco F, Doliana R, Colombatti A**. EMILIN1 represents a major stromal element determining human trophoblast invasion of the uterine wall. *J Cell Sci*. (2006) Nov 1;119(Pt 21):4574-84.
- **Spessotto P, Cervi M, Mucignat MT, Mungiguerra M, Sartoretto I, Doliana R, Colombatti A.** β1 integrin-dependent cell adhesion to EMILIN-1 is mediated by the gC1q domain. *J Biol. Chem*. (2003) vol. 278, no. 8, pp. 6160–6167.
- **Spessotto P, Giacomello E, and Perri R**. Improving fluorescence-based assays for the in vitro analysis of cell adhesion and migration. *Mol. Biotechnol.,* (2002) vol. 20, no. 3, pp. 285–304.
- **Spessotto P, Lacrima K, Nicolosi PS, Pivetta E, Scapolan M, Perris R.** Fluorescence-based assays for in vitro analysis of cell adhesion and migration. *Methods MolBiol*. 522 (2009) 221–250. doi:10.1007/978-1-59745-413-1_16.
- **Stacker SA, Caesar C, Baldwin ME, Thornton GE, Williams RA, Prevo R, et al.** VEGF-D promotes the metastatic spread of tumor cells via the lymphatics. *Nat Med (*2001); 7: 186-191.
- **Stepp MA, Zhu L.** Upregulation of alpha 9 integrin and tenascin during epithelial regeneration after debridement in the cornea. *J. Histochem. Cytochem*. (1997). 45**:**189–201.
- **Su JL, Yen CJ, Chen PS, Chuang SE, Hong CC, Kuo IH, et al.** The role of the VEGF-C/VEGFR-3 axis in cancer progression. *Br J Cancer (*2007); 96: 541-545.
- **Tammela T, Alitalo K.** Lymphangiogenesis: Molecular mechanisms and future promise. *Cell (*2010); 140: 460-476.
- **Tanaka T, Kohno H, Suzuki R, Yamada Y, Sugie S, and Mori M.** A novel inflammation-related mouse colon carcinogenesis model induced by azoxymethane and dextran sodium sulfate. *Cancer Sci.* (2003) 94, 965–973.
- **Taooka Y, Chen J, Yednock T, Sheppard D.** The integrin alpha 9 beta 1 mediates adhesion to activated endothelial cells and transendothelial neutrophil migration through interaction with vascular cell adhesion molecule-1. *J. Cell Biol***. (**1999). 145**:**413–420.
- **Tenesa A, Dunlop MG.** New insights into the aetiology of colorectal cancer from genome-wide. *Nature Reviews Genetics* (2009) volume10, pages353–358.
- **Terzic J, Grivennikov S, Karin E, Karin M. Inflammation and Colon Cancer.** *Gastroenterology (*2010); 138:2101–2114.
- **Verdone G, Corazza A, Colebrooke SA, Cicero D, Eliseo T, Boyd J, Doliana R, Fogolari F, Viglino P, Colombatti A, Campbell ID, Esposito G.** NMR-based homology model for the solution structure of the C-terminal globular domain of EMILIN1. *J Biomol NMR*. (2009) Feb;43(2):79-96.
- **Verdone G, Doliana R, Corazza A, Colebrooke SA, Spessotto P, Bot S, Bucciotti F, Capuano A, Silvestri A, Viglino P, Campbell ID, Colombatti A, Esposito G.** The solution structure of EMILIN1 globular C1q domain reveals a disordered insertion necessary for interaction with the alpha4beta1 integrin. *J Biol Chem.* (2008) Jul4;283(27):18947-56.

- **Vetrano S, Borroni EM, Sarukhan A, Savino B, Bonecchi R, Correale C, et al.** The lymphatic system controls intestinal inflammation and inflammation-associated Colon Cancer through the chemokine decoy receptor D6. *Gut*. (2010); 59:197–206.
- **Watson A J, Collins PD.** Colon cancer: a civilization disorder. *Dig Dis* (2011); 29:222-28.
- **Wiig H, Gyenge C, Iversen PO, Gullberg D, Tenstad O.** The role of the extracellular matrix in tissue distribution of macromolecules in normal and pathological tissues: potential therapeutic consequences. *Microcirculation (*2008); 15: 283-296.
- **Wirtz S, Neufert C, Weigmann and Neurath MF.** Chemically induced mouse models of intestinal inflammation. *Nature Protocols* (2007) volume2, pages541–546.
- **Xavier RJ, Podolsky DK**. Unravelling the pathogenesis of inflammatory bowel disease. *Nature.* (2007); 448:427–34.
- **Yang GX, Hagmann WK**. VLA-4 antagonists: potent inhibitors of lymphocyte migration. *Med Res Rev*. (2003) May;23(3):369-92.
- **Yang XD, Karin N, Tisch R, Steinman L and McDevitt HO.** Inhibition of insulitis and prevention of diabetes in nonobese diabetic mice by blocking L-selectin and VLA-4 adhesion receptors. *Proc. Nat. Acad. Sci.USA* (1993) 90, 10494-10498.
- **You TJ, Maxwell DS, Kogan TP, Chen Q, Li J, Kassir J, Holland GW, Dixon RA.** A 3D structure model of integrin alpha 4 beta 1 complex: I. Construction of a homology model of beta 1 and ligand binding analysis. *Biophys J.* (2002) Jan;82(1 Pt 1):447-57.
- **Yusuf-Makagiansar H, Anderson ME, Yakovleva TV, Murray JS, Siahaan TJ**. Inhibition of LFA-1/ICAM-1 and VLA-4/VCAM-1 as a therapeutic approach to inflammation and autoimmune diseases. *Med Res Rev*. (2002) Mar;22(2):146-67.
- **Zacchigna L, Vecchione C, Notte A, Cordenonsi M, Dupont S, Maretto S, Cifelli G, Ferrari A, Maffei A, Fabbro C, Braghetta P, Marino G, Selvetella G, Aretini A, Colonnese C, Bettarini U, Russo G, Soligo S, Adorno M, Bonaldo P, Volpin D, Piccolo S, Lembo G, Bressan GM**. Emilin1 links TGF-beta maturation to blood pressure homeostasis. *Cell*. (2006) Mar 10;124(5):929-42.
- **Zanetti M, Braghetta P, Sabatelli P, Mura I, Doliana R, Colombatti A, Volpin D, Bonaldo P, Bressan GM**. EMILIN-1 deficiency induces elastogenesis and vascular cell defects. *Mol Cell Biol*. (2004) Jan;24(2):638-50.
- **Zhang X, Groopman JE and Wang JF**. Extracellular matrix regulates endothelial functions through interaction of VEGFR-3 and integrin alpha5beta1. J Cell Physiol (2005), 202:205–214.
- **Zisman TL, Rubin DT**. Colorectal cancer and dysplasia in inflammatory bowel disease. *World J Gastroenterol* (2008); 14:2662–2669.

PUBLICATIONS

1. **Capuano A, Pivetta E, Baldissera F, Bosisio G, Wassermann B, Bucciotti F, Colombatti A, Doliana R, and Spessotto P.** Integrin binding site within the gC1q domain orchestrates EMILIN-1 induced lymphangiogenesis. 2018, *Matrix Biology* (in press).

   https://www.sciencedirect.com/science/article/pii/S0945053X18303445

2. **Pivetta E, Wassermann B, Del Bel Belluz L, Danussi C, Modica TME, Maiorani O, Bosisio G, Boccardo F, Canzonieri V, Colombatti A, and Spessotto P.** Local inhibition of elastase reduces EMILIN1 cleavage reactivating lymphatic vessel function in a mouse lymphoedema model. *Clin. Sci. (Lond).,* vol. 130, no. 14, pp. 1221–36, 2016.

   http://www.clinsci.org/content/early/2016/02/25/CS20160064